December 2012

SCR-Based Wind Energy Conversion Circuitry and Controls for DC Distributed Wind Farms

Ravi Nanayakkara
University of Wisconsin-Milwaukee

SCR-BASED WIND ENERGY CONVERSION CIRCUITRY AND CONTROLS FOR DC DISTRIBUTED WIND FARMS

By

Ravi Nanayakkara

A Dissertation Submitted in

Partial Fulfillment of the

Requirements for the Degree of

Doctor of Philosophy

in Engineering

at

The University of Wisconsin-Milwaukee

December 2012

ABSTRACT

SCR-BASED WIND ENERGY CONVERSION CIRCUITRY AND CONTROLS FOR DC DISTRIBUTED WIND FARMS

By

Ravi Nanayakkara

The University of Wisconsin-Milwaukee, 2012

Under the Supervision of Professor Adel Nasiri

The current state of art for electrical power generated by wind generators are in alternating current (AC). Wind farms distribute this power as 3-phase AC. There are inherent stability issues with AC power distribution. The grid power transfer capacity is limited by the distance and characteristic impedance of the lines. Furthermore, wind generators have to implement complicated, costly, and inefficient back-to-back converters to generate AC. AC distribution does not offer an easy integration of energy storage. To mitigate drawbacks with AC generation and distribution, direct current (DC) generation and high voltage direct current (HVDC) distribution for the wind farms is proposed. DC power distribution is inherently stable. The generators convert AC power to DC without the use of a back-to-back converter. DC grid offers an easy integration of energy storage.

The proposed configuration for the generator is connected to a HVDC bus using a 12 pulse thyristor network, which can apply Maximum Power Point Tracking (MPPT). To properly control the system, several estimators are designed and applied. This includes a firing angle, generator output voltage, and DC current estimators to reduce noise effects. A DSP-based controller is designed and implemented to control the system and provide gate pulses. Performance of the proposed system under faults and drive train torque pulsation are analyzed as well. Additionally, converter paralleling when turbines operate at different electrical power levels are also studied. The proposed new Wind Energy Conversion System (WECS) is described in detail and verified using MATLAB®/ Simulink® simulation and experimental test setup. The proposed solution offers higher reliability, lower conversion power loss, and lower cost. The following is proposed as future work:

1) Study different control methods for controlling the SCR's.

2) Investigate reducing torque pulsations of the PMSG and using the proposed power conversion method for DFIG turbines.

3) Explore options for communication/control between PMSG, circuit protection and grid-tied inverters.

4) Investigate the best possible configuration for DC storage/connection to the HVDC/MVDC bus.

5) Study the filtering needed to improve the DC bus voltage at the generator.

To my daughter and son

TABLE OF CONTENTS

LIST OF FIGURES

LIST OF TABLES

ACKNOWLEDGEMENTS

I would like to thank my thesis advisor, Dr Adel Nasiri for his guidance, knowledge and encouragement. I Would also like to thank my dissertation committee: Dr. David Yu, Dr. Jugal Ghorai, Dr. Mahsa Ranji and Dr. Al Ghorbanpoor. Without their advice this thesis would not be possible. I would like to thank Rockwell Automation, my employer for supporting me with hardware for the lab setup. This allowed me to build the prototype system rapidly.

I also thank my fellow colleagues Bora Novakovic, Zeljko Jankovic, Ahmad Hamidi and Goran Mandic for their help with the project.

I appreciate the tedious task of proof reading by my parents Amarasena and Padma Nanayakkara, Dineshi Burchi and Georgia Hill.

Finally, I thank my family for encouragement, understanding and support.

LIST OF ABBREVIATIONS

HVDC – High Voltage Direct Current

MVDC – Medium Voltage Direct Current

DC – Direct Current

AC – Alternating Current

SCR – Silicon Controlled Rectifier

VSC – Voltage Source Converter

CSC – Current Source Converter

PMSG – Permanent Magnet Synchronous Generator

MPPT – Maximum Power Point Tracking

PE – Power Electronic

RMS – Root Mean Square

WECS- Wind Energy Conversion systems

DFIG –Doubly Fed Induction Generator

DSP –Digital Signal Processor

Chapter 1

1.0 Wind Energy

Wind Energy is becoming a sizeable contributor to the ever-expanding energy market. Given the impact on the environment from the use of fossil fuels, there is even a bigger interest in alternative energy sources today [1]. Wind energy is proven as a viable source of clean energy. Over the past decade, there had been numerous advances in the design, control, fault tolerance, and power distribution associated with Wind Energy Conversion systems (WECS).

According to American Wind Energy Association (AWEA), 48,611 MW of wind power capacity was installed in the U.S as of first quarter 2012. This represents 20% of world's installed wind power capacity. The U.S wind industry has added over 35% of all new generating wind power capacity in the last 5 years. U.S is also well suited for wind energy penetration. There is a massive demand for electrical energy as well as an abundance of wind resources. The wind potential is one of the best in the world. It is estimated that the wind capacity is in the range of 37 trillion kilowatt hours of electricity annually. This is 10 times the existing power requirements of the country.

The U.S Department of Energy and National Renewable Energy Laboratory has studied the scenario of 20% wind energy by 2030. It also contrast not adding any new wind power capacity by 2030. To meet this goal, wind power capacity would have to be increased to 16,000 MW per year by 2018, and grow at this rate until 2030. It also assumes that the prevailing technology is sufficient to meet this demand. The net result of this study is that U.S energy production would be diversified and wind electricity

would stabilize the energy markets from volatile price swings. This also would greatly reduce the dependence of foreign energy sources.

Currently the following states in the U.S. lead in wind energy production. Texas 10,085 MW, Iowa 3,675 MW, California 3,177 MW, Minnesota 2,192 MW and Washington 2,104 MW. Offshore wind is a new opportunity for US. The first offshore wind farm was established off the coat of Denmark. It is estimated by the National Renewable Energy Laboratory (NREL) that the estimated offshore capacity is 4 times the country's current generating capacity from all sources. Other countries in the world have taken lead in increasing the off shore wind capacity. Europe is planning to have 40,000 MW of wind power by 2015 and China is planning 30,000 MW of installed capacity by 2015.

1.1 Environmental Impact

Wind energy produces zero emissions in generating power from the wind. Electricity generation in the U.S. is one of the largest sources of air pollution. It is estimated that 40% of Co2 emissions are generated by power generation facilities. The AWEA has suggested that if a 20% of total energy is generated by wind energy by 2030, it would reduce Co2 emissions by 825 million metric tons. This is a real benefit to reducing greenhouse gasses that are directly linked to increasing global warming.

1.2 Wind Generators.

We have been harnessing the power of wind for many years. Wind mills have been used to pump water and grind grain. The first modern wind turbine was built in 1957. Gedser wind turbine was 200 kW wind turbine with horizontal axis and three blades connected to a three phase AC grid [26] . Many different concepts and technology have been tested since. During 1970's, due to oil crises, the small wind turbines (22 kW) were built using inexpensive parts for house hold applications.

In the last three decades, wind turbine rating has increased from 20 kW to 5 MW. The new concepts such as pitch control and variable speed control methods have been developed and introduced to the wind industry. Since 1993, wind turbine manufacturers have changed the generator from the AC induction generator to the synchronous generator and induction generator with wounded rotor. The new machines have better capability of handling power in the wind turbine systems [26].

The progression of power electronics both in switches with better power handling capability and cost/kW encourages the manufacturers to employ sophisticated power electronic equipment. In fact, power electronics is the basis for most new developments in wind turbines [26].

Figure 1.1 shows the configuration of a simple wind turbine. A wind turbine simply consists of blades, a generator, a power electronic converter, and power grid. Sometimes, wind turbine work in islanding mode; therefore, there is no grid. Usually, there are two or three blades on a wind turbine. There were some wind turbines with more than three

blades. But based on aerodynamics, three blades is the optimum number of blades for a wind turbine [27].

Asynchronous and synchronous AC machines are the main generators that are used in the wind turbines. Based on the generator, the form of the connections of the machine to the grid and the drive method of the generator, there are numerous wind turbine configurations. Besides that, manufacturers may use their own configuration to overcome the high price of the equipment, design constraints and other regulations.

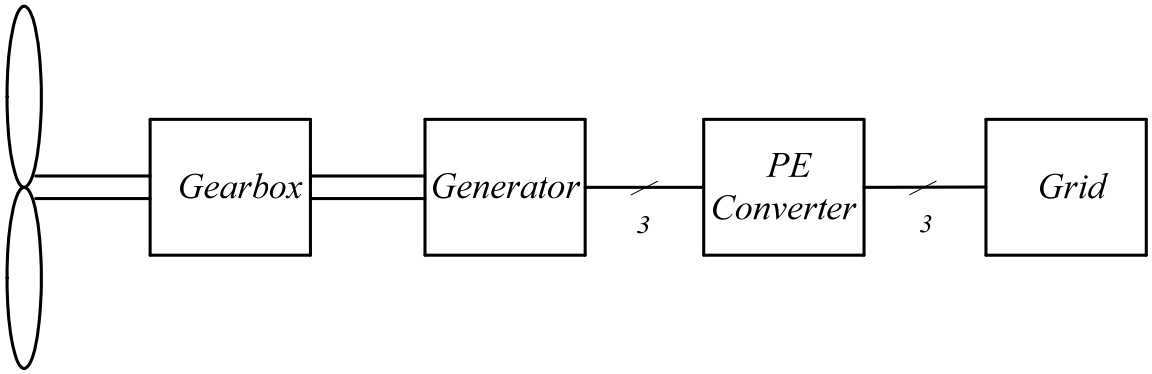

Figure 1. 1 The configuration of a typical wind turbine.

Figure 1.2 shows several configurations of the wind turbines. Type A uses the AC induction generator. There is also a gearbox to drive the generator. This type is the most common wind turbine in the wind farms. Type B is called the Doubly Fed Induction Generator (DFIG) wind turbine. The wounded induction generator is used. A power electronic converter is used to feed the rotor windings of the generator. The generator is driven by a gearbox. Type C uses Permanent Magnet Synchronous Generator (PMSG). If a gearbox is not used, it is called direct driven wind turbine. A full range power

converter is used to connect the generator to the grid. Table 1.1 compares these configuration in different aspects [26].

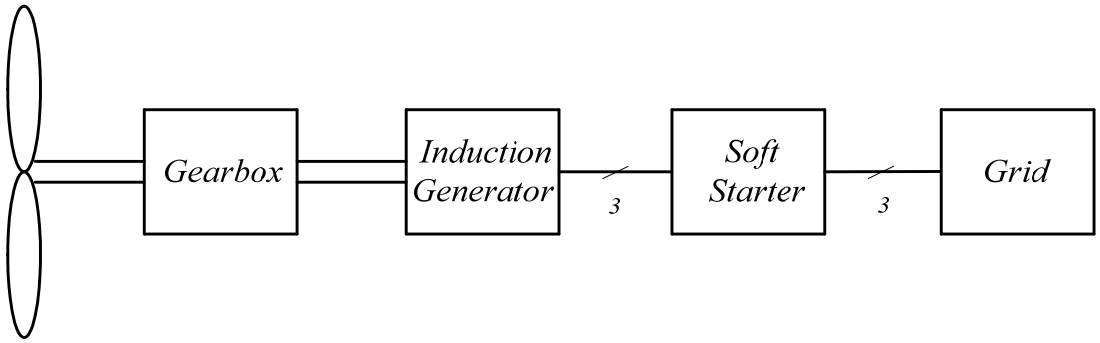

Type A

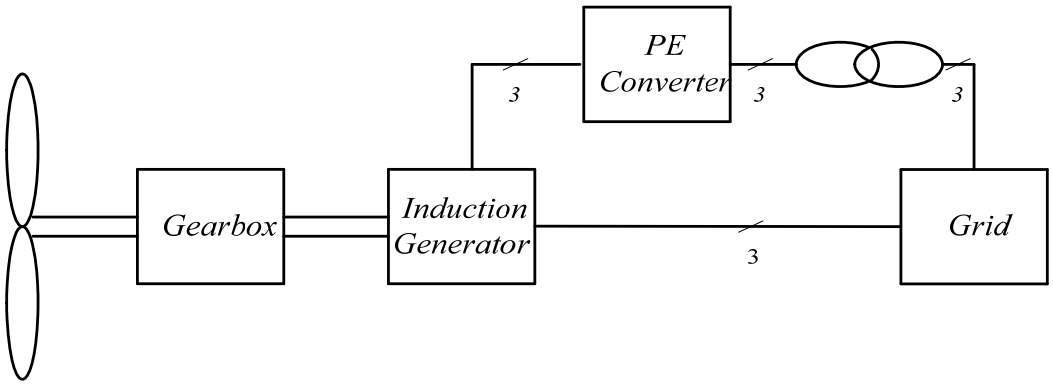

Type B

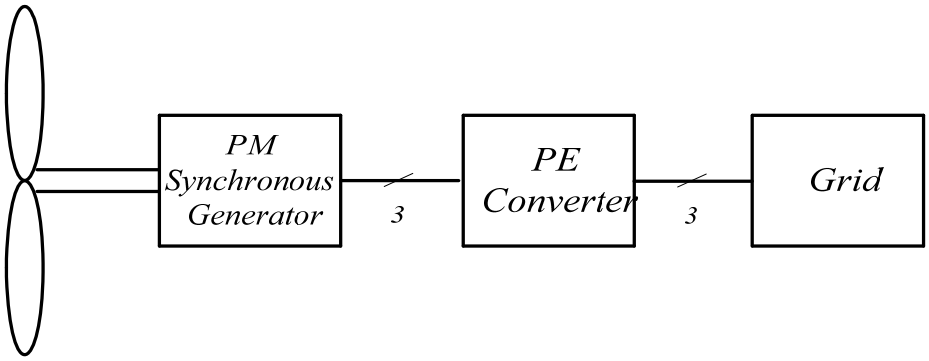

Type C

Figure 1.2 Different configurations of wind turbines with different generators.

Table 1.1. Comparison of different types of wind turbine.

Configuration	PE converter	Drive	Operation
A	Soft starter	Gearbox	Fixed speed
B	Back-to-back converter	Gearbox	Variable speed
C	Back-to-back converter	Direct	Variable speed

1.3 Power Electronics

As the advanced technology invents high current and voltage power switches, application of the Power Electronic (PE) converter increases in the industry. Power electronic equipment is an attractive means to improve the performance of wind turbines. Many types of power converters are used in the wind industry. The power converter must be capable of connecting an AC source that is variable voltage and frequency to a fixed voltage and frequency.

The soft starter is a type of power converter that is used with induction machines in fixed speed wind turbines. It reduces the transient current during the startup period of a wind turbine. Figure 1.3 shows a soft starter for one phase. When the speed of the generator is more than the synchronous speed, the soft starter connects the generator to the grid

smoothly, using the firing angle of the thyristors. When the generator is fully connected, the thyristors will be bypassed by a bypass switch.

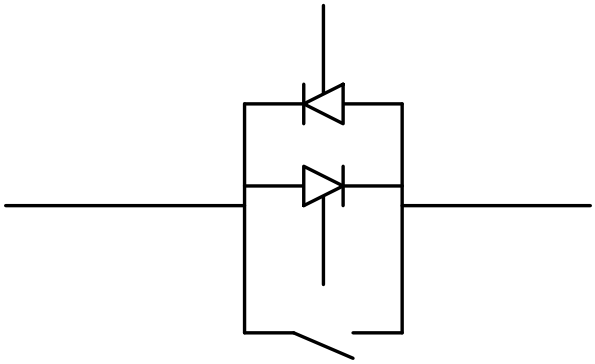

Figure 1.3 A single phase circuitry of a soft starter.

A Back-to-Back Converter (BBC) is another type of power electronic converter that is used in the wind industry. Figure 1.4 shows a back to back converter circuitry. It consists of a PWM rectifier and a PWM inverter. Therefore, the AC input voltage of the generator is first rectified and then converts into AC using the inverter. A BBC is a very powerful PE converter and is capable of controlling active and reactive power. Therefore, it is used in a variable speed wind turbine. The rectifier sometimes is called generator side converter and the inverter is called grid side converter.

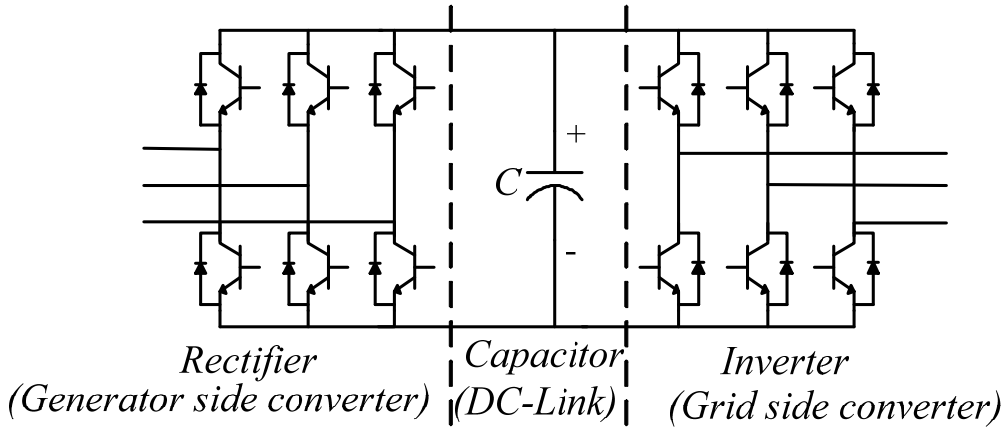

Figure 1.4 The circuitry of a back to back converter.

Besides the PE converters that are mentioned above, there are other PE converters that can be used such as Matrix converters, capacitor banks, Tandem converters, Multi-level converters, etc. [43].

1.4 Statement of thesis subject

- The electrical power generated by the wind generator are alternating current (AC).
- AWind farm power distribution is 3-phase AC. An offshore wind farm or a wind farm located far from the energy consumers would have to distribute the power generated using a 3-phase grid connection.
- There are inherent stability issues with AC power distribution. AC distribution does not offer an easy integration of energy storage.
- The power transfer capacity of AC lines is limited.
- Wind generators have to implement complicated, costly, and inefficient back- to -back converters to implement AC generation.

1.5 Proposed solution

- The wind turbine output power is in DC form after SCR-based rectification.
- Wind farm power distribution is HVDC/MVDC . An offshore wind farm or a wind farm located far from the energy consumers would distribute the power generated using DC grid connection.
- DC power distribution is inherently more stable.
- Wind generators convert AC to HVDC directly without a back-to-back converter.
- DC grid offers an easy integration of energy storage.

1.6 Configuration of the proposed solution

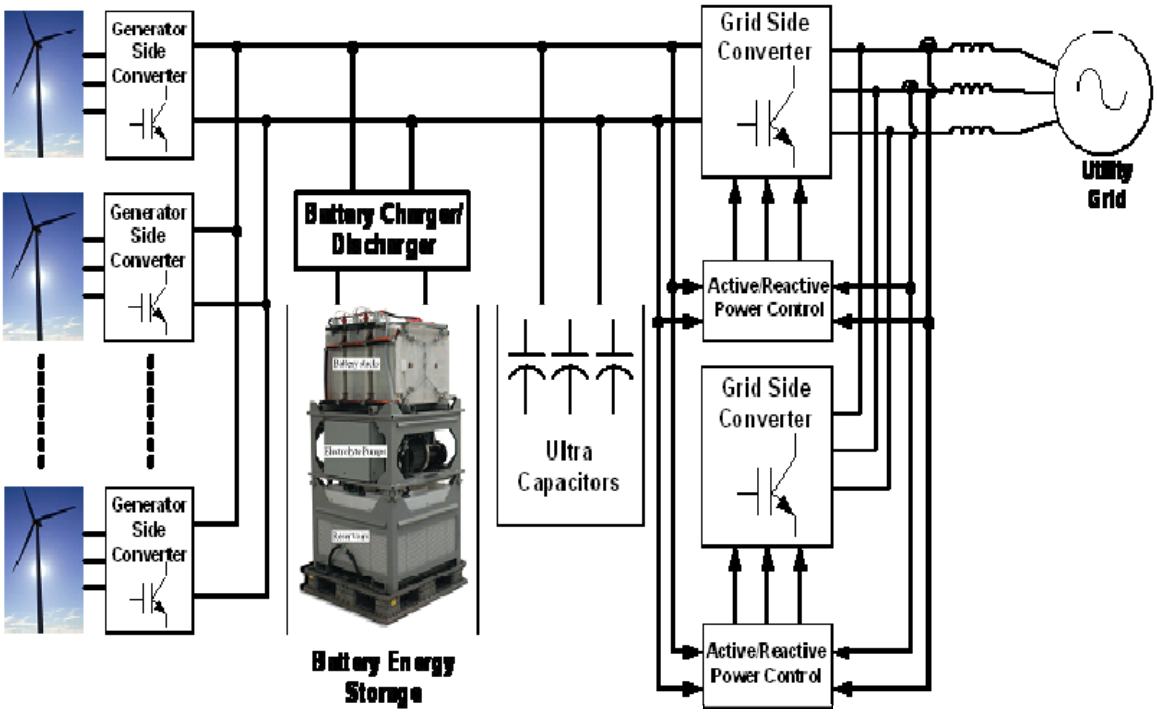

Figure 1.5 Architecture of the proposed wind energy conversion system.

The proposed solution is to convert the AC voltage generated by the wind generators to HVDC. A common HVDC bus would be used to distribute this power to the grid via inverters. DC storage can be easily integrated to the HVDC bus. This will allow the stabilization and smoothing of grid voltage. The nacelle of the wind generator is made lighter by bringing the power converter and associated circuitry to the base of the tower. This would allow easy access for maintenance. The proposed solution is fully simulated and a hardware setup is built to verify this proposed system and control.

1.7 Prior art

The current technology related to wind generators and use of HVDC as distribution in literature is limited to all generators having a back-to-back converter or the conversion of AC power to DC using a voltage source converter. The AC power is then converted to HVDC for distribution. In [6] a line commutated HVDC bus is introduced. Also the optimal condition for DC power distribution is discussed, but generators still used produce AC power and not DC. In the paper [16] the controls of a DFIG system connected to a HVDC are discussed. STATCOM is used to support the generator side grid. In [17] Voltage source converters are used per generator to convert AC to DC. HVDC light is used as the distribution method. In[18] Current Source Inverters are ganged together to produce HVDC.

1.8 Thesis organization

The thesis is organized in to the following chapters:

- Introduction on wind energy and need for DC wind farms.
- HVDC systems.
- System architecture and modeling.
- Estimation of Alpha, HVDC Currents and PMSG voltage.
- System Implementation and control.
- Maximum Power point tracking.
- Paralleling of wind generators.
- DC Power inversion to Grid.

Chapter 2

2.0 HVDC/MVDC SYSTEMS

Note: High Voltage Direct Current (HVDC) or Medium Voltage Direct Current(MVDC) will be referred as HVDC in this chapter.

HVDC systems have been in existence since the early 1930's with the advent of mercury arc rectifiers. Today HVDC technology is considered mature, and is used for transmission of bulk power. The transmission and distribution of electrical energy started with direct current. The first know transmission link was built in Germany in 1882. It was capable of transmitting at 2kV for 50 km. One issue faced was the conversion of DC voltage levels to lower consumer levels. This was accomplished by using rotating DC machines. On the other hand, AC voltage conversion was easily accomplished by using a transformer. This was a simple low cost device. AC three-phase generation using synchronous generators is far more superior to DC generation. These reasons led to the early adaptation of AC distribution.

However, high voltage AC generations has many disadvantages.[28]

- Transmission capacity is limited by inductive and capacitive elements of the overhead lines and cables and the distance power can be transmitted.
- Charging currents limit the distance of transmission from 40 to 100 km.
- Connecting two different AC systems with different frequencies is not possible.

HVDC Transmission advantages.

- DC link allows transmission of power between different AC networks.
- DC conductor is fully utilized. There is no skin effect.
- Transmission distance is not limited by inductive and capacitive elements in the cable.
- For power distribution of 40 km and above, the only solution is HVDC. The charging currents of AC cable limits the distance the power can be distributed.
- For wind generation the DC link eliminates the flicker due to wind turbulence and tower shadow.
- DC cables need less space and can carry more power than AC cables.

2.2 HVDC Sytem.

The HVDC transmission system consist of a AC to DC converter, HVDC Line and DC to AC inverter. Figure 2.1 gives this representation [28].

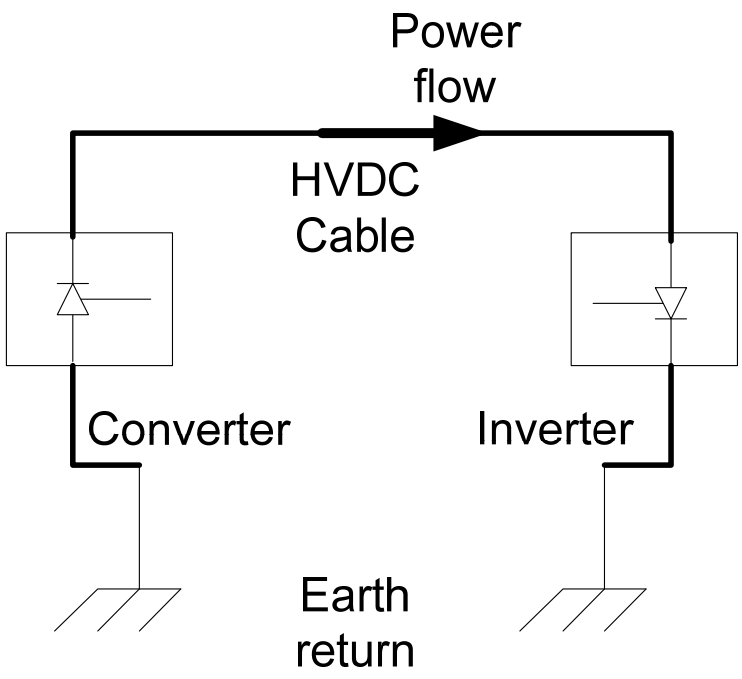

Figure 2.1 HVDC System.

The power flow or the current flow is only in one direction. The power will flow from the converter to the inverter. This is accomplished by controlling the voltage at the converter. There are two main converter topologies that are used today to the converter 3 phase AC to DC [13].

- Current source converter (CSC)
- Voltage source converter (VSC)

2.3 Current source converter

Current source converters use SCR as a fundamental switching device. In the early days, mercury arc valves were used. A current source converter converts a constant voltage source in to a current source. Figure 2.2 shows the overview of such a system [13].

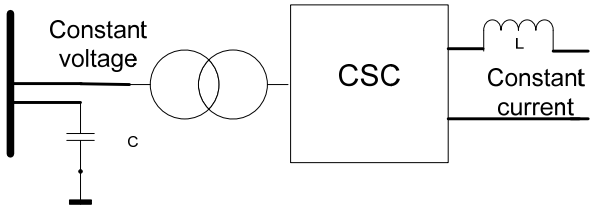

Figure 2.2 Current Source Converter.

The building block for a CSC is 6 SCR connected to a 3-phase balanced AC system as following in figure 2.3.

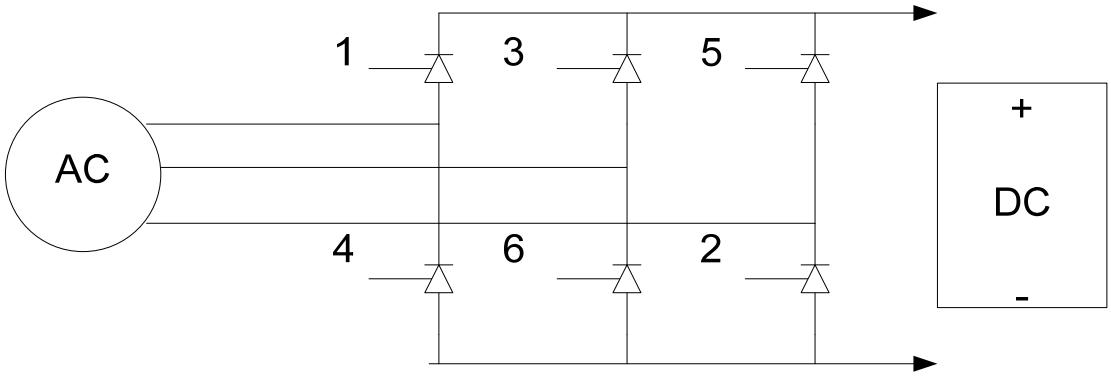

Figure 2.3 CSC with 6 SCR and firing order.

Due to the inductance, the 6-bridge SCR would overlap. At any given time two or three valves can overlap. It can be shown that the converter DC voltage that is rectified is equal to 1.35 VLL where the VLL is the line-to-line voltage of the 3-phase system. The SCR are line commutating. Therefore, only the turn on angle in relationship to the forward biasing voltage can be adjusted to change the output DC voltage.

2.4 Voltage source converter

A voltage source converter uses a IGBT or GTO as switching devices. These devices can be forced commutated as shown in figure 2.4 [12].

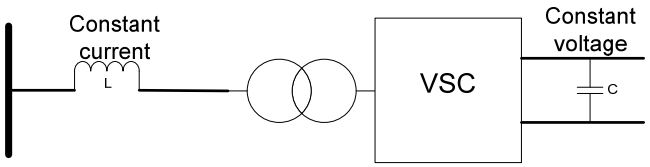

Figure 2.4 Voltage Source Converter.

This allows the switch to be turned on-off anywhere in the cycle. Therefore, these devices are PWM at a higher frequency than the line frequency of the system.

The VSC convert can operate in four quadrants. Either rectifier/inverter with leading or lagging power factor. This is given in figure 2.5.

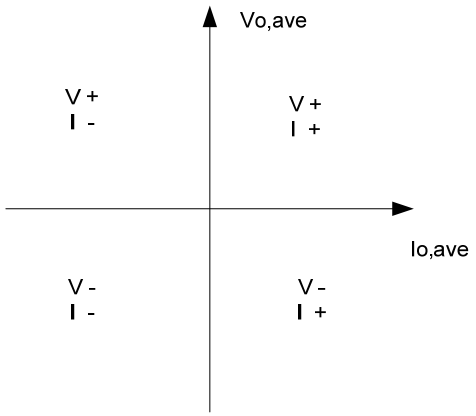

Figure 2.5 VSC Four quadrant operation.

We can compare the advantages and disadvantages of the two topologies. These are given in the table below.

Table 2.1 Comparison of the two converter topologies [13]

	Converter type	
	CSC	VSC
AC Side	Acts like a constant voltage source.	Acts like a constant current source.
	Requires a capacitor as energy storage.	Requires an inductor as its energy storing device.
	Requires filters for harmonic elimination.	requires a small filter for harmonic elimination.
	Requires reactive power supply for power factor correction.	Reactive power supply is not required.
DC side	Acts like a constant current source.	Acts like a constant voltage source.
	Requires an inductor as its energy storage.	Requires capacitor as energy storage.
	Requires DC filters.	Capacitor provides DC filtering.
	Provides inherent fault current limit.	Problamatic for DC line side shorts faults since the charge capacitor will discharge in to fault.
Switches	Line or force commutated with series capacitor.	Self -Commutaed.
	Switching occurs at line frequency	Switching occurs at high frequency.
	Lower switching losses.	Higher switching losses.
Rating	0-500 MW per converter	0-200 MW per Converter.
	Upto 600kV	Upto 100kV

2.5 HVDC Distribution.

HVDC systems can be configured in many ways for distribution.

- Monopole Distribution.

The monopole distribution system uses a single over head or marine cable for DC power distribution. The ground is used as a return path. If the ground cannot be used for a return path a low voltage dedicated metal return path can be used. These two configuration are given in figures 2.6 and figure 2.7[28].

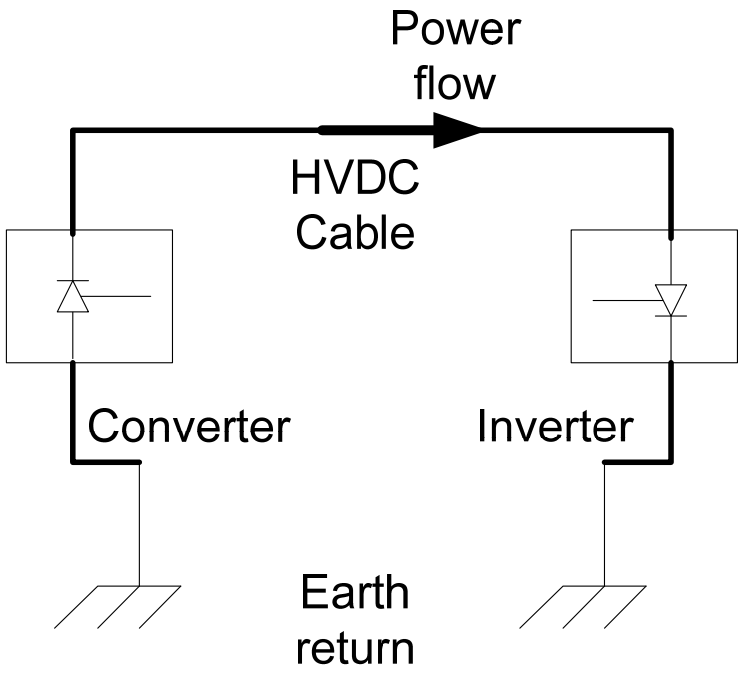

Figure 2.6 Monopole distribution.

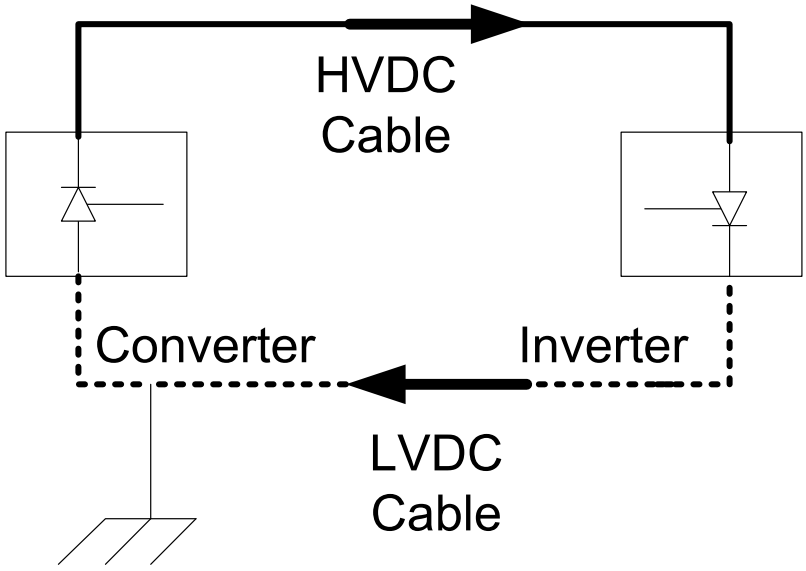

Figure 2.7 Monopole distribution with low voltage return.

- Electrochemical corrosion of long buried metal objects such as pipelines is a concern with this system.
- Underwater earth-return electrodes in seawater may produce chlorine or otherwise affect the water chemistry.
- An unbalanced current path may result in a net magnetic field, which can affect magnetic navigational compasses for ships passing over an underwater cable.
- Modern monopole systems for pure overhead lines carry typically 1,500 MW. If underground or underwater cables are used, the typical value is 600 MW.

- Bipolar Distribution.

The bipolar uses two poles and uses two high voltage lines for power distribution. The main advantage is that you can transmit twice the power compared to a monopole configuration. In this configuration there is negligible current flowing in the ground return path. A dedicated ground return cable can be added to this configuration. These two configurations are given in figure 2.8 and figure 2.9.

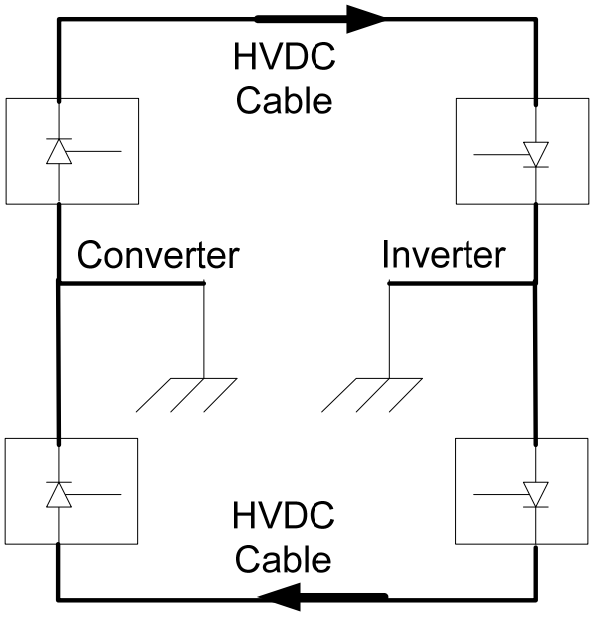

Figure 2.8 Bipolar Distribution.

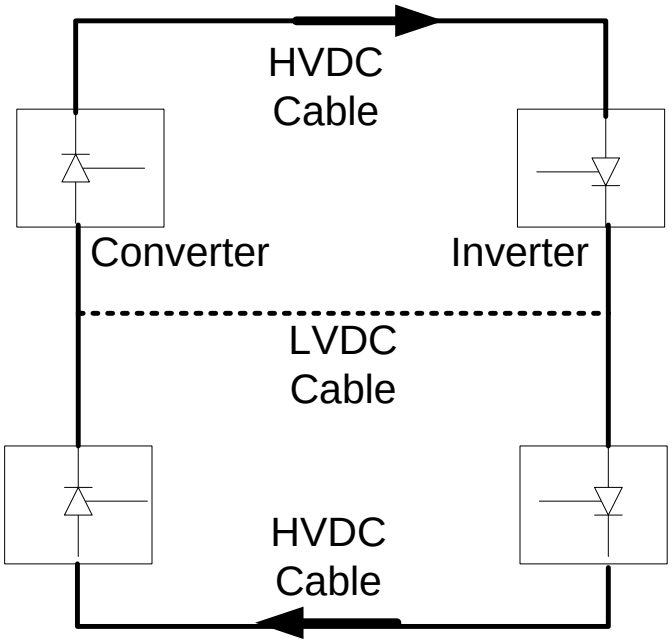

Figure 2.9 Bipolar distribution with dedicated ground return.

Under a normal load, negligible earth-current flows, as in the case of monopolar transmission with a metallic earth-return. This reduces earth return loss and environmental effects.

When a fault develops in a line, with earth return electrodes installed at each end of the line, approximately half of the rated power can continue to flow using the earth as a return path, operating in monopolar mode.

Due to the fact that for a given total power rating, each conductor of a bipolar line carries only half the current of monopolar lines, the cost of the second conductor is reduced compared to a monopolar line of the same rating.

In a very adverse terrain, the second conductor may be carried on an independent set of transmission towers, so that some power may continue to be transmitted, even if one line is damaged.

Bipolar systems may carry as much as 3,200 MW at voltages of +/-600 kV. Submarine cable installations initially commissioned as a monopole may be upgraded with additional cables and operated as a bipole.

- Multi-terminal DC distribution

Multi-terminal DC distribution is considered in urban areas were space is limited. It is similar to AC distribution system. This is a meshed DC system. It is given in figure 2.10. As we can see, we can use a common DC bus to do DC distribution to urban city centers. The power from alternative energy sources like wind and solar can be converted back to AC [13].

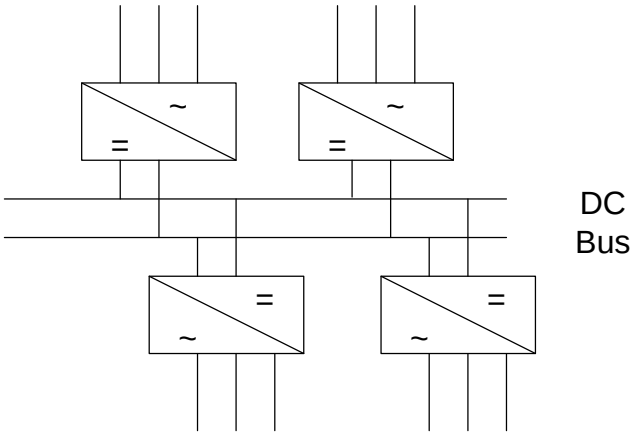

Figure 2.10 Meshed DC systems.

2.4 Bipole fault operation

It is necessary to understand the robustness of the system. Part of that analysis is to understand kinds of faults can be tolerated by the system. In the case of a bipole configured system there can be two types of faults. This is depicted in the following figures 2.11,2.12 [28].

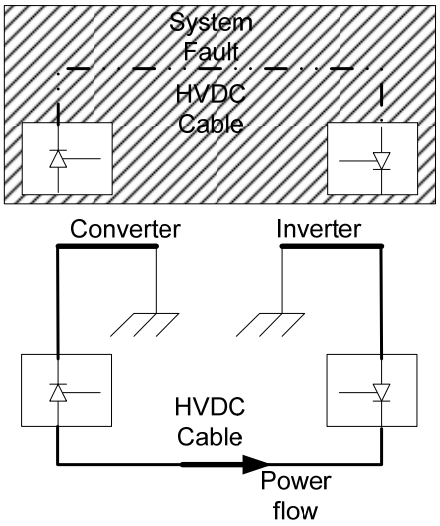

Figure 2.11 Configuration of a HVDC system under overhead line fault.

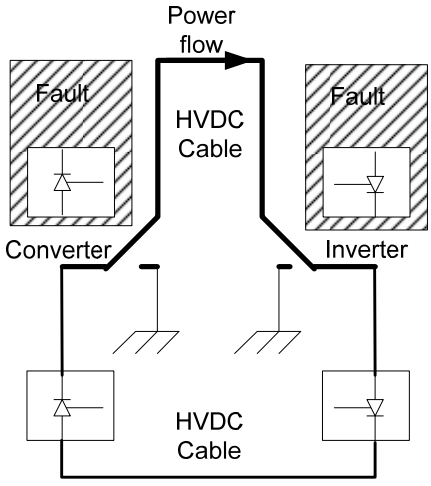

Figure2.12 Configuration of a HVDC system underground return fault.

- Overhead line fault – Transmit in monopole configuration using the ground return.
- Ground return fault- Transmit in monopole configuration using the overhead line as return.

Both modes will transmit 50% of power.

It is important to have redundancy in the system. This is a crucial consideration in building a HVDC system so power can be transmitted from the point of generation to the consumers.

Chapter 3

3. 0 System architecture and modeling

3.1 System architecture

Modern PMSG generators are variable speed generators allowing the generation of power from variable wind. This is possible due to a back-to-back power electronic converter. This allows variable frequency AC to be converted to DC and inverted back to AC synchronized to the grid frequency. The proposed system eliminates the need for a back-to-back converter by using a step-up transformer and 12 pulse thyristor converter which converts AC to DC.

Figure 3.1 shows the configuration of the system. The DC power is fed to a common DC bus for distribution. The power flow to the DC bus is controlled by changing the firing angle of the thyristors. The use of 12 pulse thyristor network reduces the harmonics in the DC bus, thus reducing the size of the filters needed. Since many of these installations are offshore, it is also important to reduce the weight of the nacelle. In the proposed system, the power electronic converter and transformer will be located on the base of the tower allowing easy access for maintenance.

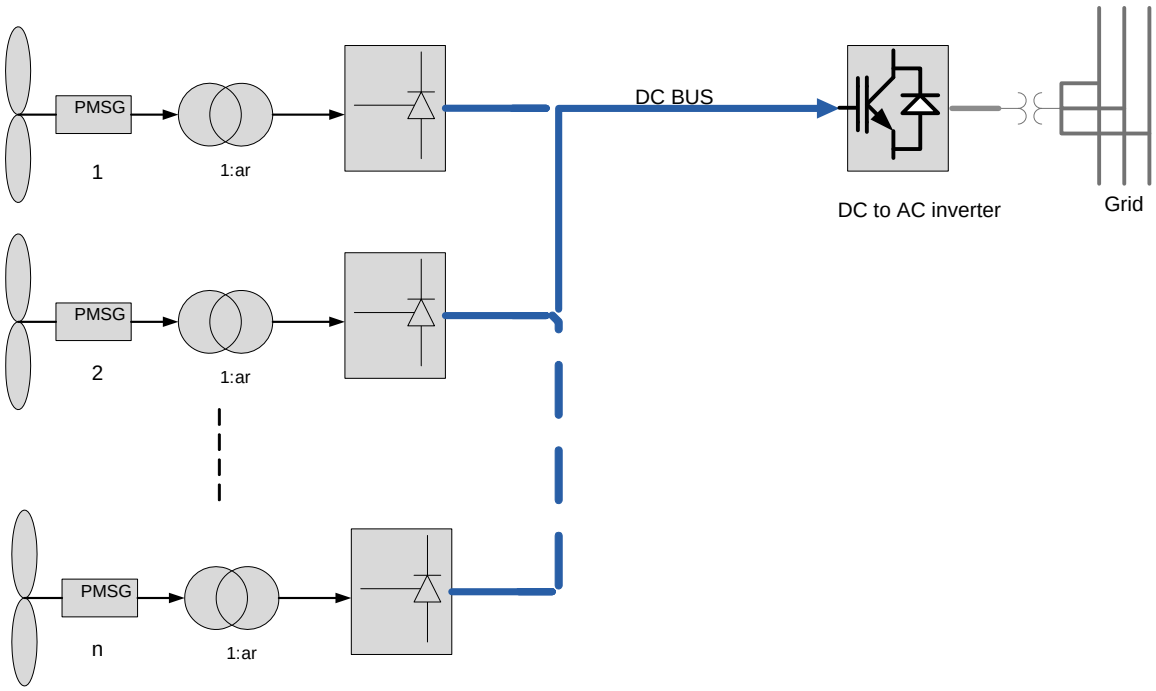

Figure 3.1 System architecture for the proposed DC distribution.

The wind farm would have many generators connected to a common HVDC bus. Each generator would produce variable voltage and current that would be fed to a step-up transformer to increase the voltage to the desired DC link voltage. The proposed architecture is scalable to any number of generators. The DC link voltage would be determined by many factors such as:

- The distance power is transmitted.
- The maximum power generated.
- Whether the wind farm is located offshore or not, in this case, offshore wind farm submarine cables would have to be considered.
- Cost of HVDC cabling.

- Geographical issues related to the conductivity of the earth will affect using earth as a return path for HVDC distribution.
- Power semiconductor ratings.
- Desired voltage for the inverters that will be converting DC to AC power.
- Power characteristics of the step-up transformer.
- DC link storage device ratings.

Once the DC link voltage is determined, the power converter and the transformer can be selected. For each wind generator, the three main components would be the Permanent magnet generator, high voltage step up transformer, and power converter. This is depicted in figure 3.2.

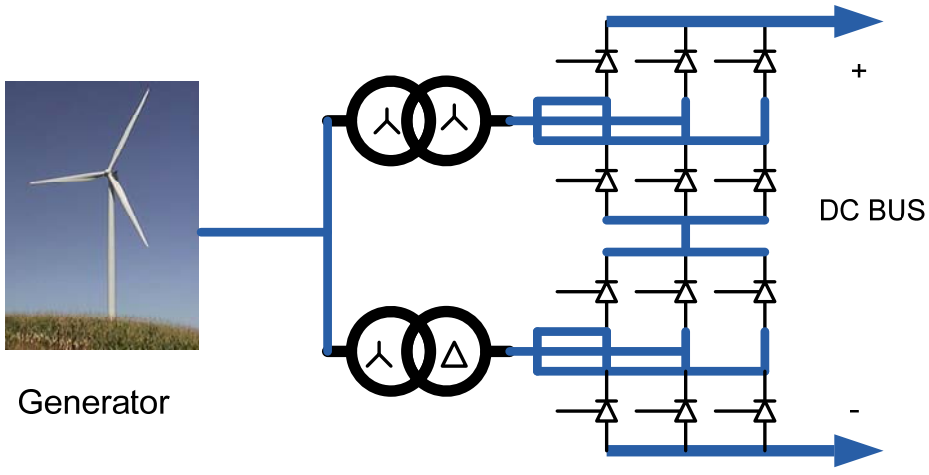

Figure 3.2 PMSG, “STAR-DELTA” transformer and 12-pulse SCR configuration.

3.2 Thyristor Power converter

The power converter for converting variable frequency AC generated by the PMSG will be SCRs (Sillicon Controlled Rectifier). When you compare a SCR to IGBT performance, the current technology is such that the SCR have the following advantages:

- Better cost structure for the same power rating.
- Ability to block voltage vs IGBT inability to block due to inherent body diode.
- Lower power loss.

Given the above advantages, SCR are well suited for the application of converting AC/DC. This is also an industry proven solution for this type of application. In many very high voltage applications, SCR are used in a series to achieve higher blocking capacity. For higher current capability, SCR can be paralled. Current technology offers SCR in the range of 4 kAmpers and 8 kVolt blocking capacities. Some application also use light triggered SCR for isolation from high voltage.

The SCR is a 3 terminal device and is shown in figure 3.3. The SCR has 3 operating modes as following:

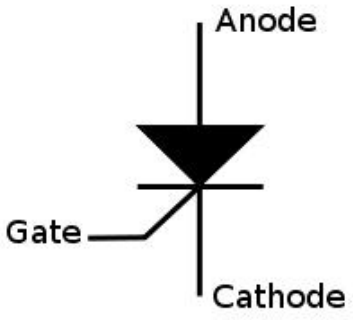

Figure 3.3 Electrical symbol of an SCR.

- Reverse blocking mode- Positive voltage applied to the cathode referenced to anode.
- Forward blocking mode – Positive voltage is applied to anode referenced to cathode, gate has not been triggered.
- Forward conducting mode- The SCR is triggered and is carrying positive voltage and will be in conduction till the current drops below the holding current. (line commutating device)

Since we can control the gate when the SCR is forward biased, we can change the average voltage that the converter sees by changing the angle that is used to trigger the SCR. The time that the Anode of the voltage became positive to the time that the SCR is trigged, is called the "firing angle" [28].

It can be shown that the DC Voltage that is produced for this converter is as following:

$$V_{dc} = 1.35 V_{LL} \cos \alpha \qquad (3.1)$$

Where V_{LL} is the line to line voltage. We can see that by changing α we can change the output voltage. When $\alpha = 0^0$, the SCR bridge works as 6 –pulse diode bridge. When $\alpha = 90^0$, output voltage is zero. When $\alpha > 90^0$ the voltage is negative. Another angle of interest is γ (extinction angle), which is describes as following:

This is the angle (time) that a thyristor takes to turn off. A reverse voltage must be applied across the device, current through the device becomes negative first and recovers to zero. The γ angle is equal to 180^0- (α+u); where u is the commutation angle.

3. 3 Power converter -12 pulse

To reduce the harmonics on both the AC and the DC side a 12pulse converter is used. The harmonics that are produced are following:

The 3 phase currents in a 6 SCR converter are rectangular in shape and have an amplitude of Id. The currents are also phase shifted by alpha angle. Alpha is the delay angle for the SCR firing.

The currents can be described as following [14]:

$$i_a(\omega t) = \sqrt{2}I_{S1}\sin(\omega t - \alpha) - \sqrt{2}I_{S5}\sin[5(\omega t - \alpha)] - \sqrt{2}I_{S7}\sin[7(\omega t - \alpha)] + \sqrt{2}I_{S11}\sin[11(\omega t - \alpha)] + \sqrt{2}I_{S13}\sin[13(\omega t - \alpha)] \ldots \quad (3.2)$$

Where only the nontriplen odd harmonics “h” are present.

$$h = 6n \pm 1 \quad (n = 1,2, \ldots)$$

The fundamental frequency rms current value is:

$$I_{S1} = 0.78I_d \quad (3.2)$$

$$I_{sh} = \frac{I_{S1}}{h} \quad h = 6n \pm 1 \quad (n = 1,2, \ldots) \quad (3.3)$$

In a 12 pulse system the 5 th and the 7 th components of the currents are removed. This is when a star-star and star-Delta transformers feed each of the 6 pulse SCR configuration

that make up the 12 SCR's. There is an electrical phase shift of 30 degrees between the star and delta transformers. The phase current is given as following:

$$I_a = \frac{2\sqrt{3}}{N\pi} I_d(\cos\theta - \frac{1}{11}\cos 11\theta - \frac{1}{13}\cos 13\theta \ldots) \qquad (3.4)$$

To mitigate the harmonics, two 3-phase systems that are 30^0 electrical degrees apart are used to feed 12 pulse SCR's as the following figure 3.4.

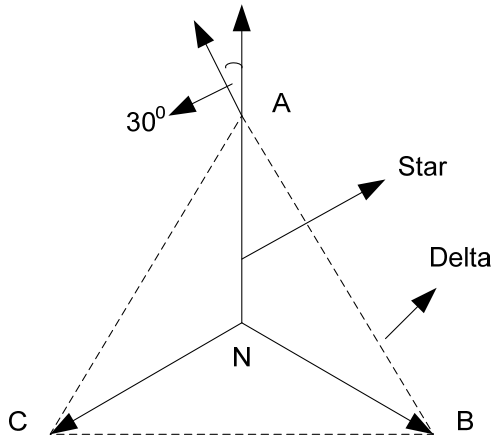

Figure 3.4 30^0 Phase shift between star and delta winding.

3.4 Phase firing of the 12 pulse SCR

Each SCR is forward biased 120^0 in a given cycle. The below figure shows when each of the 12 SCR can be fired. This figure is given for A,B,C rotation of the 3-phase. "Y" is the 6 SCR of the Y connected transformer and "D" is the delta connected transformer. Also shown are the Phase A-B,B-C,C-A Sync signals.

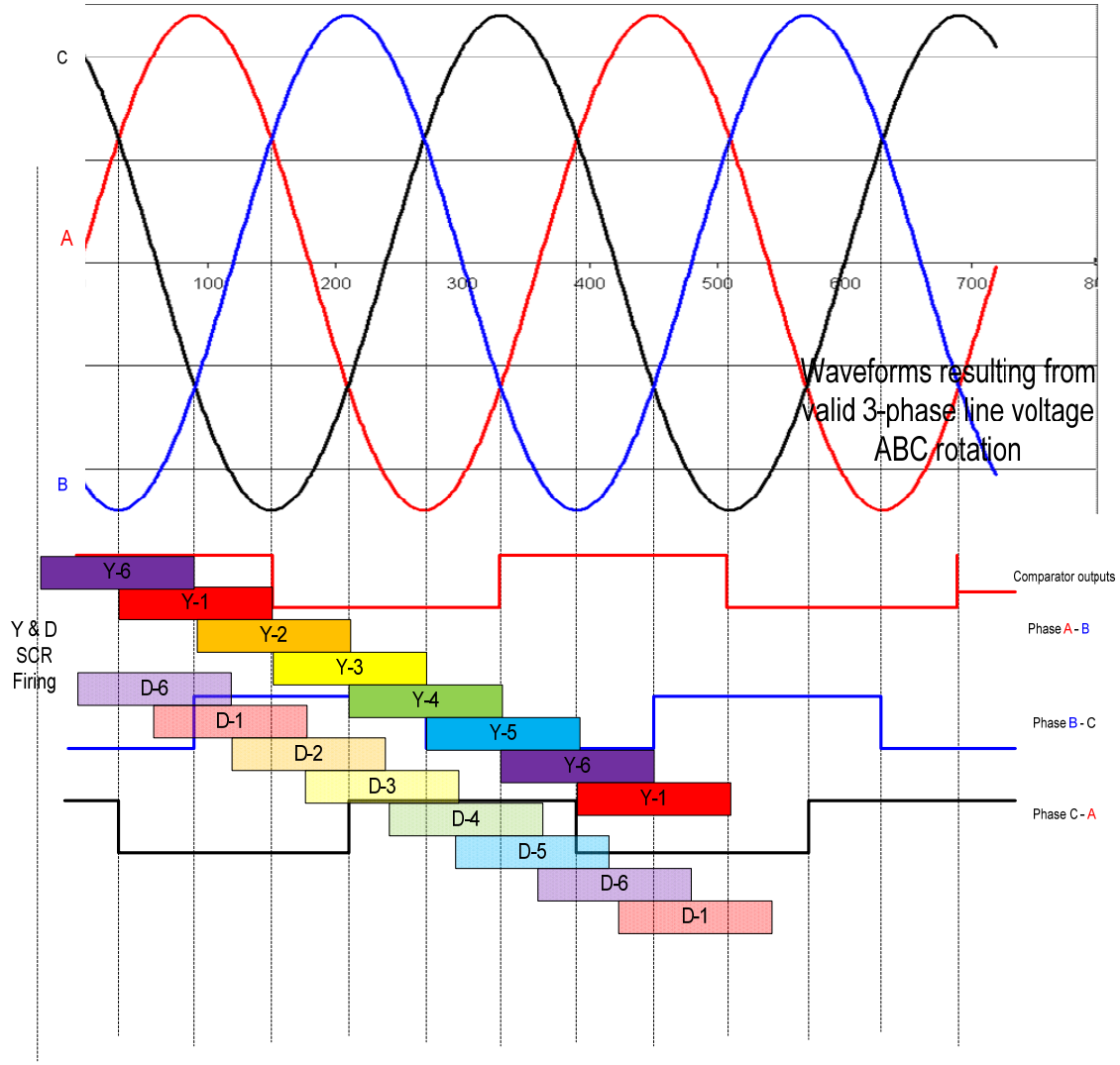

Figure 3.5 Phase firing of SCR's

3.5 HVDC bus power flow

The power flows from the converter to the DC bus, provided the converter voltage is higher than the DC bus voltage. Figure 3.6 shows this system. VR1 and VR2 are the "Star" and "Delta" converters. The DC bus resistance is R. VDC is the bus DC voltage. α is the firing angle of the SCR.

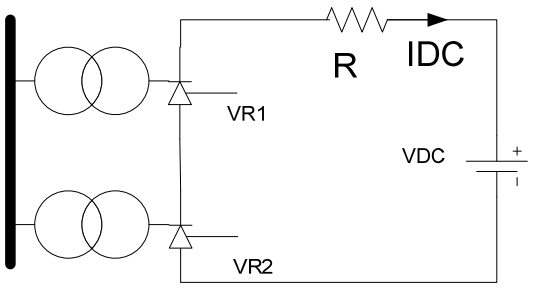

Figure 3.6 Converter power flow for the 12-pulse rectifier.

$$VR1 = \sqrt{3} \times VR2 = 1.35V_{LL}\cos\alpha \qquad (3.5)$$

$$IDC = \frac{(\frac{(1+\sqrt{3})}{\sqrt{3}} \times 1.35V_{LL}\cos\alpha - VDC)}{R} \qquad (3.6)$$

$$IDC = 0; \cos\propto = \frac{VDC}{\frac{(1+\sqrt{3})}{\sqrt{3}} \times 1.35V_{LL}} \qquad (3.7)$$

$$IDCMAX = \frac{(\frac{(1+\sqrt{3})}{\sqrt{3}} \times 1.35V_{LL} - VDC)}{R} \qquad (3.8)$$

Where $VLL = n \times VPMSG.\ n = Turns\ ratio\ of\ trasnformer$

It can be seen that the range of α is limited to 0 to α at (IDC=0). This is also the range that the power can be controlled over MPPT.

This assumes that the voltage source has no impedance. If impedance is present the VR1 and VR2 voltages will be reduced by $\frac{3\times\omega\times LINE}{\pi}$, where the "LINE" is inductance of the line impedance.

3.3 Step up transformer

The two 3 –phase systems are obtained by two step-up transformers that are wound "star-star" and "star-delta". The primaries of each transformer is connected to the PMSG 3-phase output. This enables it to increase the PMSG output voltage to the desired HVDC bus, as well as achieve 30^0 degrees of electrical phase shift to mitigate some of the harmonics of the converter.

3.4 DFIG

The proposed system is only valid for PMSG since this type of generator, and the field for excitation of the stator windings are provided by the Permanent magnets. DFIG type generators need grid connection to provide the field unless an inverter is used to provide necessary voltage/current to setup this field as seen in figure 3.7 below:

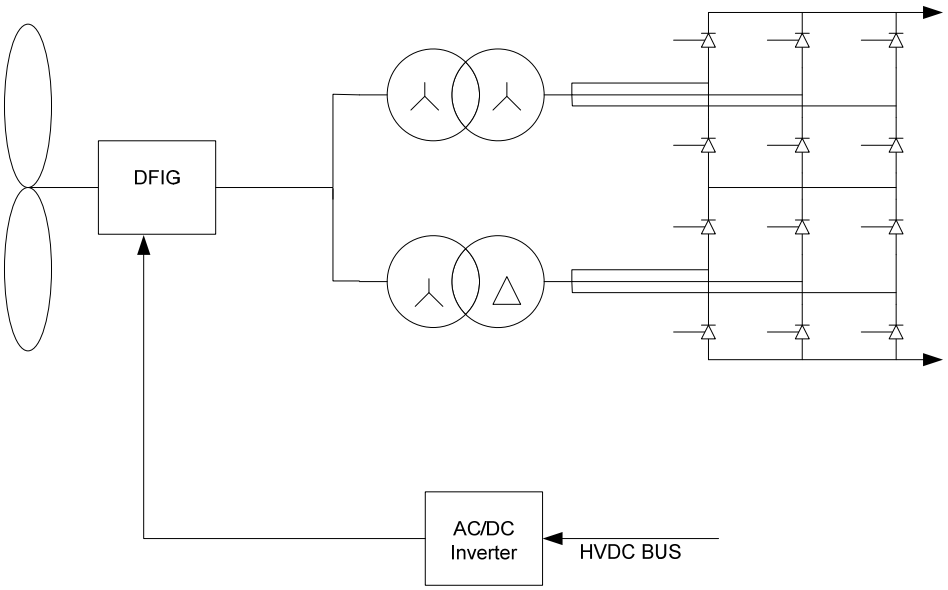

Figure 3.7 Proposed SCR-based rectifier for DFIG wind turbine.

The work will be limited to using PMSG type generators. It should also be mentioned that a direct drive PMSG can be used in this system[42,43].

3.4 Modeling

The proposed system was fully modeled in MATLAB® and Simulink®. Figure 3.8 represents this system.

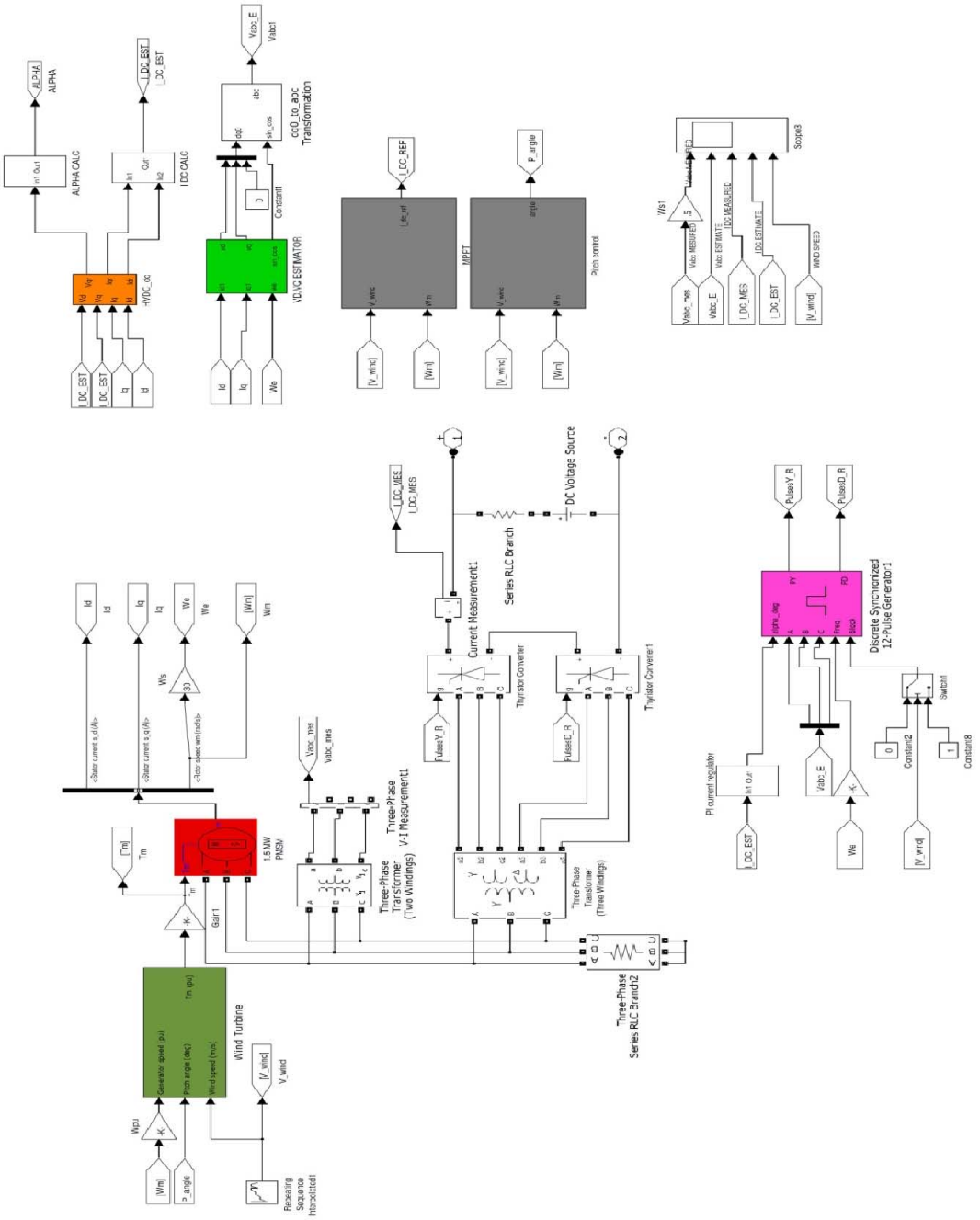

Figure 3.8 Complete configuration of the system in Simulink® environment.

3.5 Wind Turbine model

The model that is used for the wind turbine is based on following turbine characteristics:

Table 3.1 Turbine Parameters.

		1500 KW RATING	REMARK
Rated shaft power	kW	1670	
Rated electrical power	kW	1562	
Rated shaft torque	kNm	862	
Rated voltage	V	3000	rms, fundermental
Rated current	A	325	rms, fundermental
Power factor		0.93	Inductive,underexcited
Rated frequency	Hz	9.5	
Rated speed	rpm	19	
Pole number		60	
Load angle	deg	33	
Rs	ohm	0.225	(20ºc)
Xds	PU	56%	Unsaturated
Xqs	PU	46%	

The Matlab wind turbine model is given in figure 3.9. The inputs to this block are generator speed (PU), pitch angle of the blade and wind speed. The output is the mechanical torque that is generated (PU).

Figure 3.9 Simulink® Wind turbine model.

Other parameters for the generator are as following:

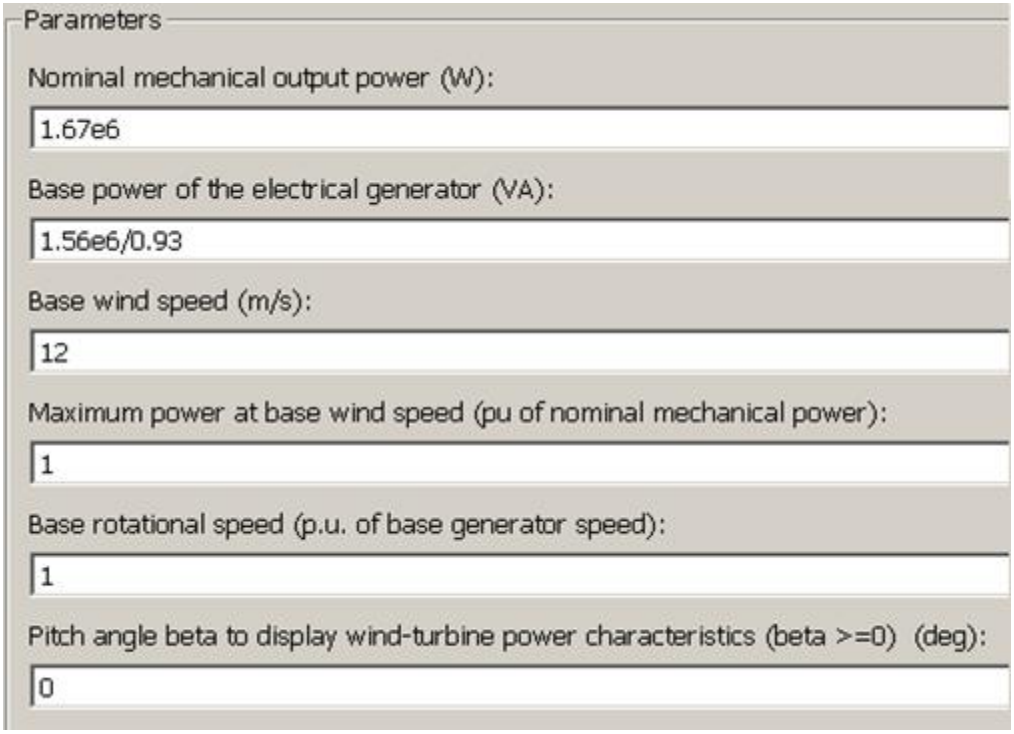

Figure 3.10 Simulink® Wind turbine model parameters.

The base wind speed for this turbine is set at 12 m/s. The turbine characteristics and output power characteristics are given as following:

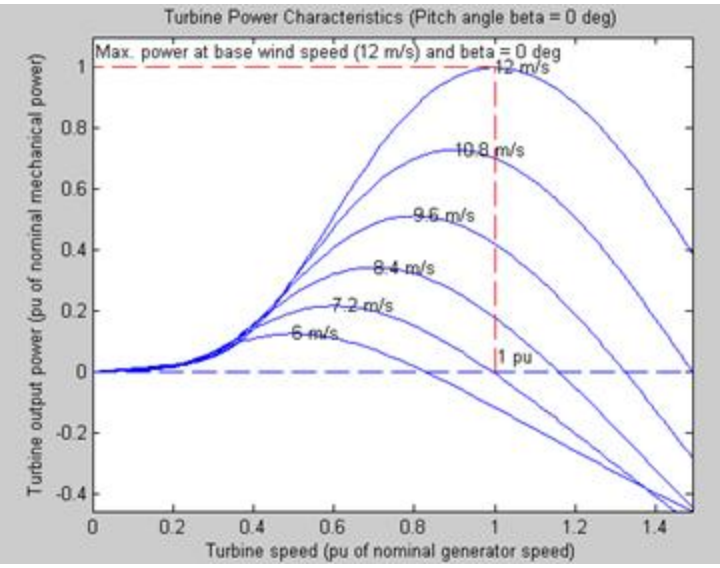

Figure 3.11 Turbine Power Characteristics (MATLAB®/ Simulink®).

3.6 PMSG Model

The PMSG is modeled as a 1.5 Megawatt generator. The input is the mechanical motor torque and the output is 3 phase current/voltage.

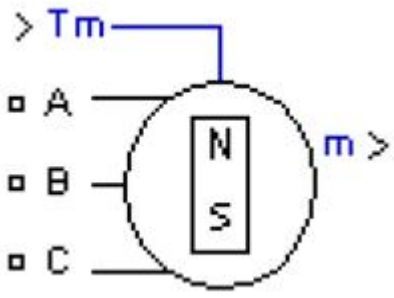

Figure 3.12 MATLAB®/ Simulink® PMSG model.

The following motor parameters are established for this generator.

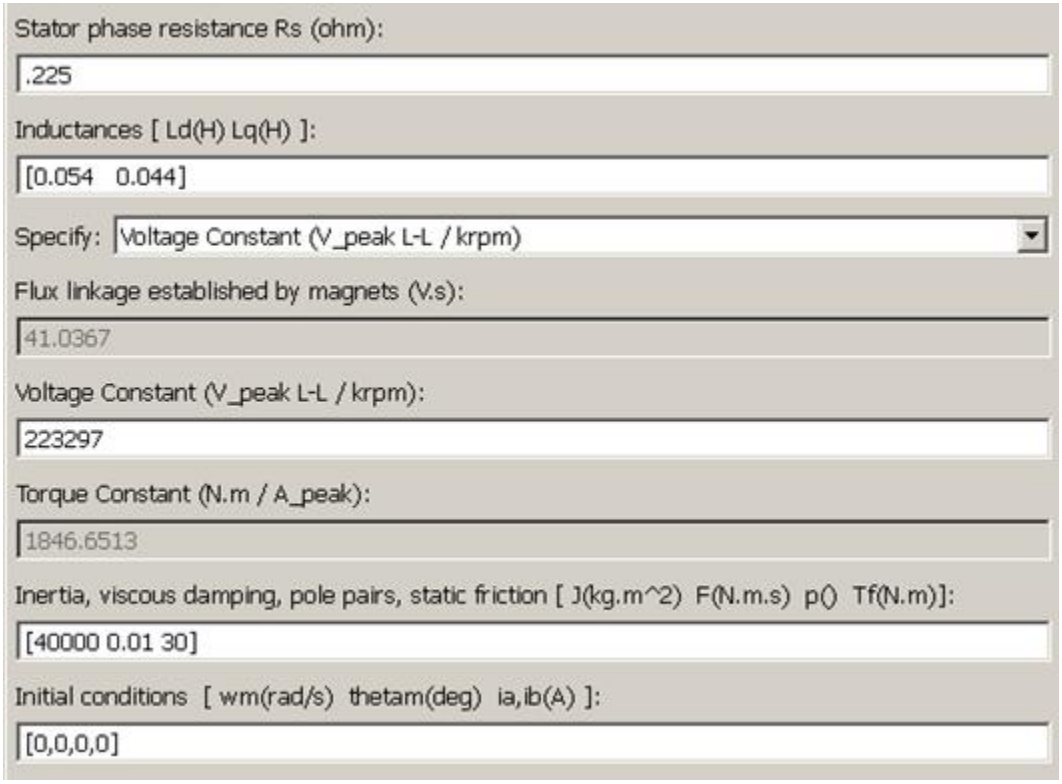

The generator is also setup as a salient-pole generator with sinusoidal back emf. Simulation uses the following signals:

- Stator current (is_d)
- Stator current (is_q)
- Rotor speed wm (rad/s)

The stator currents is_d, is_q is used as the inputs to the estimators. Rotor speed is used to generate the electrical rotation speed by multiplying by pole pairs .

$$\omega_m = \frac{2}{p}\omega_e \qquad (3.9)$$

The rotor speed is fed to the wind turbine generator model as pu speed calculated as following:

$$Generator\ p.u\ speed = \omega_m \frac{60}{(19*2*\pi)} \qquad (3.10)$$

For a salient round rotor the the d-q inductance is given by:

$$L_d = \frac{\max\ (L\ pase\ to\ phase)}{2} \qquad (3.11)$$

$$L_q = \frac{\min(L\ pase\ to\ phase)}{2} \qquad (3.12)$$

3.7 V_d,V_q estimator

Estimator inputs are is_d, is_q and ωe. The output is is Vd and Vq and the sin and cosine of the electrical rotational angle. This estimator provides the estimation of the d-q axis voltages of the PMSG.

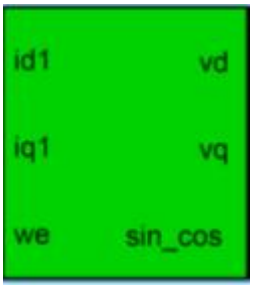

The results of this estimator is scope plots. These are provided in figure 3.13.

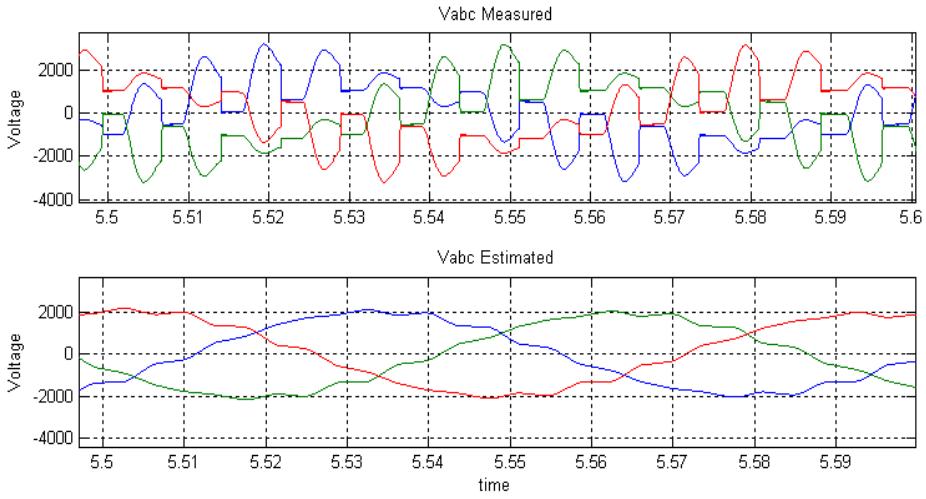

Figure 3.13 PMSG measured and estimated voltage.

The estimated voltage does not have switching noises riding on the voltage wave forms and acts as an ideal filter. The 3-phase voltage is used to determine the zero cross point to calculate the firing angle of the SCRs. If there is noise, the detection of the zero-crossing point is not accurate and could cause erratic firing of the SCR's.

3.8 HVDC Vdr,Vqr estimator

Estimator estimates the current and voltage of the SCR converter. Estimator inputs are Vd,Vq,Id and Iq. Output is the Vqr,Idr and Iqr. Converter output also allows the calculation of HVDC bus voltage and current as well as the firing angle α of the SCRs. Estimator is given in figure 3.14.

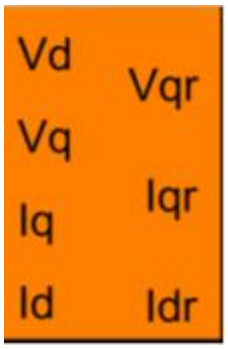

Figure 3.14 HVDC Vdr,Vqr estimator.

3.9 Step up transformer

The step up transformer has a single 3-phase primary and two 3–phase secondaries. The primary winding is in a star configuration as well as the first secondary winding. The second secondary is in a delta configuration and lagging the star secondary.

3 – phase voltage and current from the PMSG is directly fed to this transformer.

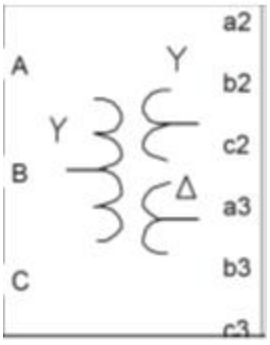

Figure 3.15 Star-Delta transformer.

Following are the parameters of the transformer. The turns ratio is 3/5

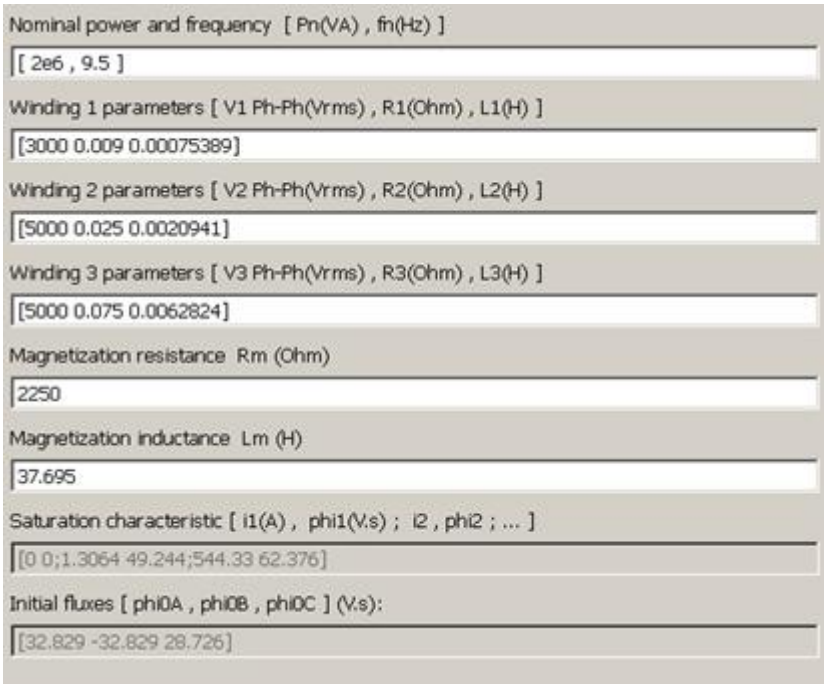

Figure 3.16 Transformer parameters.

3.10 SCR converter

The simulation uses 6-SCR bridges to convert AC to DC and are in series. The star and delta windings of the setup transformer feed these two bridges. Gate pulses are provided in the natural order of commutation, as given in figure 3.17. The output is the converted DC voltage and current.

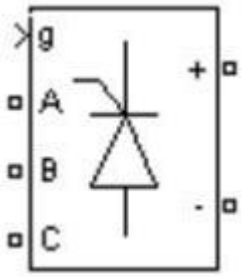

Figure 3.17 MATLAB®/ Simulink® model of an SCR module.

The simulation requires the addition of snubber for avoiding numerical oscillation. The values are selected as following:

Rs > 2 Ts/Cs

Cs < Pn/(1000 2 pi V^2

P_n = nominal power of single or three phase converter (VA)

V_n = nominal line-to-line AC voltage (V_{rms})

f = fundamental frequency (Hz)

T_s = sample time (s)

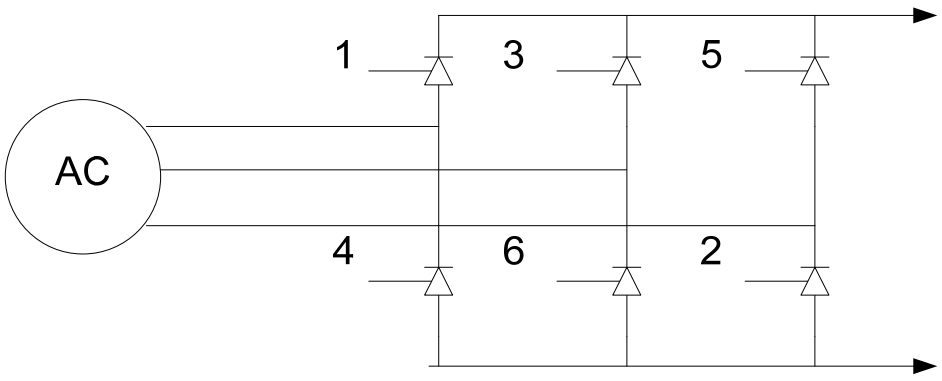

Figure 3.18 SCR firing order.

3.11 PI Current regulator

The feedback control scheme for controlling the power flow is in figure 3.19

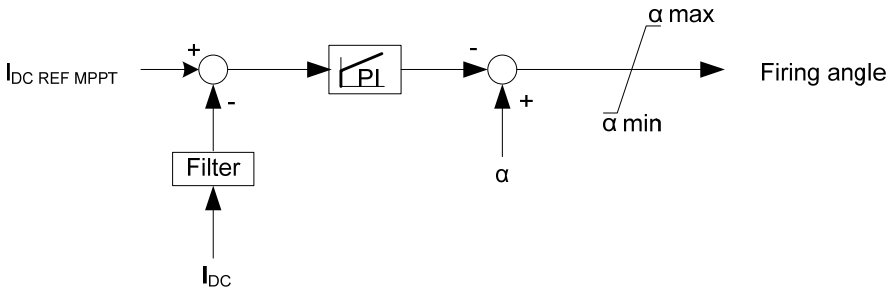

Figure 3.19 current regulator with firing angle modulation.

I_{DC} is the measured or estimated DC bus current, $I_{DC\ REF\ MPPT}$ is the reference current estimated by the MPPT calculation. The calculated angle is α. The output of the regulator is the firing angle for the converter. This angle is fed to the the 12 pulse generating block that generates the 12 SCR firing pulses[41][44].

3.12 SCR Pulse generator

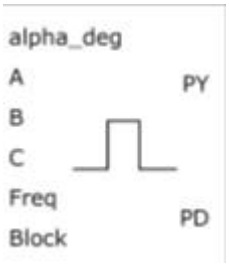

Figure 3.20 SCR firing module.

The pulse generator block generates star and delta (12 pulse) for the SCR's. The input to this block is the ABC 3 phase voltage and frequency of the 3 phase voltage. This block also allows the setting of the leading and lagging for the star and delta windings.

3.13 Simulation results

The proposed system is fully simulated. The figure x shows the result of the alpha estimators and Vqr,Iqr and Idr estimator. The wind speed is changed from 4 m/s to 12. When the speed of the wind is changed we can see the change in the all the values. As the wind speed increases the alpha angle is increases to match the MPPT torque.

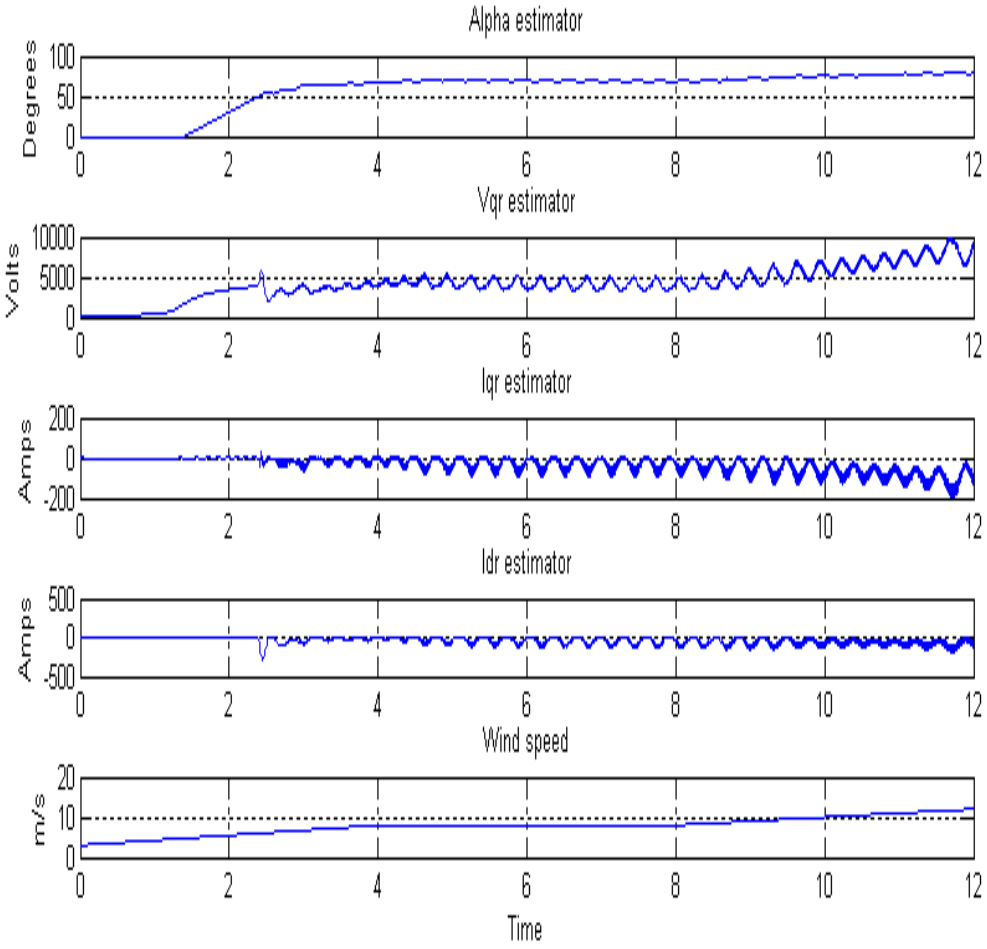

Figure 3.21 Estimated alpha, Estimated Vqr, Estimated Iqr , Estimated Idr and wind speed.

In the second result, the first two plots are the measured and estimated voltage. The second is the measured and estimated current. It is observed that the measured and estimated values closely track each other.

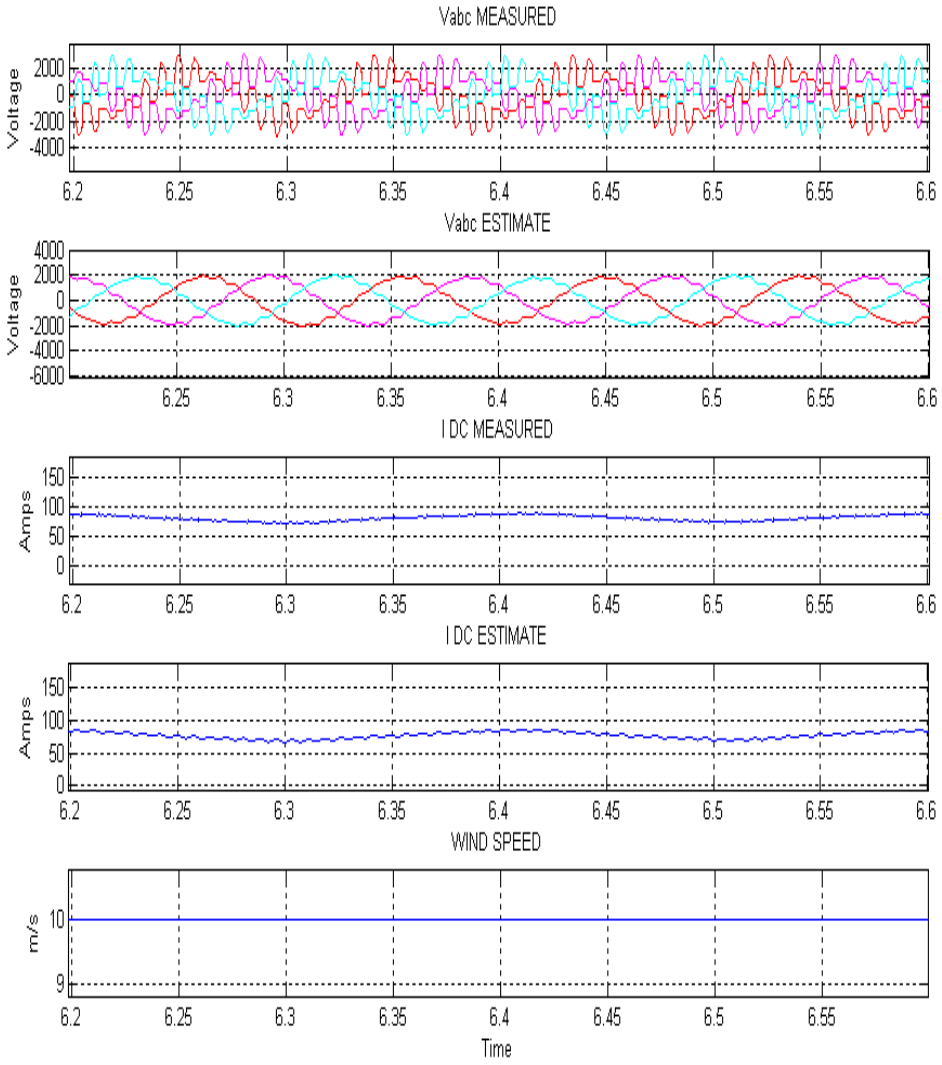

Figure 3.22 Measured Voltage, Estimated voltage, Measured Current, Estimated current and wind speed.

The third result is the estimated Vd and Vq of the PMSG generator. The Vq and Vd values were used to obtain the figure 3-phase estimated voltages by using the Clark transformations. The bottom two plots are the Id and Iq of the PMSG generator that these values were obtained from.

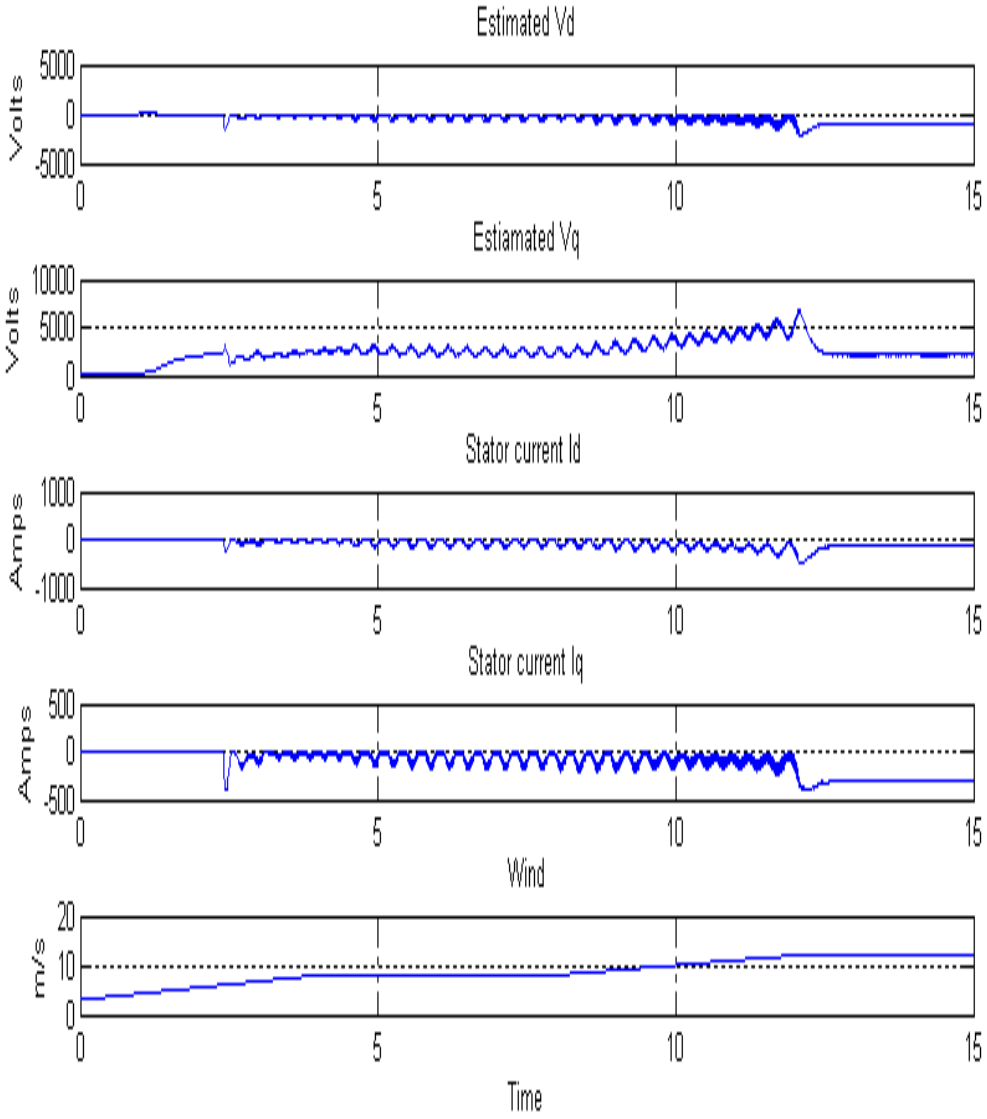

Figure 3.23 PMSG Estimated Vd voltage, Estimated Vq voltage, measured current Id, Iq and wind speed.

The fourth result is the plot of the control loop. The input to the control loop are the DC current of the HVDC bus, estimated alpha angle and the reference DC current generated by the MPPT. The output is the firing angle for the SCR's. This is graphed against the changing wind.

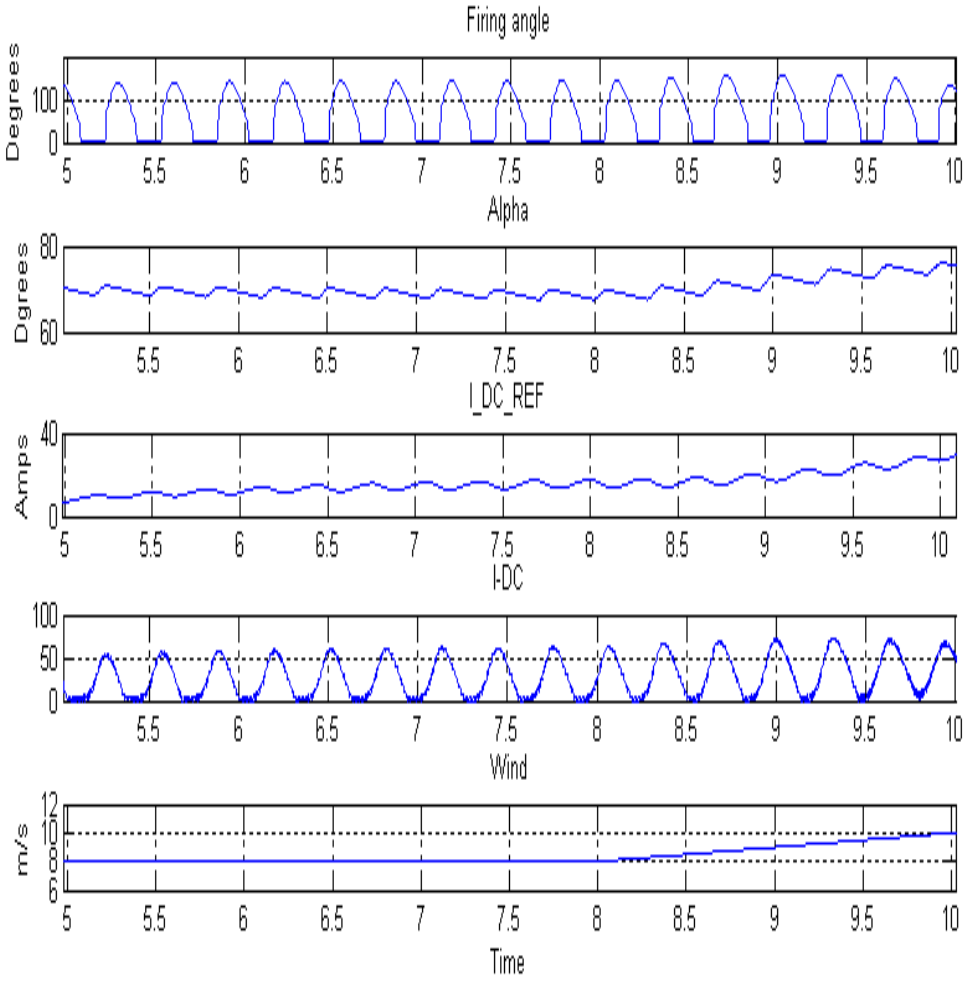

Figure 3.24 Firing angle, Estimated Alpha, Reference DC current, HVDC Current and wind speed.

The fifth result is the line to line voltage of the PMSG and the 3 phase currents feeding a load of 60 ohms. DC current thru the load is given in the last plot.

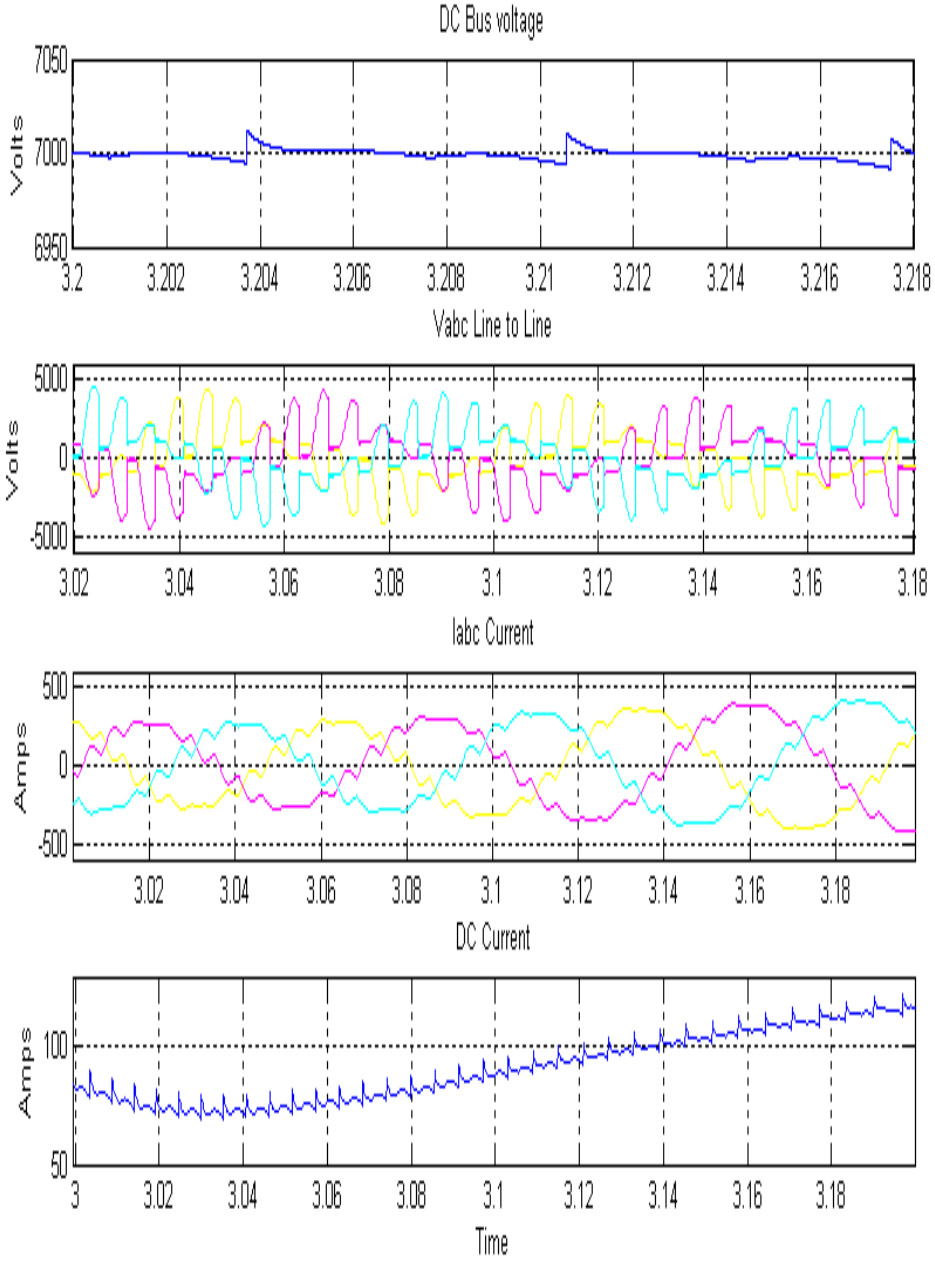

Figure 3.25 DC Bus voltage, 3 phase line to line voltage of PMSG, 3 phase current of PMSG and DC current.

Chapter 4

4.0 Estimation of Alpha, DC current, and AC voltage

4.1 Control system

In this chapter the estimation of the system will be presented. Figure 4.1 represents the control system.

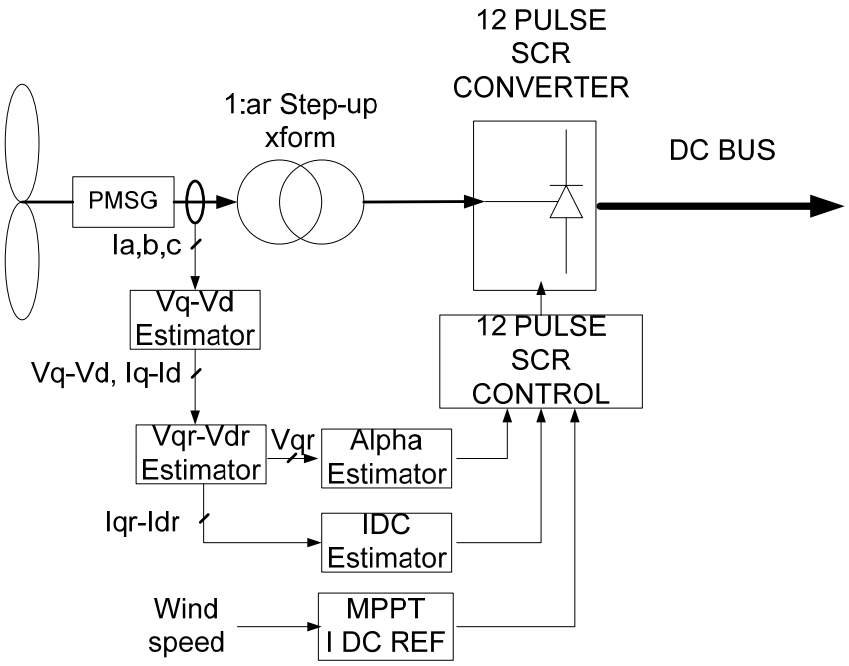

Figure 4.1 PMSG Control system.

The wind generator power flow will be as following; the generated voltage and current will flow via the step up transformer and will be fed to the 12 pulse SCR converter producing the DC voltage. The SCR converter is controlled so the desired power flow is achieved corresponding to the Maximum Power Point tracking (MPPT). To control the SCR's, the voltage, current and frequency of the generator are needed. This information will be obtained in the following manner:

The 3 phase current will be sensed. It was shown from the simulation/measured values that the current is not distorted from the switching of the SCR as much as the voltage waveforms. The 3-phase current will be used to create the estimators need to control the system. The first estimator is the "V_q-V_d estimator".

4.2 V_q - V_d Estimator

This estimator is derived from the PMSG generator model. [2] The 3 phase voltages are given as follows [7]

$$\begin{bmatrix} v_{as} \\ v_{bs} \\ v_{cs} \end{bmatrix} = \begin{bmatrix} -R_s & 0 & 0 \\ 0 & -R_s & 0 \\ 0 & 0 & -R_s \end{bmatrix} \begin{bmatrix} i_{as} \\ i_{as} \\ i_{as} \end{bmatrix} + \frac{d}{dt} \begin{bmatrix} \lambda_{as} \\ \lambda_{bs} \\ \lambda_{cs} \end{bmatrix} \tag{4.1}$$

Where *i* is the 3 phase current generated by the generator, λ is the flux linkage associated with each phase. The flux in each phase can be written as following:

$$\begin{bmatrix} \lambda_{as} \\ \lambda_{bs} \\ \lambda_{cs} \end{bmatrix} = \begin{bmatrix} L_{ls} + L_A - L_B \cos 2\theta_e & -\frac{1}{2}L_A - L_B \cos 2(\theta_e - \frac{\pi}{3}) & -\frac{1}{2}L_A - L_B \cos 2(\theta_e + \frac{\pi}{3}) \\ -\frac{1}{2}L_A - L_B \cos 2(\theta_e - \frac{\pi}{3}) & L_{ls} + L_A - L_B \cos 2(\theta_e - \frac{2\pi}{3}) & -\frac{1}{2}L_A - L_B \cos 2(\theta_e + \pi) \\ -\frac{1}{2}L_A - L_B \cos 2(\theta_e + \frac{\pi}{3}) & -\frac{1}{2}L_A - L_B \cos 2(\theta_e + \pi) & L_{ls} + L_A - L_B \cos(2\theta_e + \frac{2\pi}{3}) \end{bmatrix}$$
$$\begin{bmatrix} -i_{as} \\ -i_{bs} \\ -i_{cs} \end{bmatrix} + \begin{bmatrix} \lambda_m \cos(\theta_e) \\ \lambda_m \cos(\theta_e - \frac{2\pi}{3}) \\ \lambda_m \cos(\theta_e + \frac{2\pi}{3}) \end{bmatrix} \tag{4.2}$$

Where *Lis* is the linkage inductance of the machine and *LA* and *LB* is the mutual inductace. Θc is the electrical angle and λm is the magnitude of the flux.

$$\begin{bmatrix} f_{ds} \\ f_{qs} \\ f_o \end{bmatrix} = \frac{2}{3}\begin{bmatrix} \cos\theta_e & \cos(\theta_e - 120) & \cos(\theta_e + 120) \\ \sin\theta_e & \sin(\theta_e - 120) & \sin(\theta_e + 120) \\ 0.5 & 0.5 & 0.5 \end{bmatrix}\begin{bmatrix} f_a \\ f_b \\ f_c \end{bmatrix} \tag{4.3}$$

$$\begin{bmatrix} v_{qs} \\ v_{ds} \end{bmatrix} = \begin{bmatrix} -R_s & 0 \\ 0 & -R_s \end{bmatrix}\begin{bmatrix} i_{qs} \\ i_{ds} \end{bmatrix} + \begin{bmatrix} \frac{d}{dt} & \omega_e \\ -\omega_e & \frac{d}{dt} \end{bmatrix}\begin{bmatrix} \lambda_{qs} \\ \lambda_{ds} \end{bmatrix} \tag{4.4}$$

Figure 4.2 is the d-q axis of a typical machine. It can be seen from the above derivation that we can convert the equation governing the generator form a,b,c refrence frame to d-q axis given in (4.5) and (4.6)

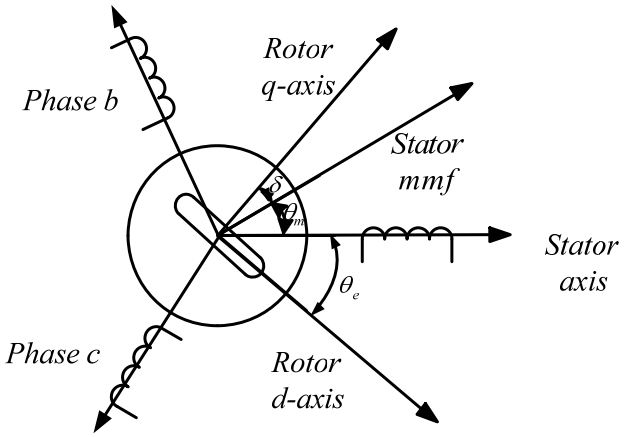

Figure 4.2 d-q axis representation of a PMSG machine.

$$u_{sd} = -R_s i_{sd} - L_{sd} \frac{di_{sd}}{dt} + L_{sq} \omega_e i_{sq} \quad (4.5)$$

$$u_{sq} = -R_s i_{sq} - L_{sq} \frac{di_{sq}}{dt} - L_{sd} \omega_e i_{sd} + \omega_e \Psi \quad (4.6)$$

The above equations allow building an estimator for the voltage if the parameters of the generator are known. Namely Rs, Lsd, Lsq, Ψ and ωe. ωe is the electrical field rotational speed. Θc, the electrical angle is obtained as following:

$$\int \omega_e = \theta_c \quad (4.7)$$

The below diagram describes the PMSG estimator which is developed from the equation (4.5,4.6). Isd and Isq is the stator d-q currents. The output of the estimator is Usd and Usq, and d-q frame voltages for the PMSG. The estimator can be thought of as an ideal filter that gets rid of the switching noise of the converter. The voltage and current is used to estimate the HVDC bus voltage and current using the "V_{qr}-V_{dr} estimator" and is given in figure 4.3

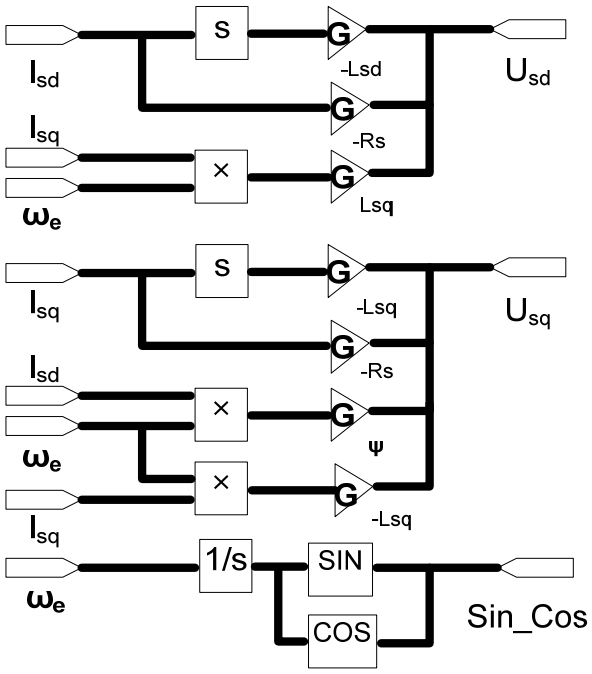

Figure 4.3 V_{qr}-V_{dr} estimator

In the above estimator, transformer inductance and resistance has to be taken in to consideration.

$$L_{sd} = L_d + L_d x \qquad (4.8)$$

$$L_{sq} = L_q + L_q x \qquad (4.9)$$

4.3 Vqr –Vdr Estimator

The 12-pulse SCR converter generates the DC voltage and current. To control this voltage and current, we need to understand the relationship of the converter and the PMSG generator. The PMSG generator described above is referenced to its stator frame or the d-q axis. There need to be a method to extrapolate this reference frame to the HVDC converter. If we create this reference frame, we can describe the PMSG and HVDC as one system. This allows us a way to understand and control the system.

The 3-phase variables voltage or current are referenced to the fixed generator reference frame as: [3-4]

$$f_a = f_q \cos\theta + f_d \sin\theta \qquad (4.10)$$

$$f_b = f_q \cos\left(\theta - \frac{2\pi}{3}\right) + f_d \sin\left(\theta - \frac{2\pi}{3}\right) \qquad (4.11)$$

$$f_c = f_q \cos\left(\theta + \frac{2\pi}{3}\right) + f_d \sin\left(\theta + \frac{2\pi}{3}\right) \qquad (4.12)$$

This assumes that the voltages and currents are balanced. Angular displacement is θ for the d-q reference frame. If we select a second set of orthoganl axis as (d`-q` axis), we can map the 3-phase variable to this new axis as follows:[3-4]

$$f_a = F`_q \cos\beta + F`_d \sin\beta \qquad (4.13)$$

$$f_b = F`_q \cos\left(\beta - \frac{2\pi}{3}\right) + F`_d \sin\left(\beta - \frac{2\pi}{3}\right) \qquad (4.14)$$

$$f_c = F`_q \cos\left(\beta + \frac{2\pi}{3}\right) + F`_d \sin\left(\beta + \frac{2\pi}{3}\right) \qquad (4.15)$$

β is the angular displacement for the new axis. It can be shown that the relationship between two axes as following:

$$F`_q = f_q \cos(\theta - \beta) + f_d \sin(\theta - \beta) \quad (4.16)$$

$$F`_d = -f_q \sin(\theta - \beta) + f_d \cos(\theta - \beta) \quad (4.17)$$

If we make$(\theta - \beta) = \delta_R$, then

$$F`_q = f_q \cos \delta_R + f_d \sin \delta_R \quad (4.18)$$

$$F`_d = -f_q \sin \delta_R + f_d \cos \delta_R \quad (4.19)$$

If we consider the synchronous machine voltage to be Vd, Vq and Id, Iq for the d-q axis reference frame, we can formulate the following equations:[3-4]

$$V_{qr}^{`} = V_q \cos \delta_R + V_d \sin \delta_R \quad (4.20)$$

$$V_{dr}^{`} = -V_q \sin \delta_R + V_d \cos \delta_R \quad (4.21)$$

$$I_{qr}^{`} = I_q \cos \delta_R + I_d \sin \delta_R \quad (4.22)$$

$$I_{dr}^{`} = -I_q \sin \delta_R + I_d \cos \delta_R \quad (4.23)$$

Since these quantities are related to the converter, we denote them with a “r” suffix. We also label the new axis as “dr” and “qr”. The relationship between the d-q and dr-qr axis is represented in figure 4.4. The vector representation allows us to map d-q axis values to dr-qr vectors[3].

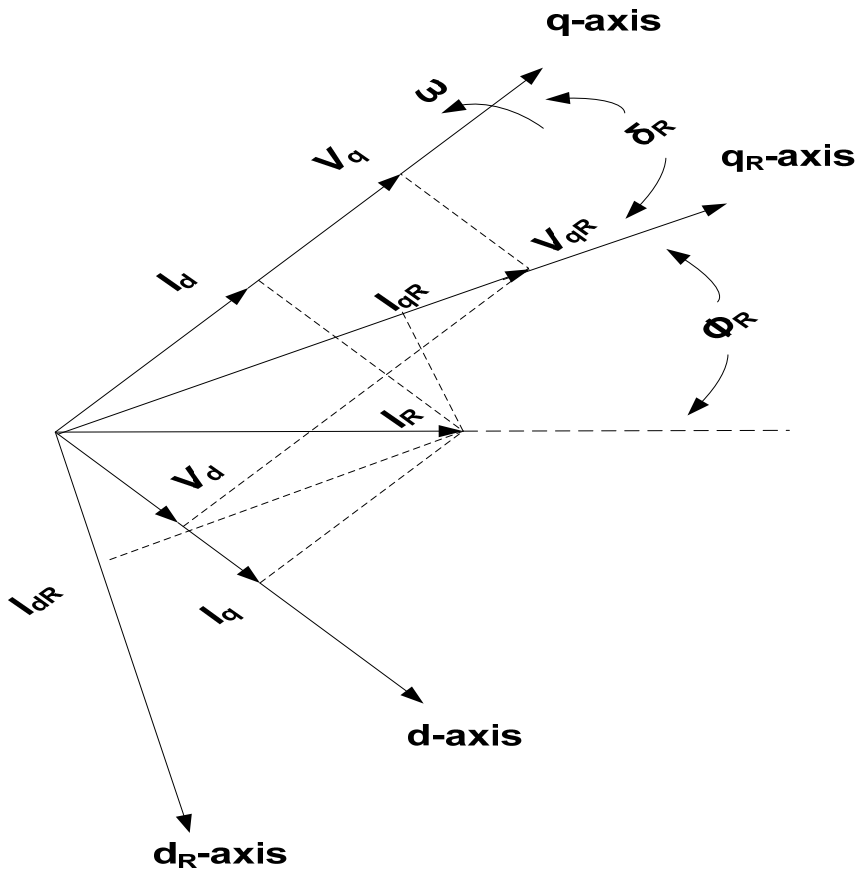

Figure 4.4 d-q and d_r –q_r axis relationship.

Since the choice of δ_R is arbitrary, we can pick this angle to satisfy the following condition for equation 4.24 as following:

$$V_d^{`} = 0 \qquad (4.24)$$

The value of the angle for this condition is:

$$\tan \delta_R = V_d / V_q \qquad (4.25)$$

It should be mentioned that it is not absolutely necessary to restrict to the equation (4.24) for the above mentioned axis, but doing so greatly reduces the complexity of the SCR converter representation. The below figure 4.5 describe the estimator.

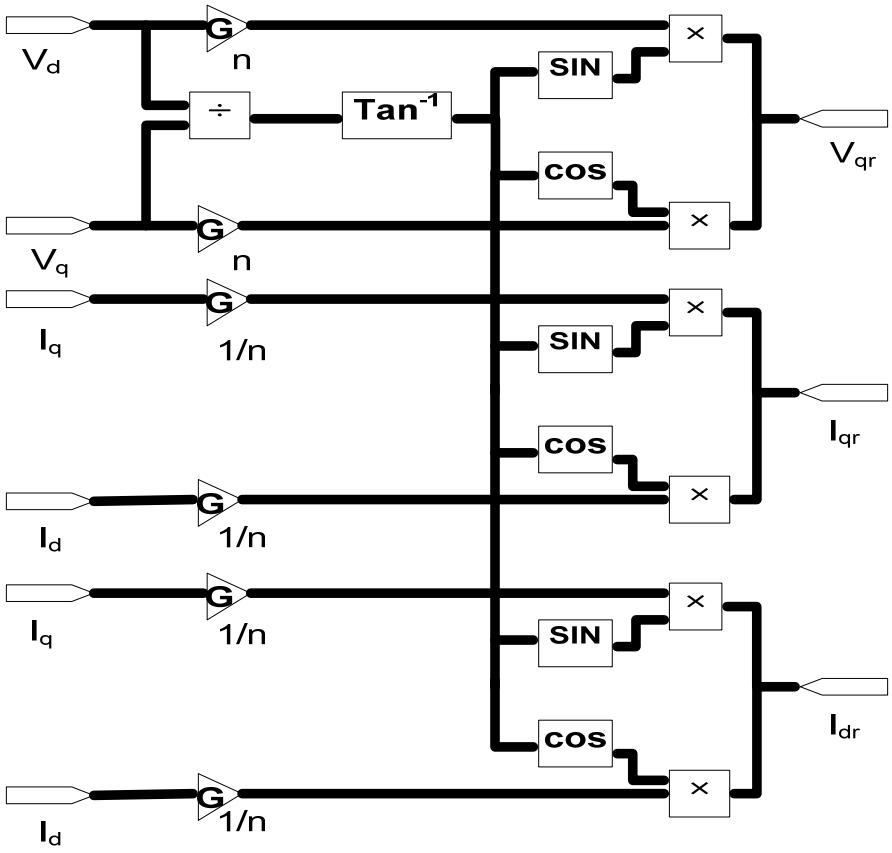

Figure 4.5 Vqr –Vdr Estimator.

The n is the transformer turns ratio.

We can represent the above derivation for the system as given in figure 4.6 below. The left hand quantities to the SCR converter describe the PMSG voltage and current. The

Right hand quantities describe the HVDC bus voltage and currents. The above calculation show the relationship between these quantities

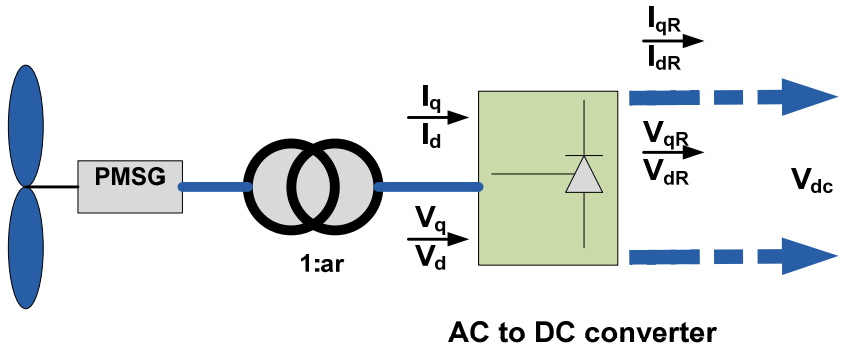

Figure 4.6 d-q and dr-qr representation of the PMSG and SCR converter.

4.4 SCR Converter – 6 pulse

A 6 pulse SCR converter will be analyzed to understand the operation of a 12 pulse SCR converter. Analysis will allow us to represent the converter in the above found reference frame and create an estimator for the voltage and current. [3]

$$Vdc = \frac{3V_q'}{\pi - 3\gamma}\left[\left(\frac{\sqrt{3}}{2} - \frac{3}{2}\sin\gamma + \frac{\sqrt{3}}{2}\cos\gamma\right)\cos\gamma + \left(\frac{3}{2} - \frac{\sqrt{3}}{2}\sin\gamma - \frac{3}{2}\cos\gamma\right)\sin\alpha\right] - 2l_{co}\frac{dI_{dc}}{dx} \quad (4.26)$$

The average output voltage for π/3 is

$$V_{dc} = \frac{3\sqrt{3}V_q'}{2\pi}[\cos\alpha + \cos(\alpha+\gamma)] - \frac{2\pi-\frac{3\gamma}{2}}{\pi} l_{co}\frac{dI_{dc}}{dx} \quad (4.27)$$

In most cases the commutation inductance is very small (less that 1%) and the last term can be ignored. [3]

$$I_{dc} = \frac{\sqrt{3}V_q'}{2\omega l_{co}}[\cos\alpha + \cos(\alpha+\gamma)] \quad (4.28)$$

By substituting in

$$V_{dc} = \frac{3\sqrt{3}V_q'}{\pi}\cos\alpha \quad (4.29)$$

This is neglecting line inductance.

$$\cos\emptyset = \frac{1}{2}[\cos\alpha + \cos(\alpha+\gamma)] \quad (4.30)$$

For the rectifier denote quintiles with R subscript.

$$V_R = \frac{3\sqrt{3}}{\pi}V_{qR}\cos\alpha_R - \frac{3}{\pi}X_{CO}I_R \quad (4.31)$$

$$I_{qR} = \frac{2\sqrt{3}}{\pi}I_R\cos\emptyset_R \quad (4.32)$$

$$I_{qR} = \frac{2\sqrt{3}}{\pi}I_R\sin\emptyset_R \quad (4.33)$$

$$I_R = I_{dc} = \frac{\pi}{4\sqrt{3}}\sqrt{\left(I_{qR}^2 + I_{dR}^2\right)} \quad (4.34)$$

$$V_R = Vdc = \frac{3\sqrt{3}}{\pi}V_{qr}\cos\alpha \quad (4.35)$$

Since we know the Vdc and Vqr from the estimation, the firing angle α can be estimated as following:

$$\cos\alpha = \frac{Vdc}{\frac{3\sqrt{3}}{\pi}V_{qr}} \tag{4.36}$$

Chapter 5

5.0 Experimental test setup

5.1 Lab setup

A lab setup was built to support the simulation results. Figure 5.1 depicts the setup that is used. It consists of two main sections, a Power section, and a Control section.

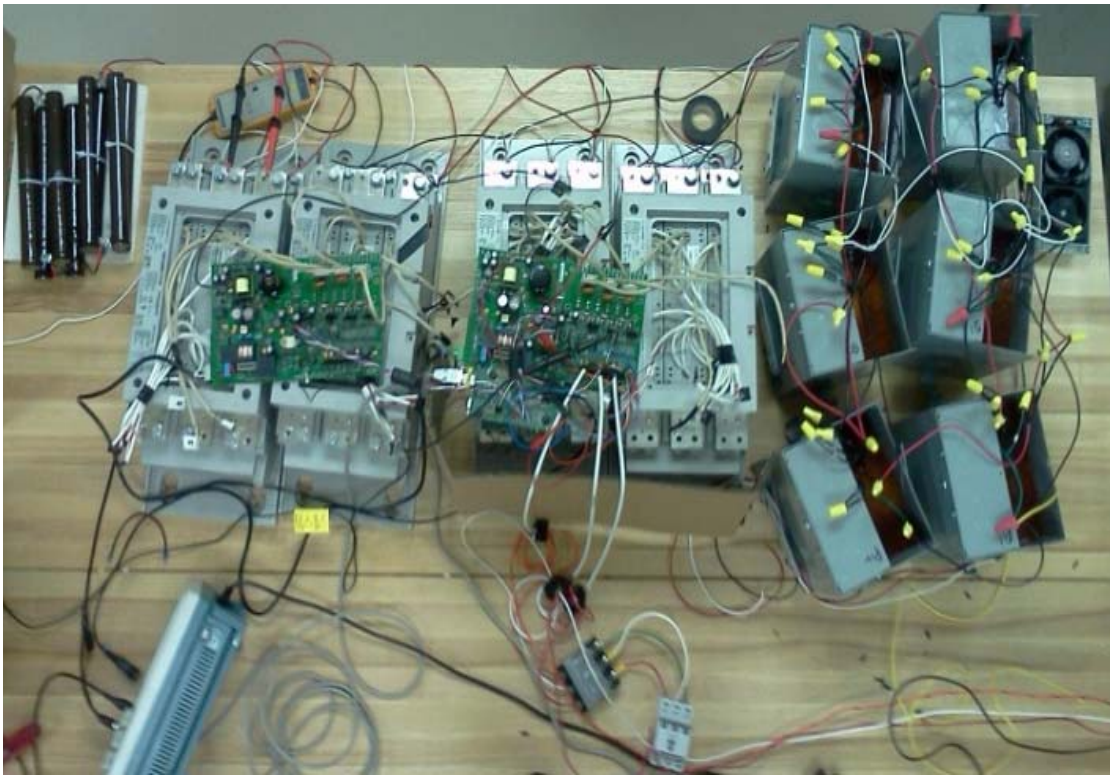

Figure 5.1 A picture of the lab setup showing SCRs, transformers, and control boards.

A block diagram of the setup is given in figure 5.2. This setup is connected to a PMSG generator to obtain the results.

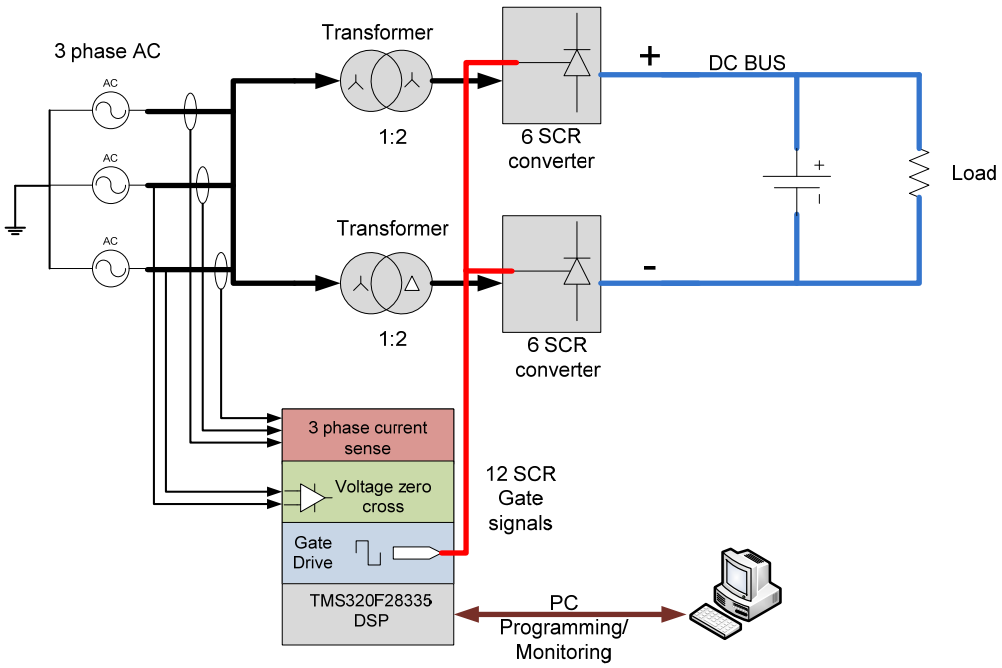

Figure 5.2 Block diagram of the test setup.

5.2 Power Section

The power section consists of the variable speed AC generator, step-up transformer, SCR's and load. The SCR's are connected in the following manner in figure 5.3.

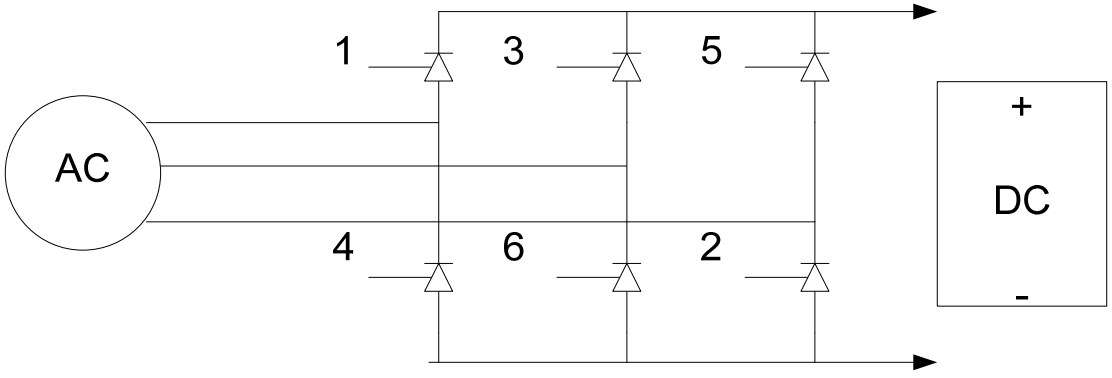

Figure 5.3 SCR connection.

The SCR's are numbered in their natural order of commutation. Each power pole consists of 3 – SCR . Four power poles are used to create the 12 SCR converter to produce DC from AC. This is given in figure 5.4. It is seen that the produced DC voltage is twice of the 6- SCR converter.

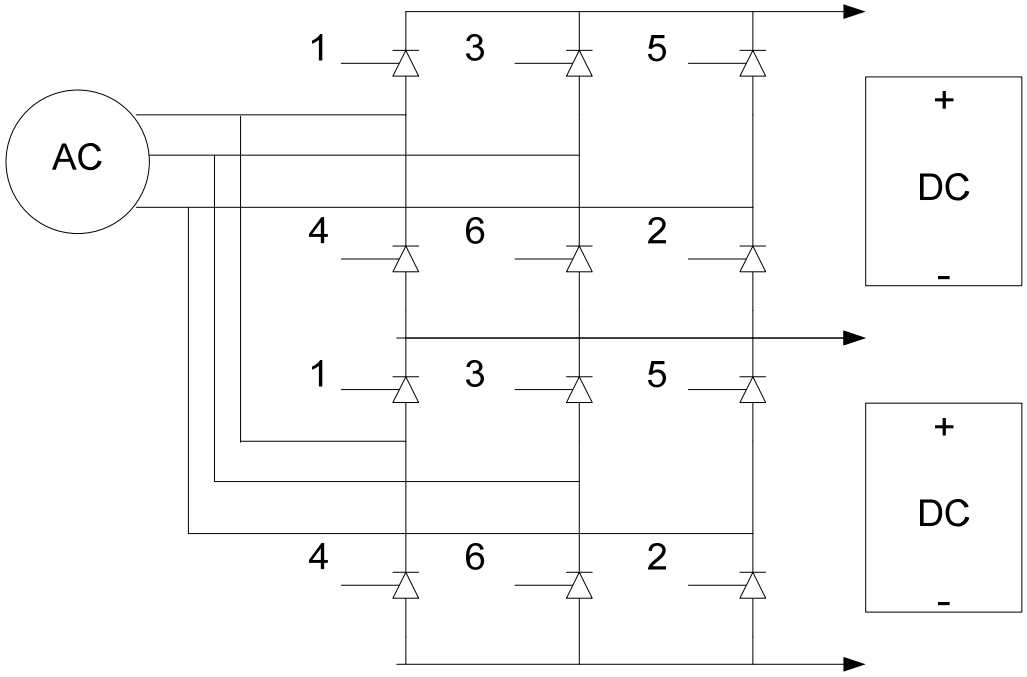

Figure 5.4 12 pulse SCR connection.

There are 6 single phase transformers used to create star-star and start-delta 3-phase configuration that feeds the 12 SCR power converter. The delta winding was connected so it lags the star winding. Each transformer is a step-up with a ratio of 1:2 turns. This is given in figure 5.5 and figure 5.6. The DC bus was formed by connecting the 1,3,5 SCR cathodes to form the positive bus and the delta 4,6,2 SCR anodes form the negative bus.

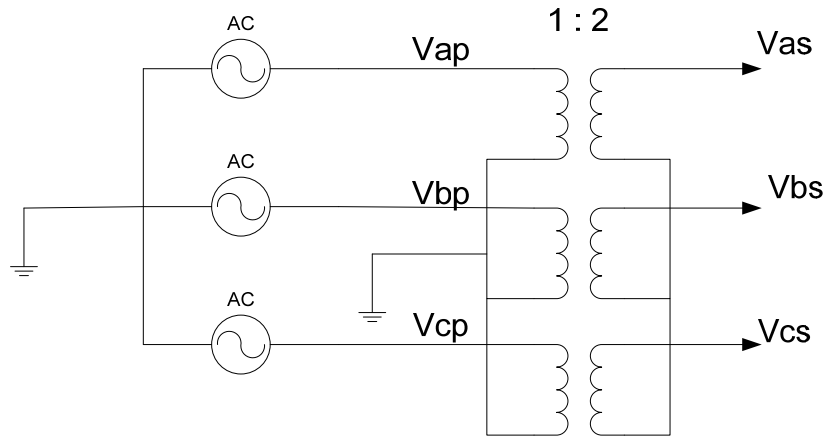

Figure 5.5 Star-Star connections.

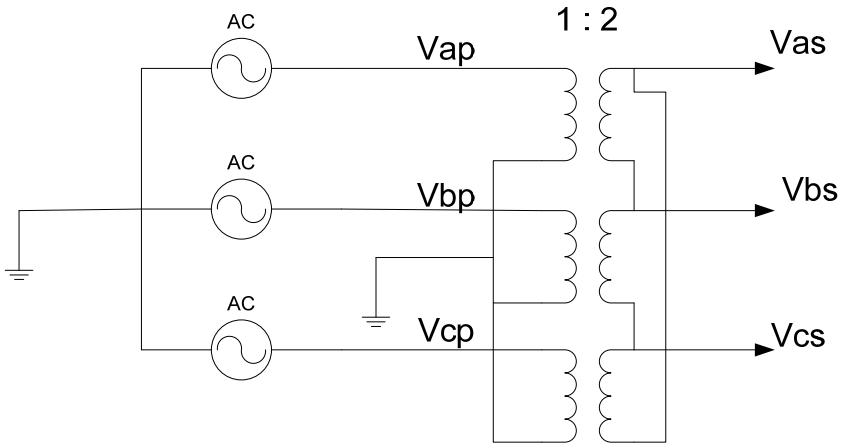

Figure 5.6 Star-Delta connections.

5.3 Control section

The control section consists of the following:

- 3 phase current sensing.
- Voltage zero cross detection.
- SCR gate drive circuits.
- Digital Signal processor.(DSP)
- AC to DC Power supplies with different voltage rails.

❖ Current sensing

This is achieved by using 3 current sense transformers (CT). Each transformer is placed in line with the 3-phase power lines. The CT produces a 0-5 volts signal that is proportional to the AC current that is flowing in each phase. The current signal is scaled to a 0-3 volts signal and is read by the Analog to Digital Converter (ADC) of the DSP.

❖ Voltage Zero crossing

The voltage zero crossing is detected by using external hardware. Each voltage is fed to a comparator to detect phase to phase zero crossing. This signal is used in a capture input of the DSP to calculate period/frequency of the incoming AC voltage.

❖ SCR Gate Drive

SCR are driven by anexternal 250 KHz PWM signal that is digitally ”NAND” with PWM produced by the DSP. There are 12 individual PWM that are used to gate the 12 SCR. The gate drives are electrically isolated from the DSP and associated circuitry using pulse transformers. The output of the pulse transformer is referenced to the anode of the SCR.

Gate drive output also has a RC snubber circuit across the SCR to reduce the voltage spikes. This reduces the chance of SCR turning on inadvertently.

DSP is TMS320F28335 manufactured by Texas Instruments Corporation. DSP is configured to run at 150 MHz. MATLAB®/ Simulink® was used to write the firmware to control this DSP.

The control board also has op-amps to condition the current that is sensed by the CT. All this circuitry is supported by many voltage rails/switching power supplies on the board. The control board generates 1.8 volts, 3.3 volts, 5 volts, +/- 12 volts and 24 volts.

5.4 Simulink DSP programming

a. DSP Program Flow

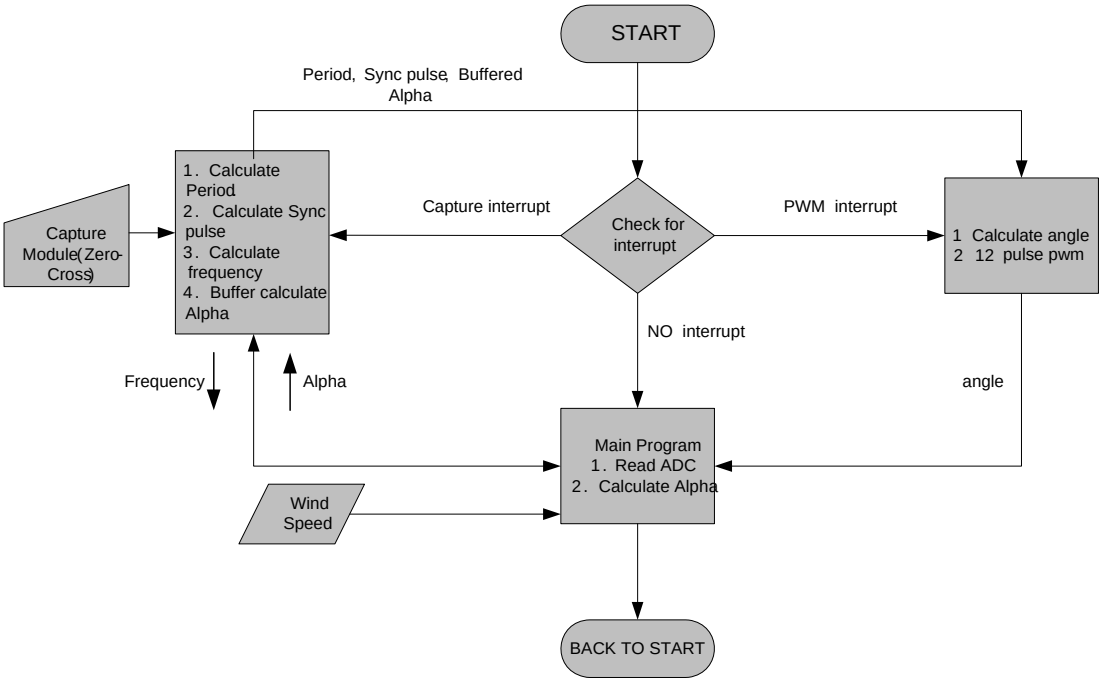

Figure 5.7 DSP Program flow

- Interrupt handler

The DSP is interrupt driven. There are two main interrupts that are used to control the program. ePWM1 and ECAPTURE. The interrupt handler handles these interrupts. ePWM1 interrupt is generated every 50 KHz. This interrupt routine is used to calculate the angle of the 3-phase voltage. This angle is critical to enable the firing of the SCR in relationship to a voltage zero-cross. The input to this routine is the period of the voltage waveform from the ECAPTURE module. The angle calculation is periodically synced to make the system time accurate. This sync signal is also generated in the ECAPTURE module. The way the angle is calculated is by generating a counter that is incremented at interrupt frequency and will count up to the value of the period. When a sync signal is asserted the counter is set to zero. Since the period that is captured is in DSP clock cycle time, the value need to be converted to real time. The value of the angle is a number between 0 and 1, the counter value is divided by the period. This number needs to be multiplied by 360 to obtain the degrees. This method allows an angle resolution of 1/50 KHz. It is accomplished by implementing the following equation:

$$Tperiod\ real = \frac{Tcap * 50\ KHz}{150\ MHz} \qquad (5.1)$$

The value of the angle also needs to be converted in to degrees. This is accomplished for each new period value by the following equation:

$$Count = Count + 1, up\ to\ the\ Tperiod\ real \qquad (5.2)$$

$$Angle = \frac{Count}{Tperiod\ real} \tag{5.3}$$

CAPTURE interrupt is asserted when the capture module sees a rising edge signal. The voltage zero cross detection hardware circuitry is connected to this interface of the DSP. The module is setup after each capture event to reset the capture counter. This way each capture is the period of the zero cross detection signal. This period represents the period of the incoming 3-phase voltage.

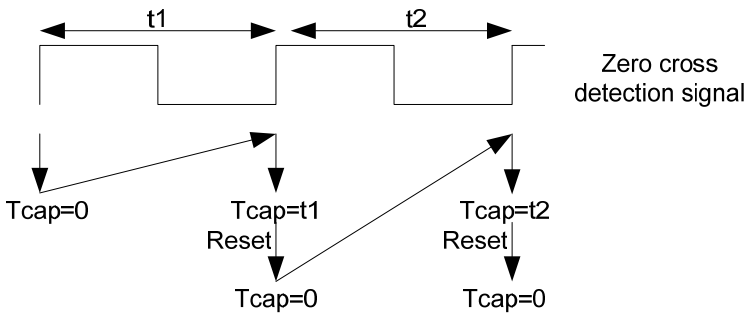

Figure 5.8 Calculation of Tcap time in the DSP module.

To keep this module from detecting spurious signals, the signal is captured only within a valid range of frequency. The reasoning behind this is that the change of frequency from one cycle to another does not happen rapidly. This is implemented in Simulink as given in figure 5.8. The whole interrupt routine is represented in figure 5.9.

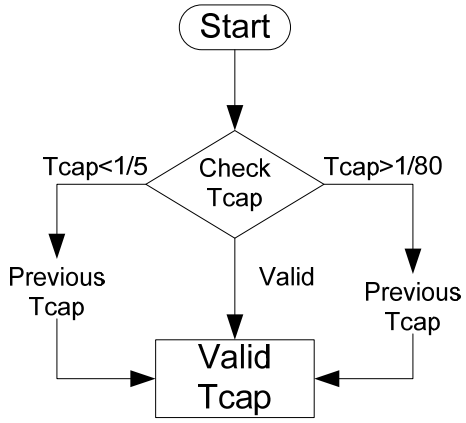

Figure 5.8 Valid capture of Tcap time flow diagram.

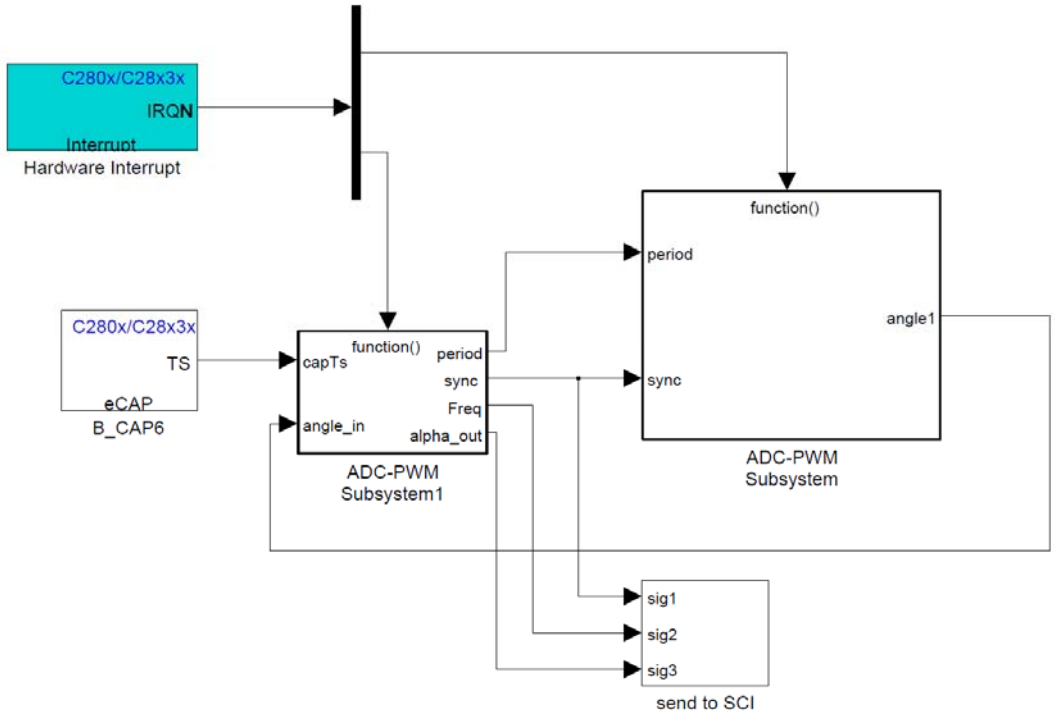

Figure 5.9 Interrupt routine for the DSP for real time control.

- SCR Firing logic.

The SCR's are fired in relationship to the zero crossing of the 3 phase voltage wave form. Each SCR can be offset from 0^0 to 180^0 degrees. This is the range for the alpha angle that is generated by the control circuit. In the case of the delta winding, the angle needs to be further delayed by 30^0 for a range of 30^0 to 210^0

The circuit has to stop firing after a certain pulse width that can be adjusted. Figure 5.10 is the Simulink code of the SCR firing and the output of the firing pulse pattern is given in figure 5.11. This firing pattern is logical "AND" with a 250 KHz square wave to produce the gate drive. The logical "AND" is accomplished by digital hardware on the drive board.

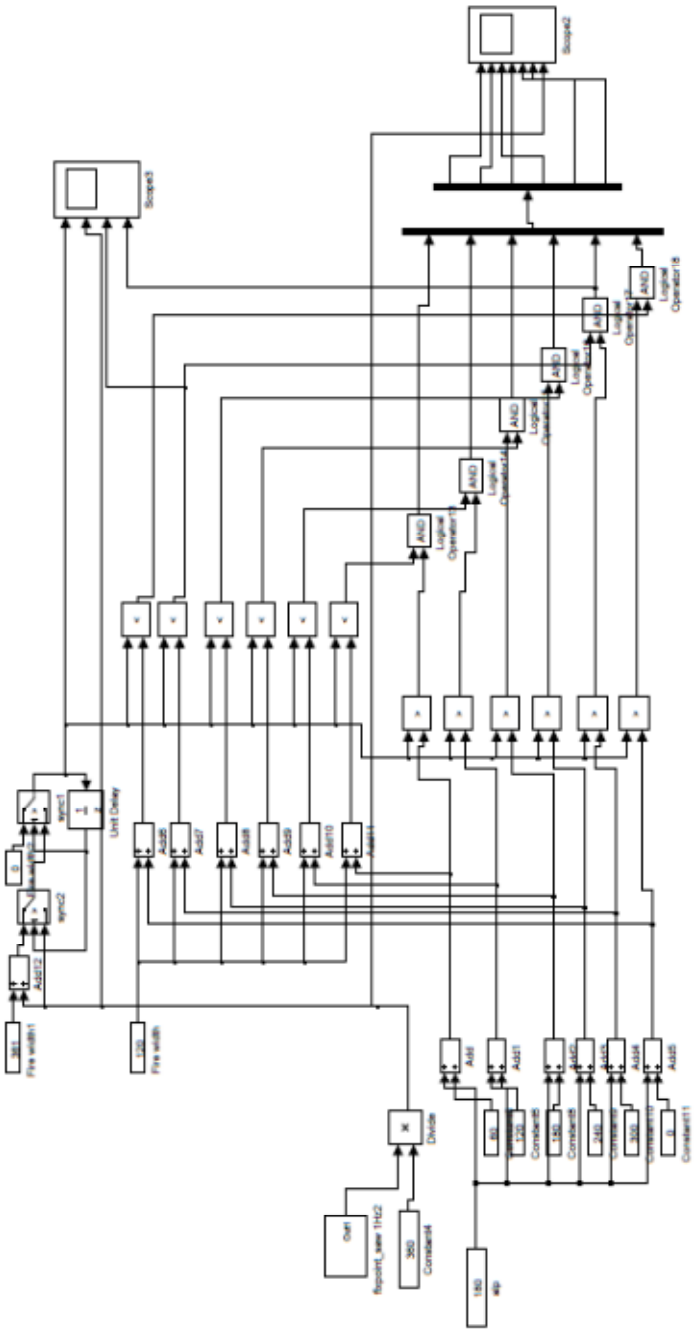

Figure 5.10MATLAB®/ Simulink® code for SCR firing circuit.

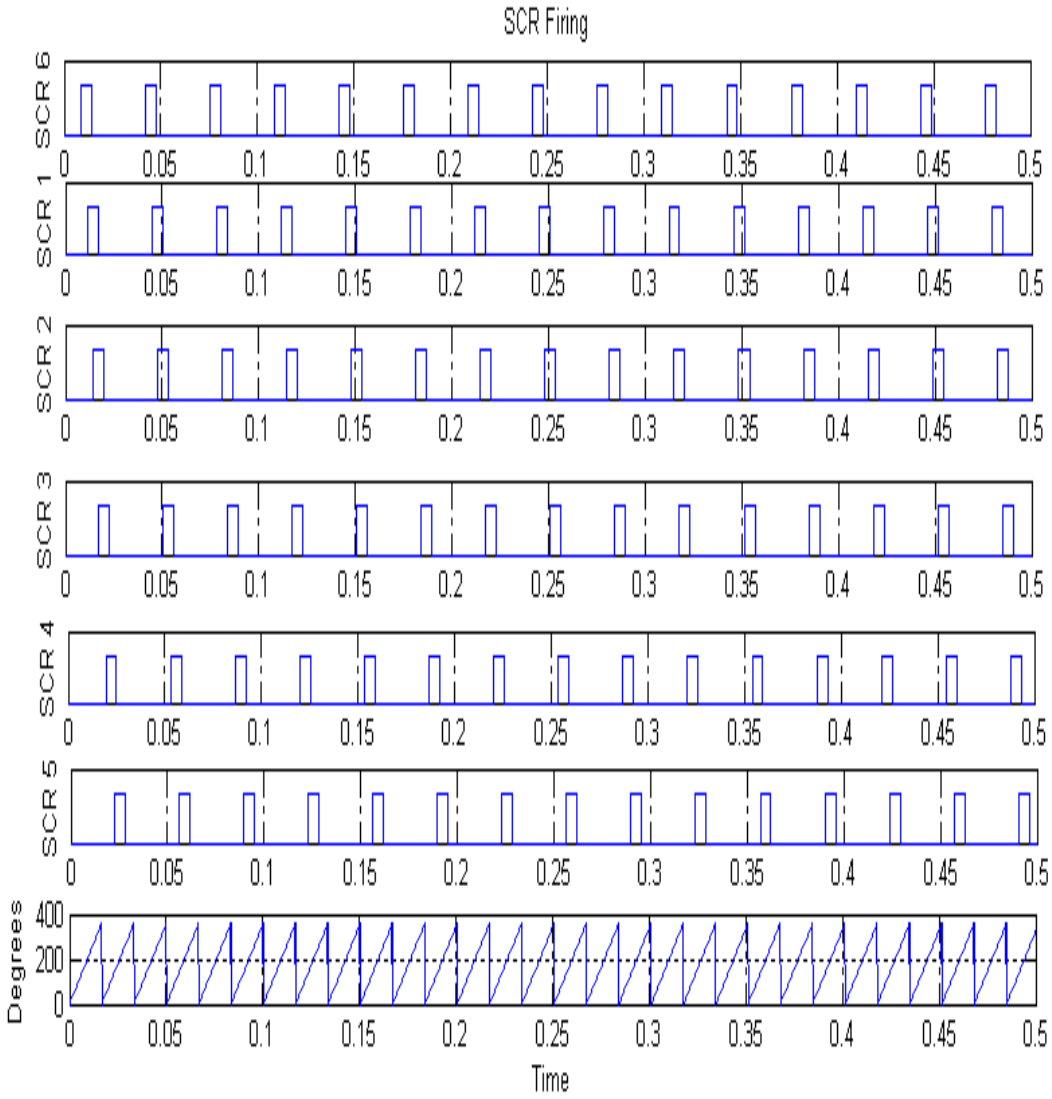

Figure 5.11 SCR firing pattern vs angle.

d. Analog to digital converter

The ADC of the DSP is used to read the voltage produced by the Current Transformers. This is the representation of the 3 phase current that is flowing via the system. The ADC is 12 bits and produces a number between 0 and 2024 with the last bit used to indicate negative or positive. The CT are calibrated to read 12 amps. An offset and a gain is applied to the reading from the ADC convert to a actual reading.

The conversion of the ADC is enabled every 50 KHz by the epwm1.

5.5 Hardware setup results

The first result is the PMSG voltage that is estimated by the DSP. This is the V_d-V_q estimation and presented in figure 5.12. The data is read by serial communication from the DSP board using a computer. We can see that it is an accurate representation of the 3 phase voltage. The voltage does not have noise due to SCR switching and the zero crossings are well defined. The simulation results are supported by this data.

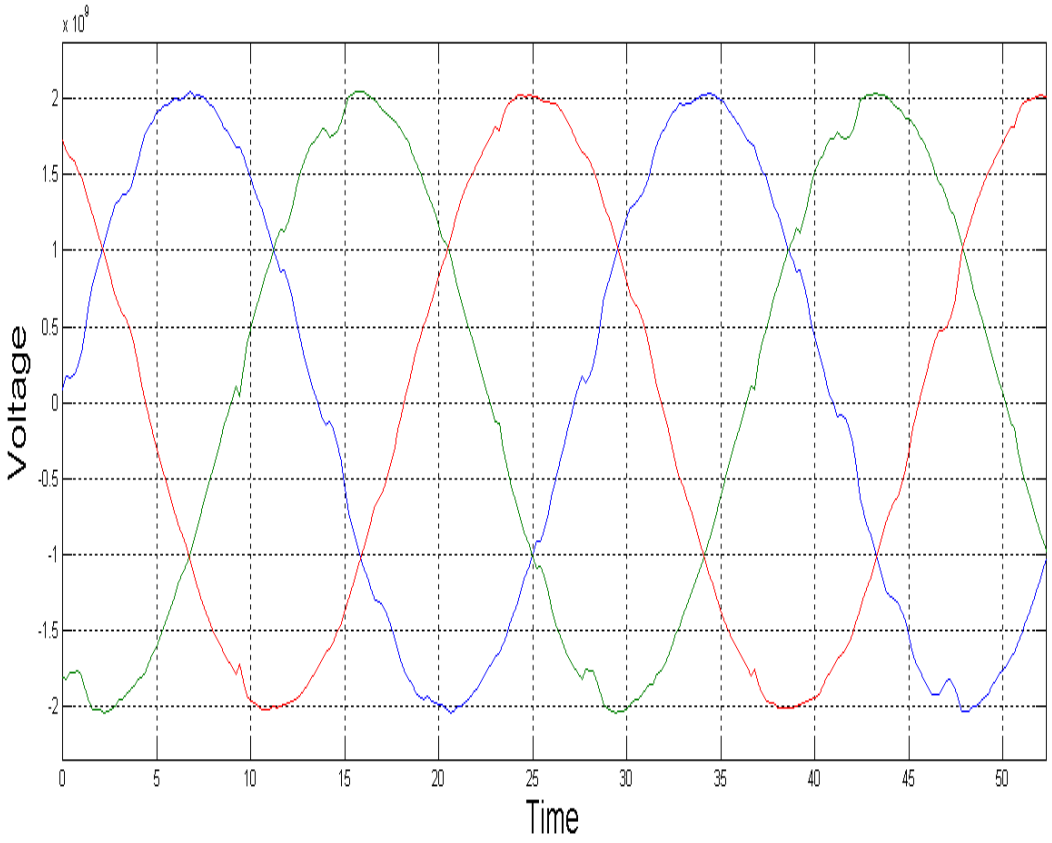

Figure 5.12 DSP Vabc estimated results of 3 phase voltage.

The second plot in figure 5.13 is the V_{qr}-V_{dr} estimation data that is read back from the DSP via serial communication to a computer. This is the DC bus voltage that is estimated. The peak to peak range of the data is from 4.5345 Amps to 4.5344 Amps. The estimation that was shown in MATLAB simulation is implemented real time in the DSP running at 150 MHz.

Results verify that the estimation of the DC current is possible for this system. It also shows that by implementing this, a current sensor can be eliminated in the system. This is an added advantage.

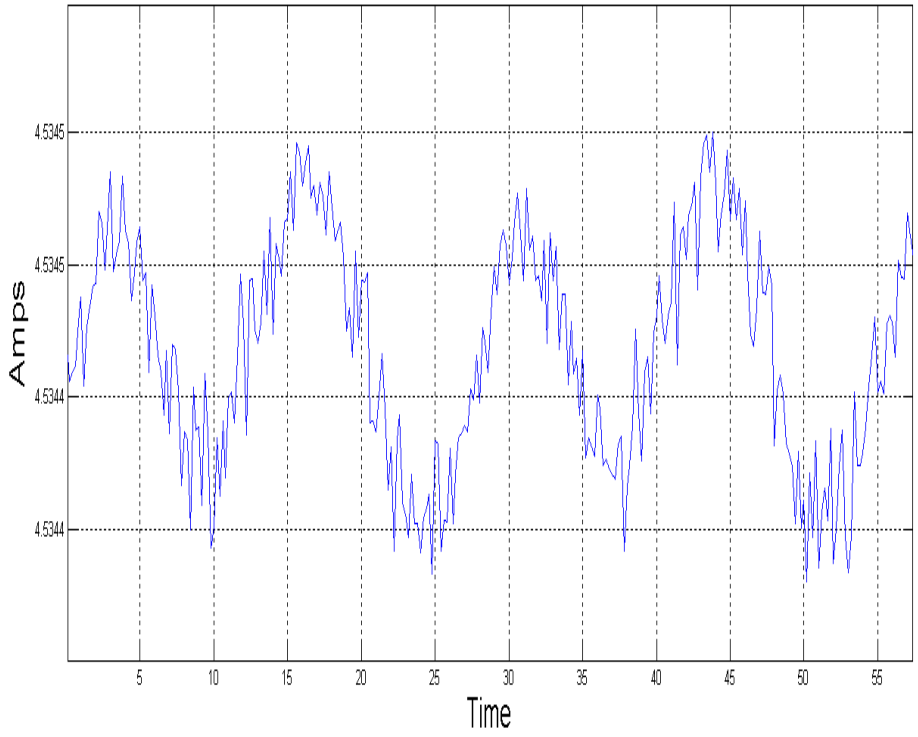

Figure 5.13 DSP V_{qr}-V_{dr} estimator results of HVDC current read via a serial port.

The third plot is the Alpha estimation from the DSP. This information is also read by using a serial communication to the DSP. The Alpha estimation is used by the control loop in determination of firing the SCR's. The range of data is from 83.772 to 83.7708. Essentially the angle estimation is close to 83 degrees in this instance.

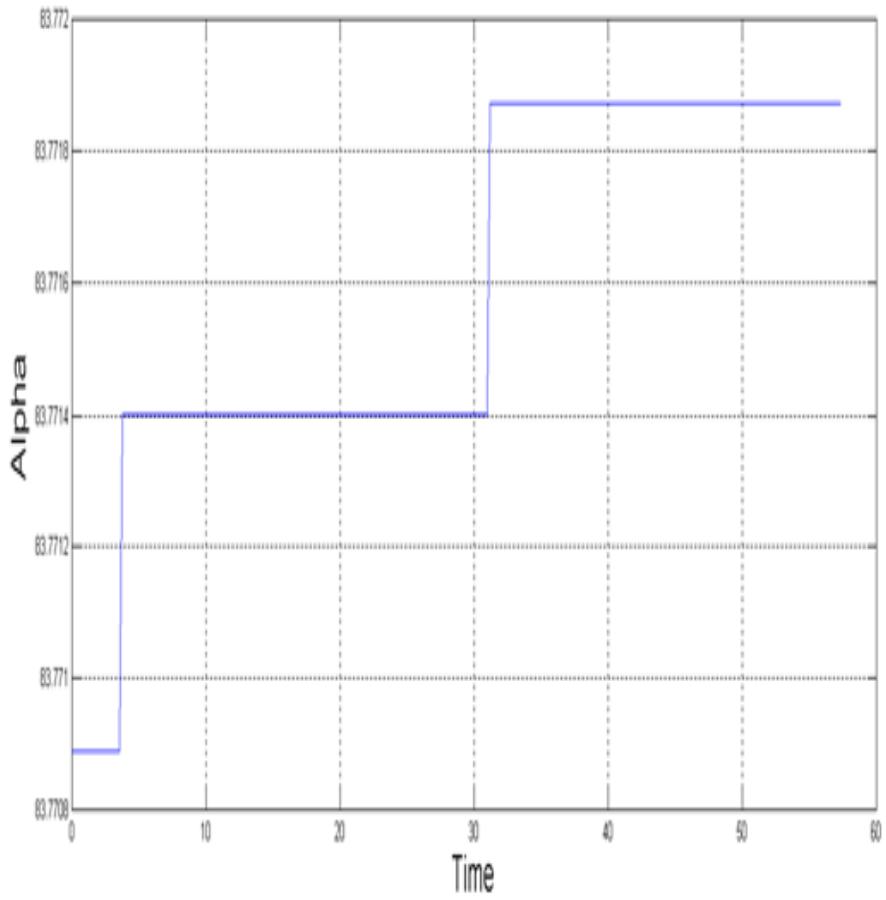

Figure 5.14 DSP Alpha estimator results read back via a serial port.

The next plots are from the scope reading of the system voltages and sync signal. It is very important for this system to sync to the incoming voltage frequency for the SCR's to be phase fired. The lab setup was connected to a variable frequency synchronous generator to produce variable frequency voltage. This represents a wind generator producing variable frequency power. The plots display this incoming voltage as well as the DC voltage that is produced by the system. The hardware generated synchronizing signal is also plotted. This signal is fed to the capture module of the DSP to generate the Tcap.

The green waveform in the plot is the DC bus voltage, Blue is one phase of the 3 Phase AC waveform. Magenta is the sync signal. Figure 5.15 shows the synchronizing signal and DC signal relationship. It is zoomed in to clearly show the synchronizing. In Figure 5.16, the frequency is at 24.23 Hz. In figure 5.17, the synchronizing is at 35.05 Hz. Figure 5.18, the synchronizing is at 43.15 Hz. Figure 5.19, the synchronizing is at 53.19 Hz. It is seen from the results, the system can synchronizing to a wide frequency range. You can also observe that the output DC voltage is rising. This is due to the PMSG voltage rising in relationship to the frequency increase. This experiment purely looks at the synchronizing capability of the system.

The system only uses the star to star winding to synchronize and has to offset to account for the star to delta winding firing of the SCR's. This is accomplished in the DSP's SCR firing algorithm. This system was setup to only synchronize between 5Hz and 80Hz.

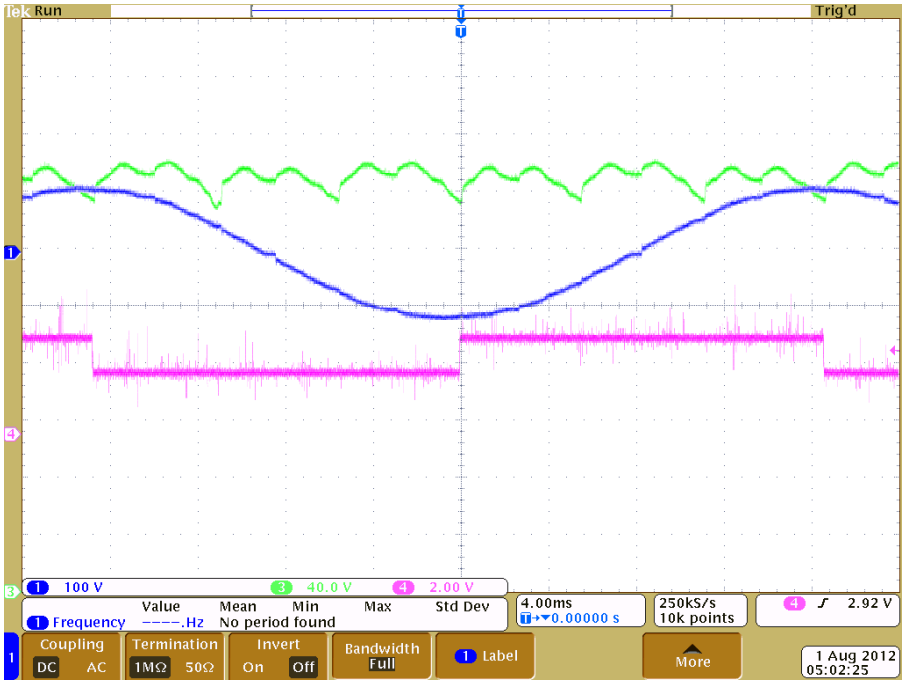

Figure 5.15 Green DC bus voltage, Blue AC voltage, Magenta synchronizing signal.

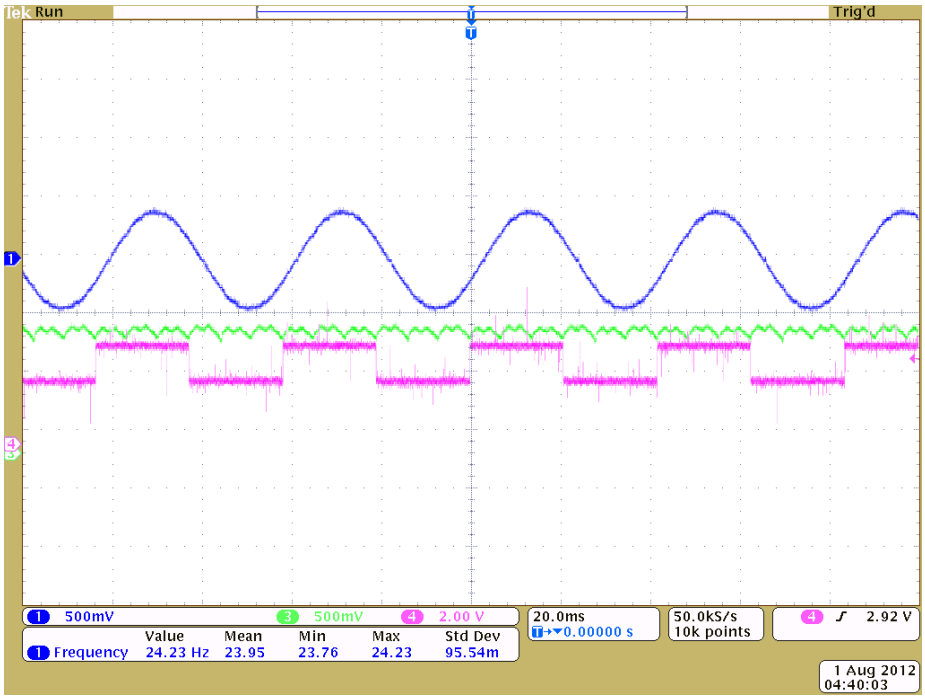

Figure 5.16 Green DC bus voltage, Blue AC voltage, Magenta synchronizing signal, frequency 24.23 Hz.

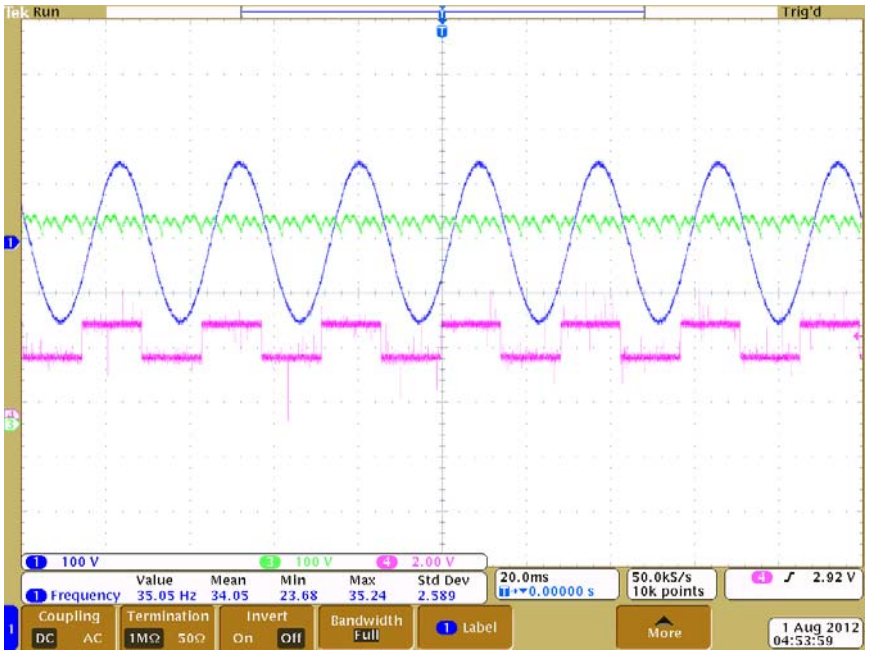

Figure 5.17 Green DC bus voltage, Blue AC voltage, Magenta synchronizing signal, frequency 35.05 Hz.

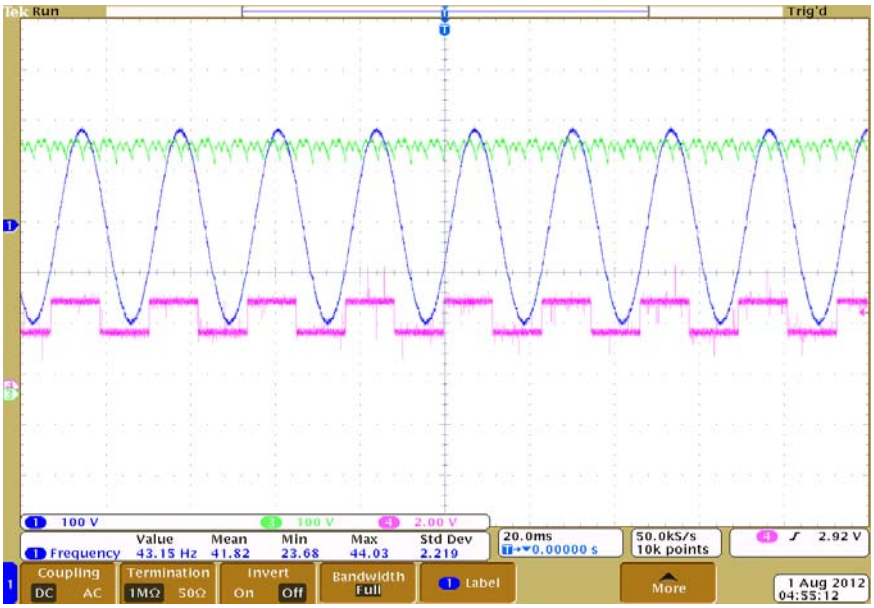

Figure 5.18 Green DC bus voltage, Blue AC voltage, Magenta synchronizing signal, frequency 43.15 Hz.

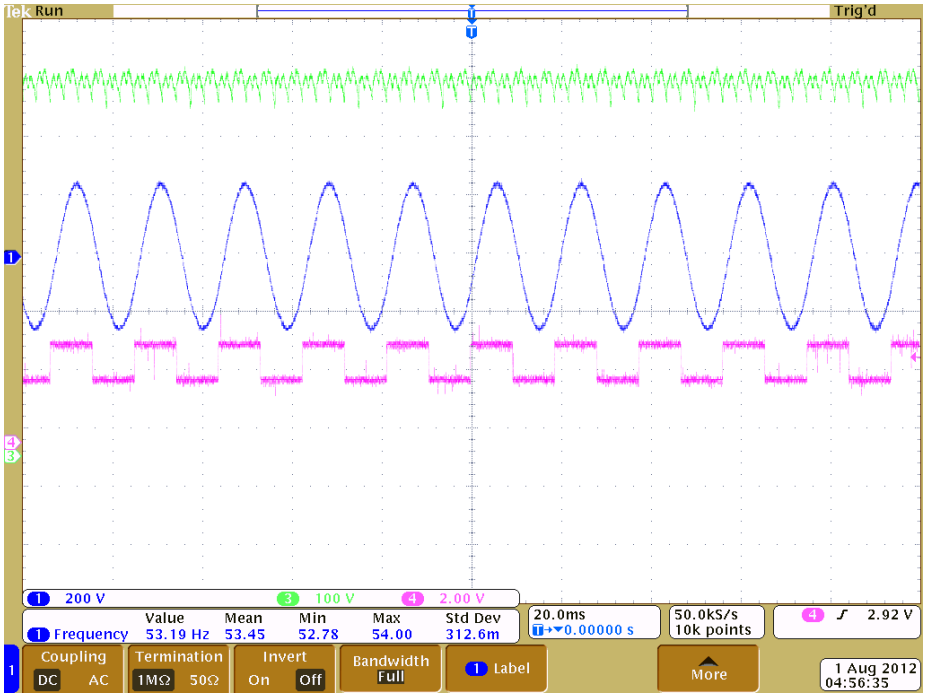

Figure 5.19 Green DC bus voltage, Blue AC voltage, Magenta synchronizing signal, frequency 53.19 Hz.

The next set of results were obtained by configuring the system to simulate a connection to a stiff DC bus. A high voltage DC power supply was connected in parallel with the output of the SCR system and load. The DC bus voltage varied to observe how the system would behave. This was crucial in seeing how the SCR based system could pump power to a constant DC bus. For the following plots in figures 5.20 and 5.21, Blue is DC bus voltage, Red is AC voltage, Green is DC current, and Magenta is AC current. When the DC bus voltage was lowered 106 volts, both the DC power supply and SCR system contributed power to the load. This is seen in figure 5.20. As the DC bus voltage was

increased to 174 volts, all the power was delivered by the DC power supply and is seen in figure 5.21. The magenta trace which is the AC current goes to zero.

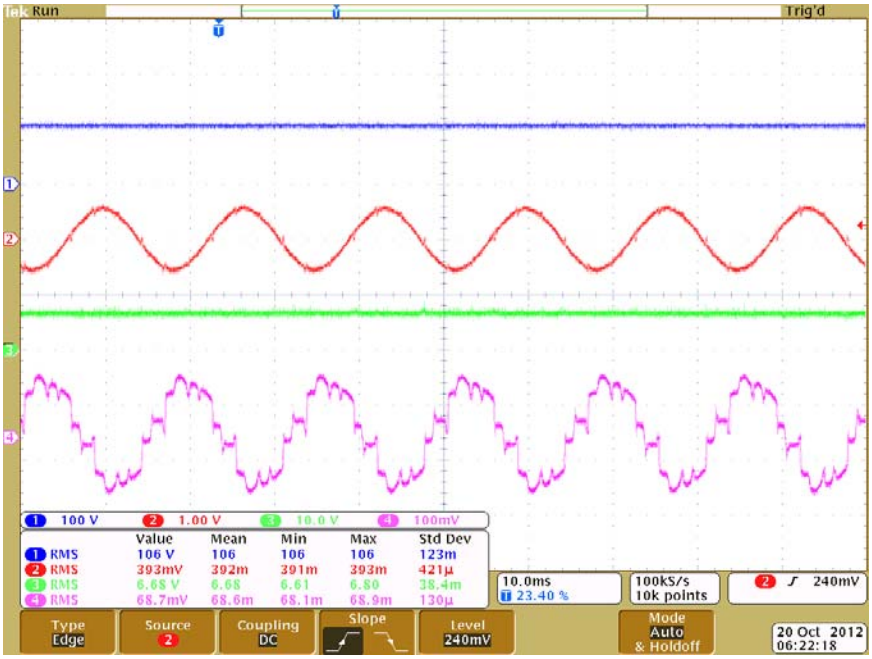

Figure 5.20 Blue DC bus voltage, Red AC voltage, Green DC current, Magenta AC current.

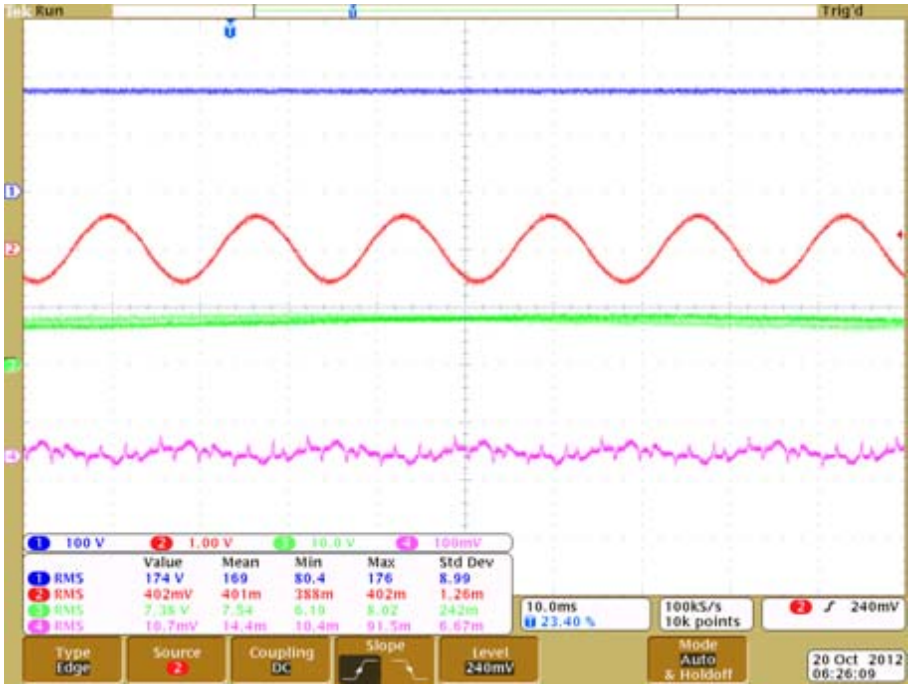

Figure 5.21 Blue DC bus voltage, Red AC voltage, Green DC current, Magenta AC current.

The next plot was obtain by changing the lab setup. The system was connected to a variable frequency synchronous generator and a DC power supply to obtain a full system performance. The system is given in figure 5.22.

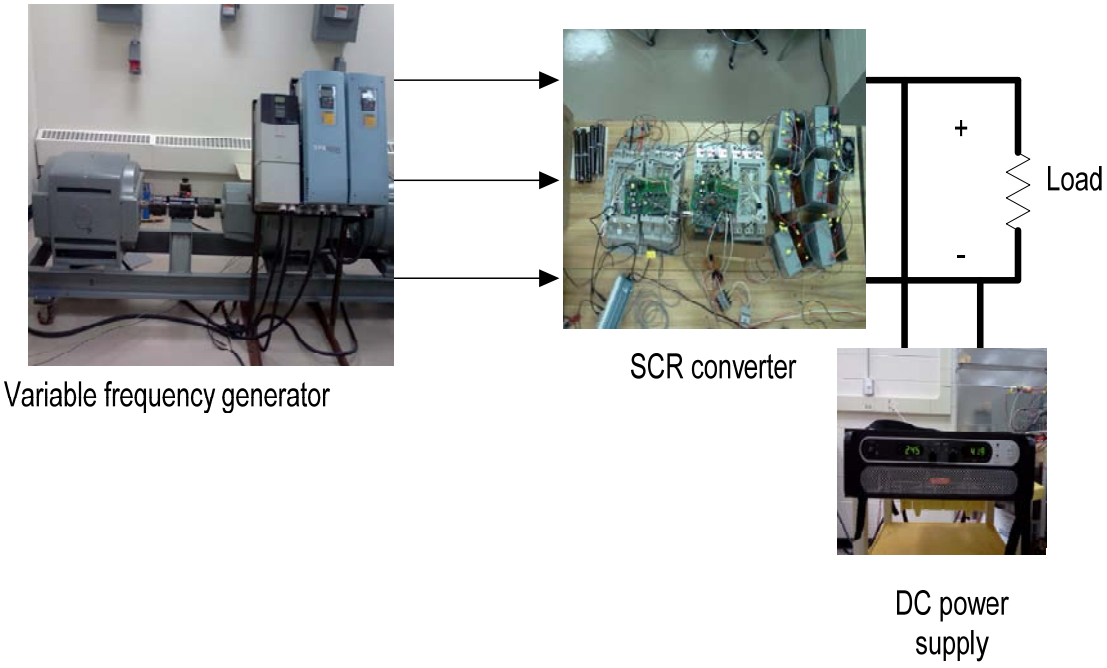

Figure 5.22 Lab setup of the complete system connected to a AC generator.

The synchronous generator in figure 5.22 represents a variable frequency wind generator. The speed of the generator can be varied by using an AC motor drive. In this setup a Rockwell Automation drive was commanded to change frequency to generate varying voltage. The SCR conversion system was fed this 3 phase voltage. A DC power supply was used to maintain a stiff DC bus voltage and a resistor bank was used as a load. The results of this set up are given in figure 5.23. Red is the DC bus voltage, Blue is the AC Voltage, Magenta is the AC current and Green is the DC current.

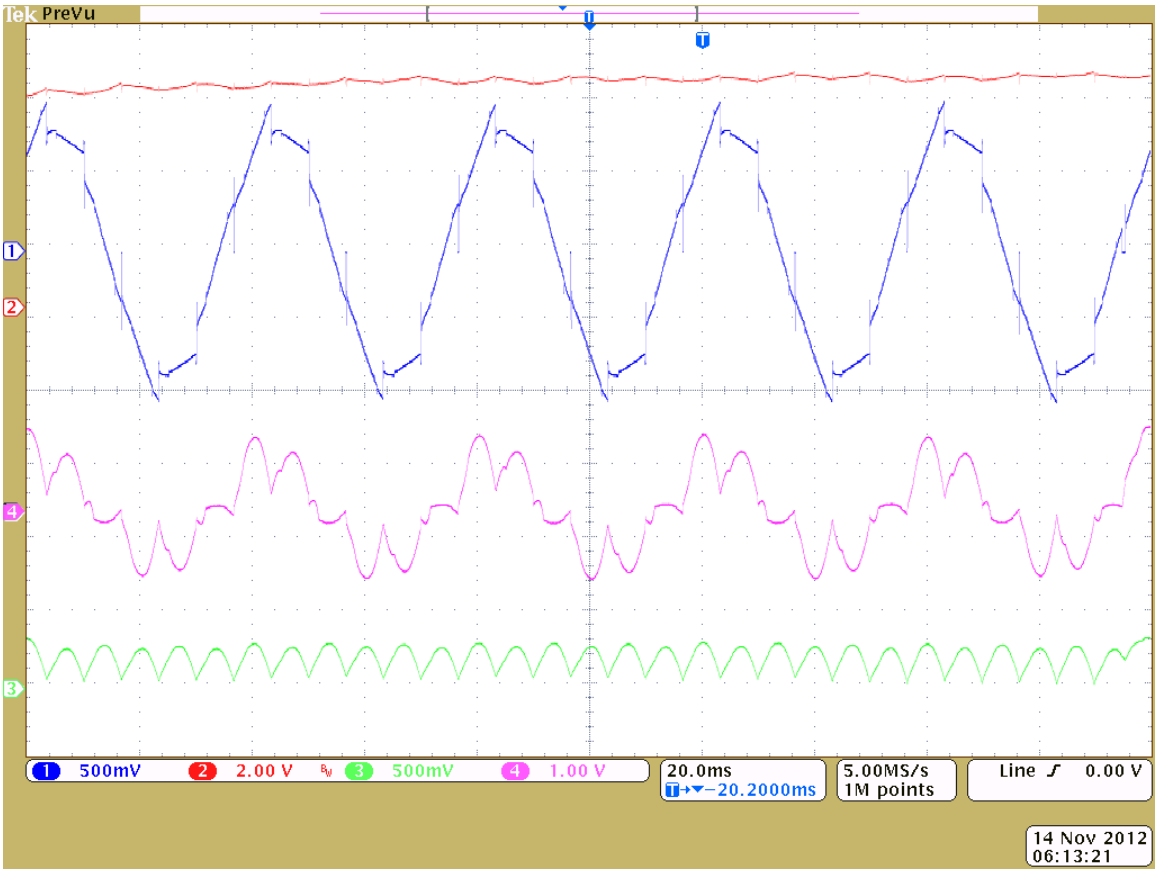

Figure 5.23 Red DC bus voltage, Blue AC Voltage, Magenta AC current and Green is DC current.

Chapter 6

6.0 Maximum Power Point Tracking (MPPT)

6.1 Wind regions of operation

Modern variable wind generators have three main regions of operation.

These regions are depicted in figure 6.1.

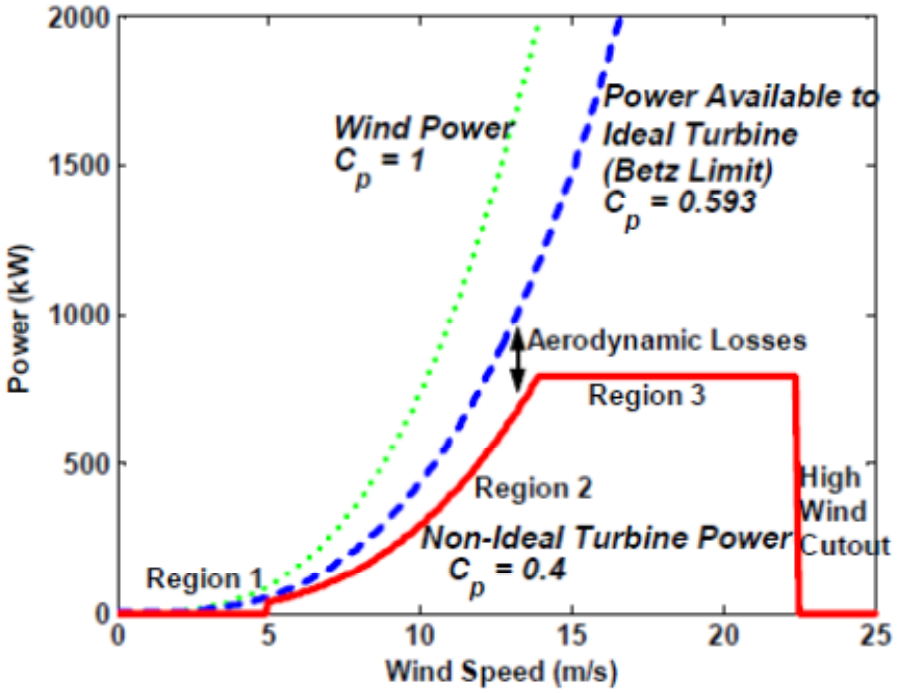

Figure 6.1 Wind Turbine regions of operation.

(Adaptive Torque control of variable speed wind turbine, Kathryn E. Johnson, NREL)

Region 1, This is the startup region. The turbine monitors for the wind speed to see if the turbine can be operated. If it can, it initiates the startup routine. This region does not use modern controls to improve the capture of wind energy [30] .

Region 2, This is the region that a wind generator should use modern control techniques to capture the most maximum energy. The maximum energy that can be captured is given by the Betz limit. The losses in a turbine keeps the generator from reaching this limit. The idea is to achieve the maximum power extraction. The controls that are available to maximize are the Yaw angle, generator torque and blade pitch. Since the wind loading in this region is minimal, it is customary to only control the Yaw angle and generator torque. Blade pitch angle is left at an optimal angle to capture the maximum energy[47].

Region 3, This is the region that the generator is operating above the rated speed. The speed of the wind is above the speed that the maximum power can be extracted. The turbine has to be protected from reaching its maximum mechanical and electrical limits. Blade pitch control is used to shed the excess wind power. The generator is held at a constant speed. Yaw angle and generator torque control also can be used to shed the excess wind power [48].

6.2 Capture of wind energy.

The performance of the wind turbine not only depends on its hardware but also wind turbine control techniques influence the performance of the wind turbines. Therefore, the wind turbine control technique can influence the output of the wind turbine. Fixed speed and variable speed control methods are two traditional control methods. Variable speed control methods divided into several control methods[45,46].

Equation (6.1) show the output power of a wind turbine.

$$P = c(\beta, \lambda)\frac{\rho A}{2}v_{wind}^3 \tag{6.1}$$

$$c(\beta, \lambda) = c_1(\frac{c_2}{\lambda_2} - c_3\beta - c_4)e^{-\frac{c_5}{\lambda_2}} + c_6\lambda \tag{6.2}$$

$$\frac{1}{\lambda_2} = \frac{1}{\lambda + 0.08\beta} - \frac{0.035}{\beta^3 + 1} \tag{6.3}$$

$$\lambda = \frac{R\omega}{v_{wind}} \tag{6.4}$$

Where $\rho = 1.2\ kg/m^3$ is the air density, A is the area swept by the turbine blades, λ is the Tip-Speed-Ratio (TSR) given by (6.4), β is the pitch angle, c is the performance coefficient of the turbine given in (6.2) and ω is the generator angular velocity. c_1-c_6 are coefficients that are dependent on the structure of the wind turbine [29].

Figure 6.2 shows the power versus TSR. Output power changes with TSR. The TSR that corresponds to the maximum output power is called optimal TSR. Figure 6.3 shows the output power versus wind turbine speed and compares wind turbine control methods. One of the lines shows the fixed speed control method and the other one shows the Maximum Power Extraction (MPE) method (MPE). In MPE algorithm the speed of the wind turbine is set so that the maximum power can be extracted from the blowing wind. This speed is called optimal speed. This control method is applicable to variable speed wind turbines and has better efficiency than the fixed speed method.

Other control methods can be implemented in the wind turbines. The control algorithm is designed to achieve a certain criteria for the wind turbines. Therefore, the wind data and geographical characteristics of the wind site are important for the wind turbine control algorithm[49,50].

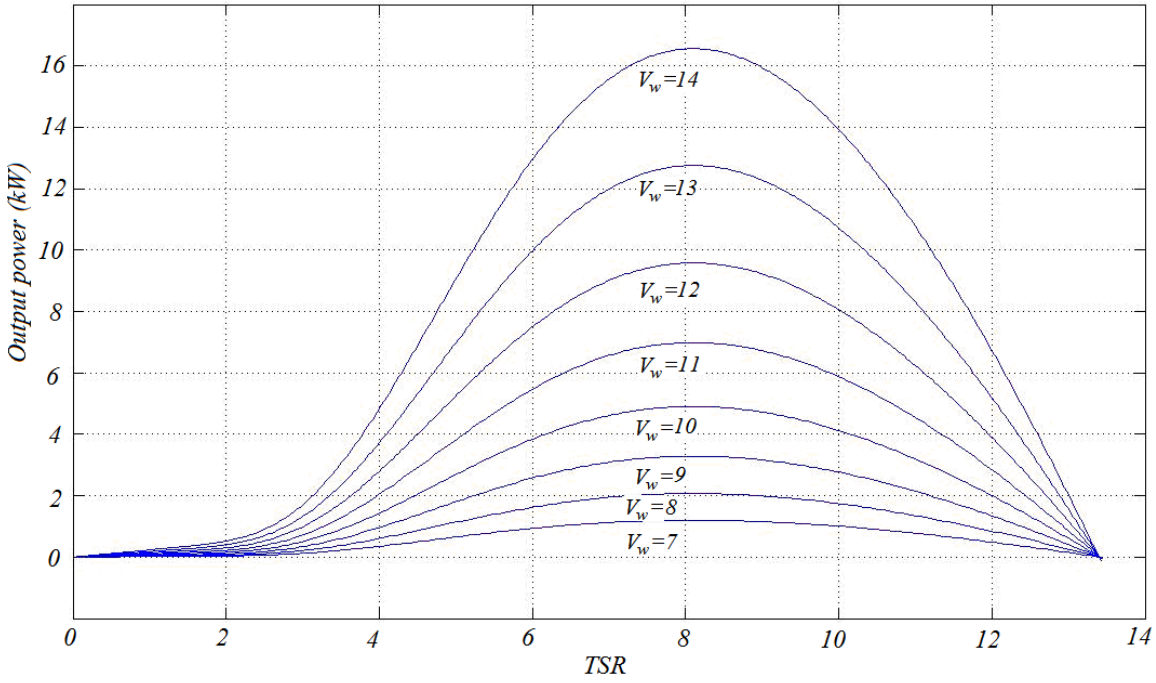

Figure 6.2 Wind turbine output power versus Tip-Speed Ratio (TSR).

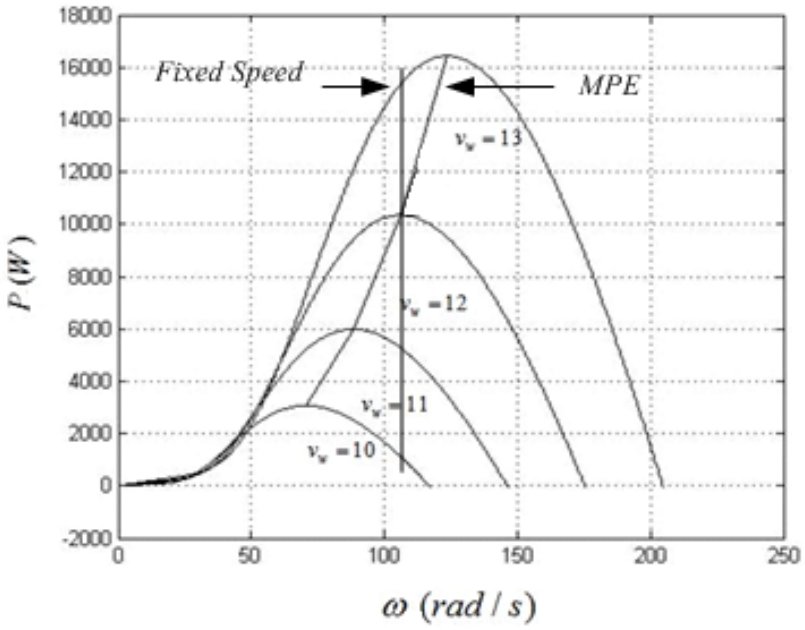

Figure 6.3 Wind turbine output power versus rotor speed.

6.3 Wind generator mechanical equations.

The wind generator captures the wind energy using the blades and transfers the power to the electrical generator. In general, a low speed shaft that is connected to the blades is fed to a gearbox. The gearbox will increase the speed and is connected to the generator via a high speed shaft. A generator without a gearbox is referred as a "direct drive" generator. This type of generator has multiple poles to compensate for the low speed rotation of the blades. Figure 6.4 is the representation of a geared system.

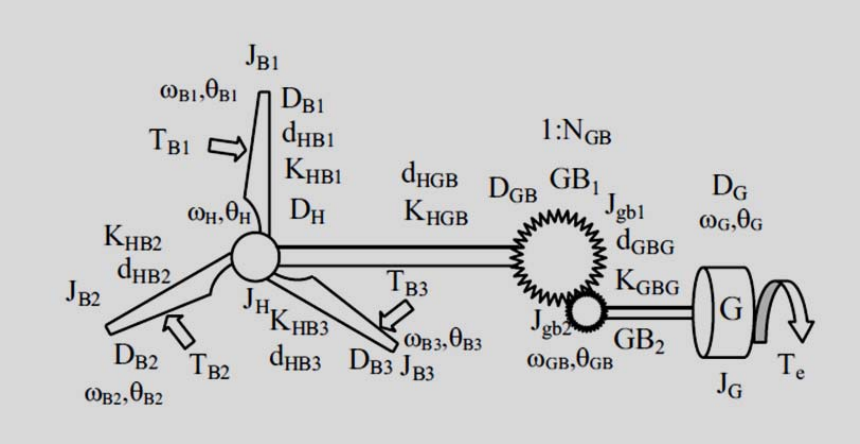

Figure 6.4 Wind Turbine mechanical system of power transfer.

The mechanical equations for the system are as following:

$$T_m = T_e + B\omega_m + J\frac{d\omega_m}{dt} \quad (6.5)$$

Where, Tm is the mechanical torque produce by the wind. T_e is the electrical torque produced by the generator. B is the frictional coefficient and J is the inertia.

$$T_m - T_e = B\omega_m + J\frac{d\omega_m}{dt} \quad (6.6)$$

The power generated by the generator is P_e

$$Pe = Vdc\ Idc = Te\ \omega e \quad (6.7)$$

Using this relationship we can generate a Idc reference related to the ω_m reference from maximum power point tracking as following:

$$Idc\ ref = \frac{Te\ \omega e}{Vdc} \quad (6.8)$$

The above derivations allows us to control a control system to track the maximum power point. The inputs to this system are the Wind speed, Radius of the blade (R) and λ nominal. ω reference compared to the ωm and the error is fed to a PI controller. The output is divided by HVDC bus voltage and divided by ωe to produce a current reference to the current control loop. This is given in figure 6.5

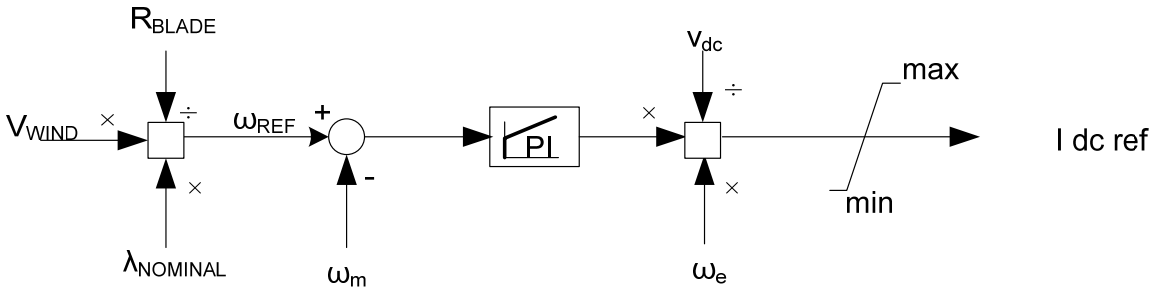

Figure 6.5 Configuration of the MPPT Control system.

The output is limited to the I dc reference range of minimum and maximum. "Anti-winding" PI controller is used.

6.4 Simulation results

The simulation results for the figure 6.5 controller is given in Figure 6.6. The first plot is the reference current corresponding to the MPPT algorithm. The second plot is the ω reference that is related to the turbine characteristics. In this case, the simulated turbine has a blade radius of 41 meters, λ nominal of 8.1. The final two plots are the ω_m the turbine speed and wind speed.

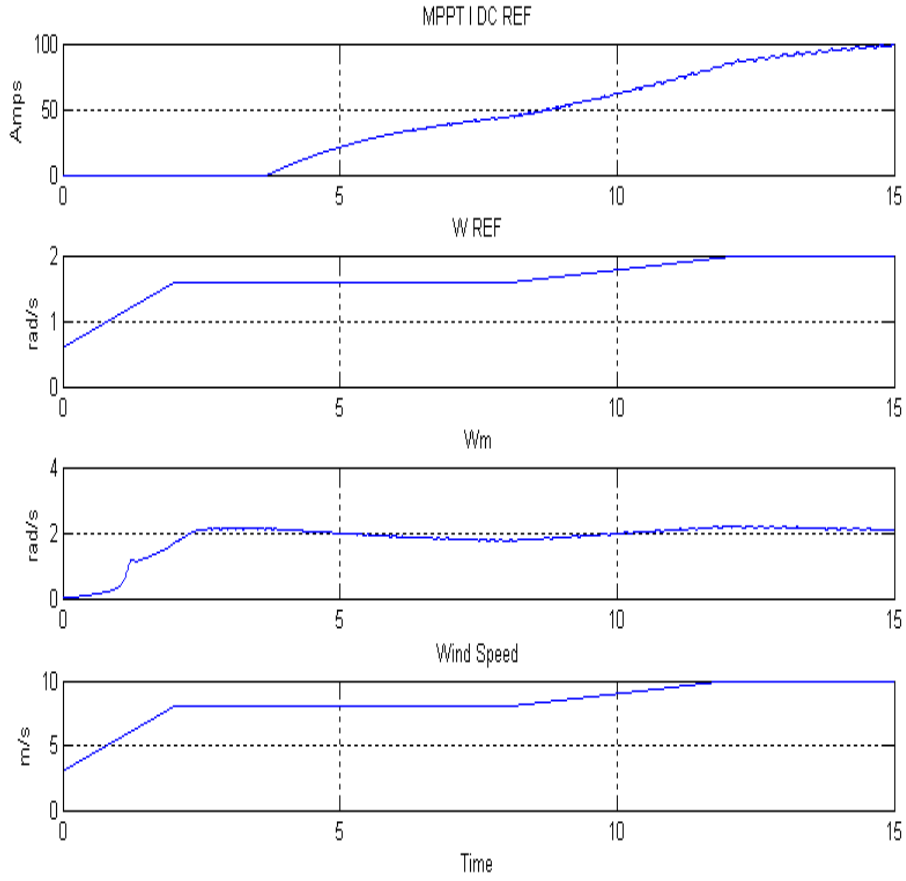

Figure 6.6 MPPT Simulation results for changing wind speed.

Chapter 7

7.0 Paralleling of wind generators, Fault analysis and Torque pulsations.

7.1 Wind farm operation

The proposed multi-terminal system is given in figure 7.1. The wind farm would have many generators connected to a common HVDC bus. Each generator would produce variable voltage and current that would be fed to a step-up transformer to increase the voltage to the desired DC link voltage. The proposed architecture is scalable to any number of generators. The HVDC bus would be inverted back to an existing 3 -phase grid for distribution for utilities.

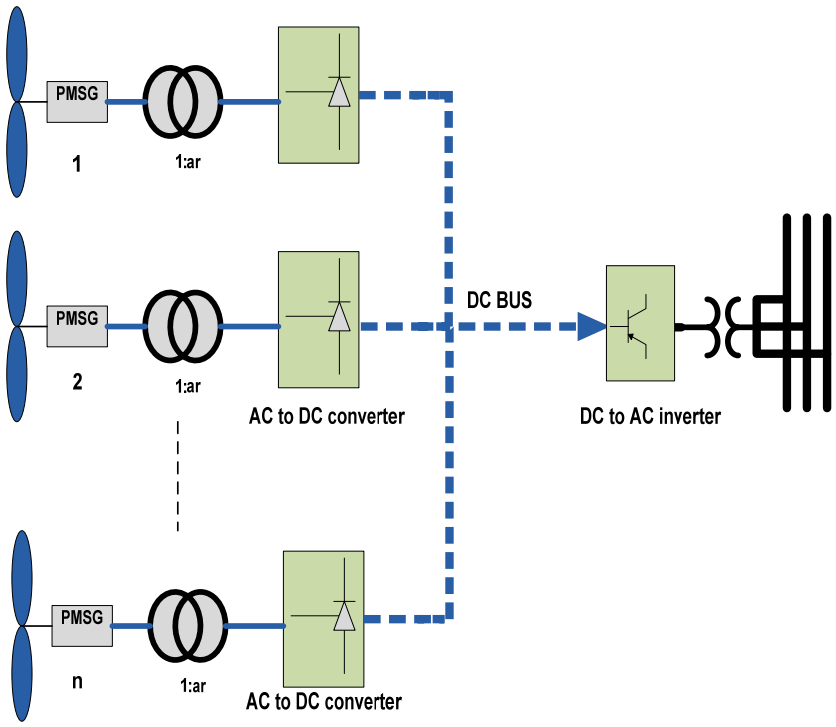

Figure 7.1 Configuration of the proposed DC distributed PMSG wind farm with multi-terminal interconnections.

Two generators tied to a common DC bus is simulated. The DC bus is held constant. The wind speed and the pitch angle to the generators are varied to simulate the varying nature of wind. Each generator is controlled to track for MPPT. The pitch angle for the generator 1 is change from 0 to 10 at 3 seconds and the same is done for the generator 2 at 6 seconds independently. The speed of wind is increased to 15 m/s at 7 seconds. In all these cases the control loop compensates for the changes and regulates the output current in each generator to track MPPT. The simulation results are given in figure 7.3

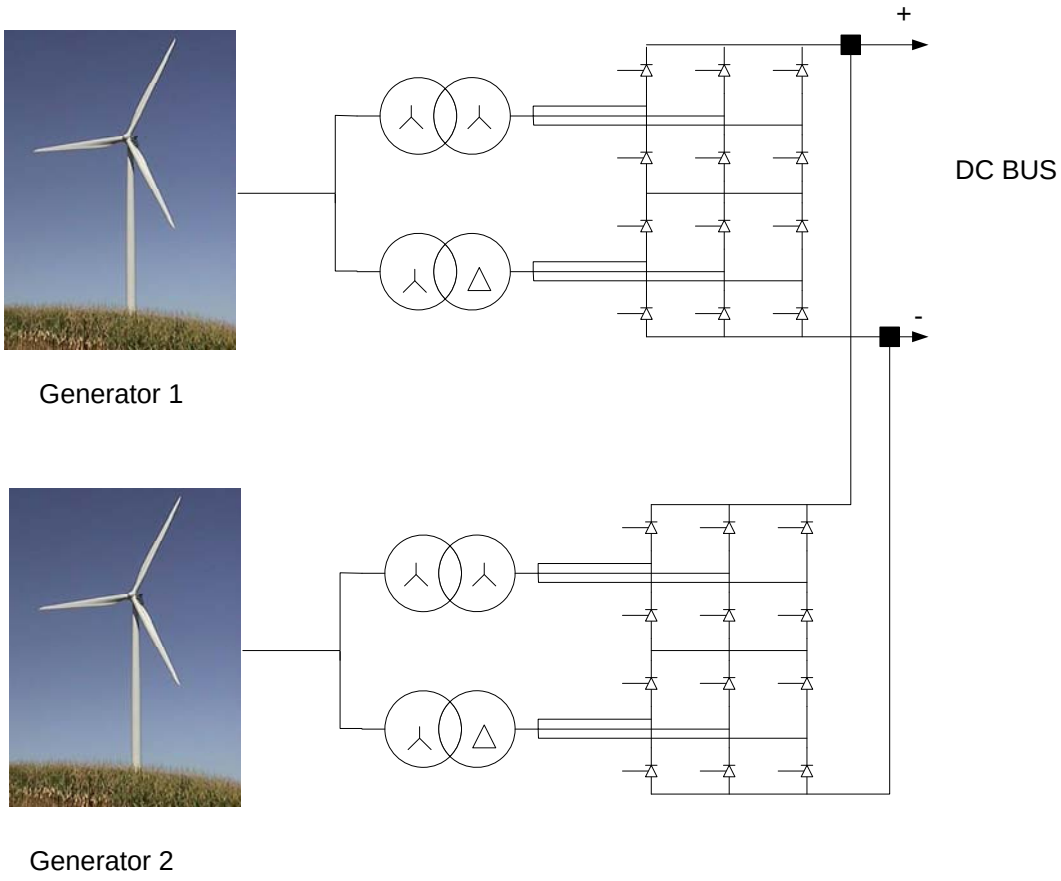

Figure 7.2 Simulation configuration of Parallel wind generators to a common DC bus.

The first plot is the total current that is produced by the generators. The second plot is the DC bus, and it is held constant. The third and fourth plots are the generator 1 and 2 pitch angle. The last plot is the wind speed change.

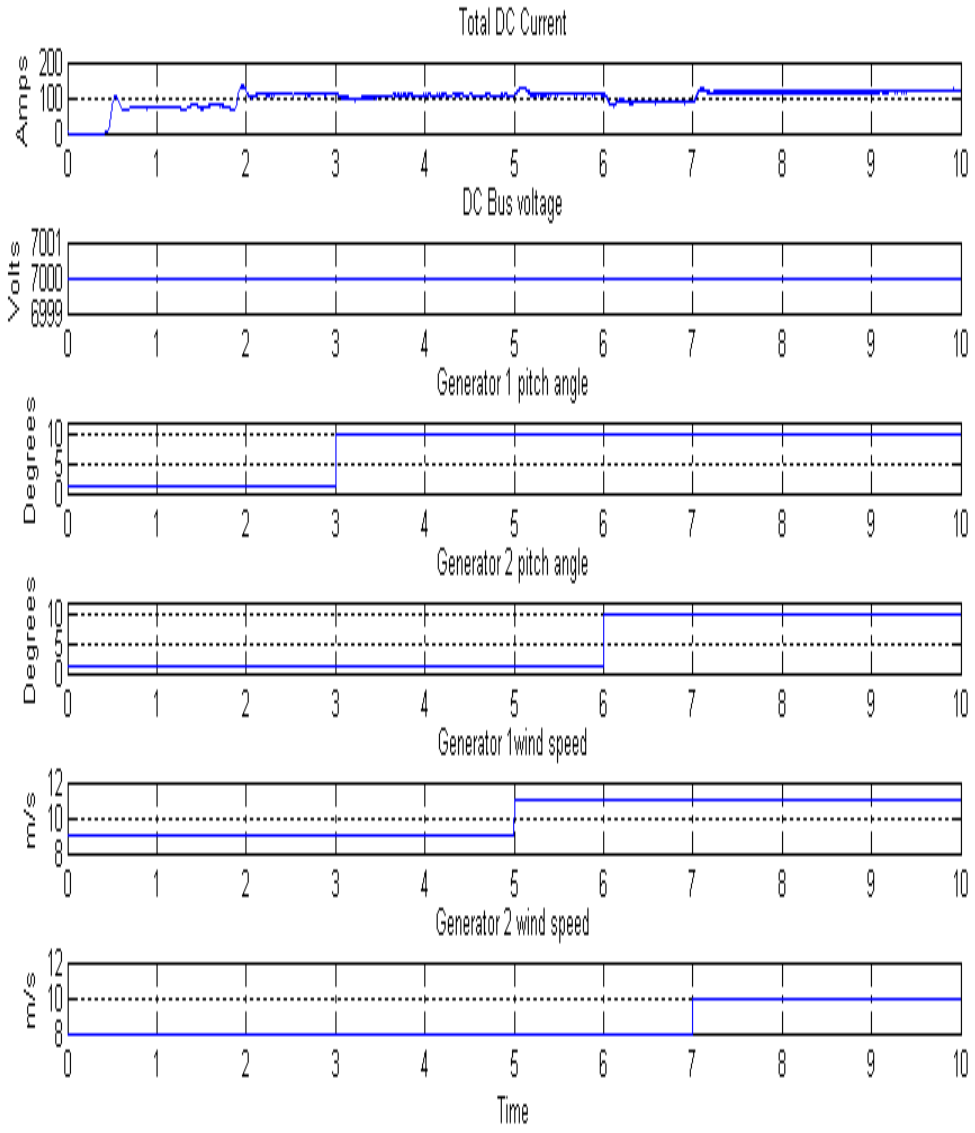

Figure 7.3 Simulation of parallel wind generators connected to a common DC bus.

7.2 Faults Analysis

There are two possible faults in the system

- Line faults – generator and inverter side.
- DC Bus faults.

A possible architecture, for a system like this is to only use AC switch gear. In the event of a Line fault at the generator, the faulty generator can be isolated from the rest of the system using an AC breaker. If the fault occurs at the inverter side, the inverter can be isolated from the utility grid using an AC breaker as well as the generators. Same holds true for DC faults where by using AC breakers the DC bus can be isolated and protected. Figure 7.4 is the proposed breaker isolation system. Figure 7.5 gives the results of a 3 phase AC ground fault, the behavior of the current and voltage estimation. It is seen from the simulation that estimators recover well after ground fault and can track the voltage and current.

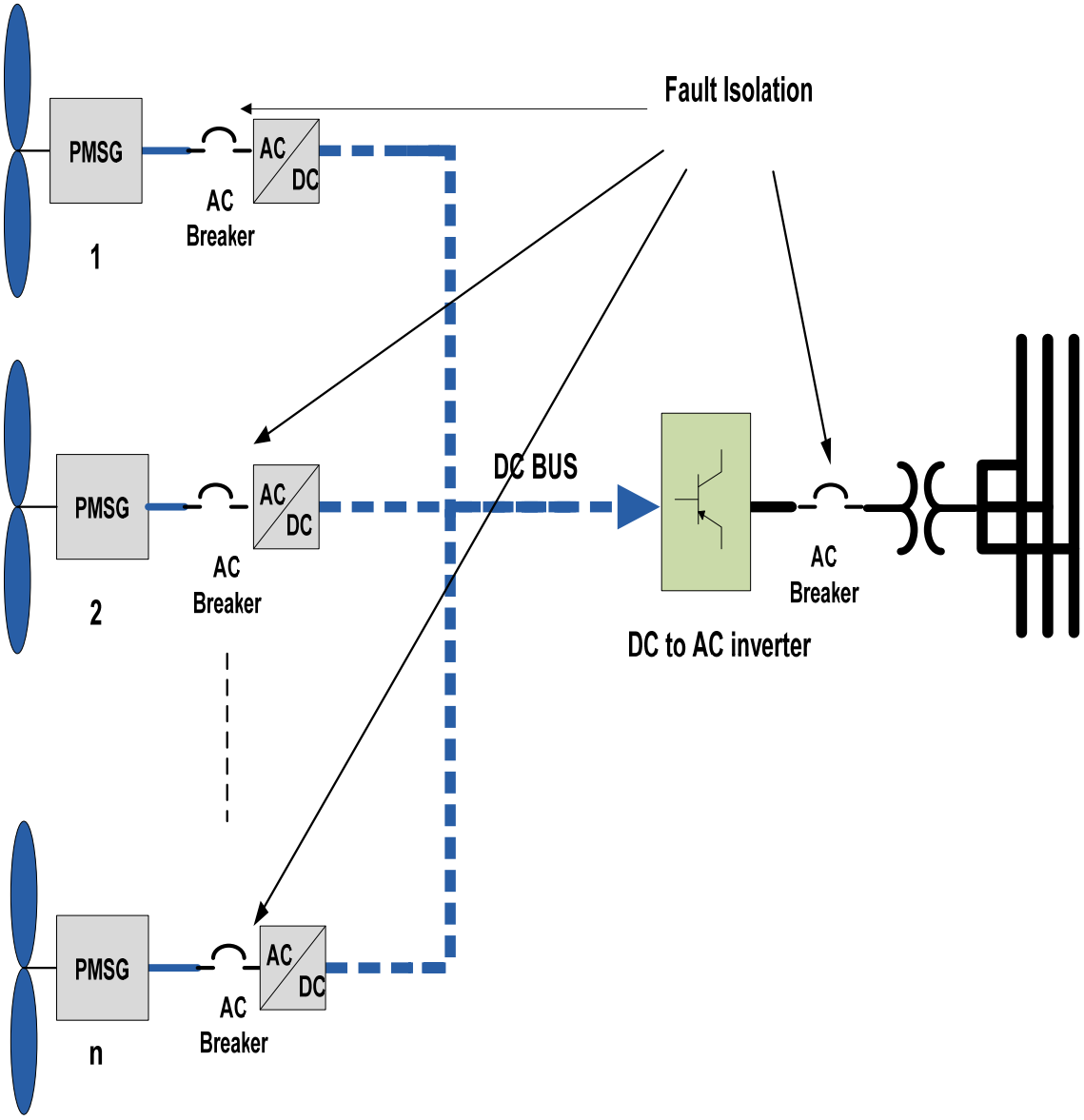

Figure 7.4 Configuration of the proposed AC fault isolation with AC breakers.

The first plot is the voltage of the PMSG and a ground fault between 2-3 seconds. The second plot is the estimation of this voltage. The third is the measured DC current. The fourth is the estimation of the DC current and the last is the wind speed.

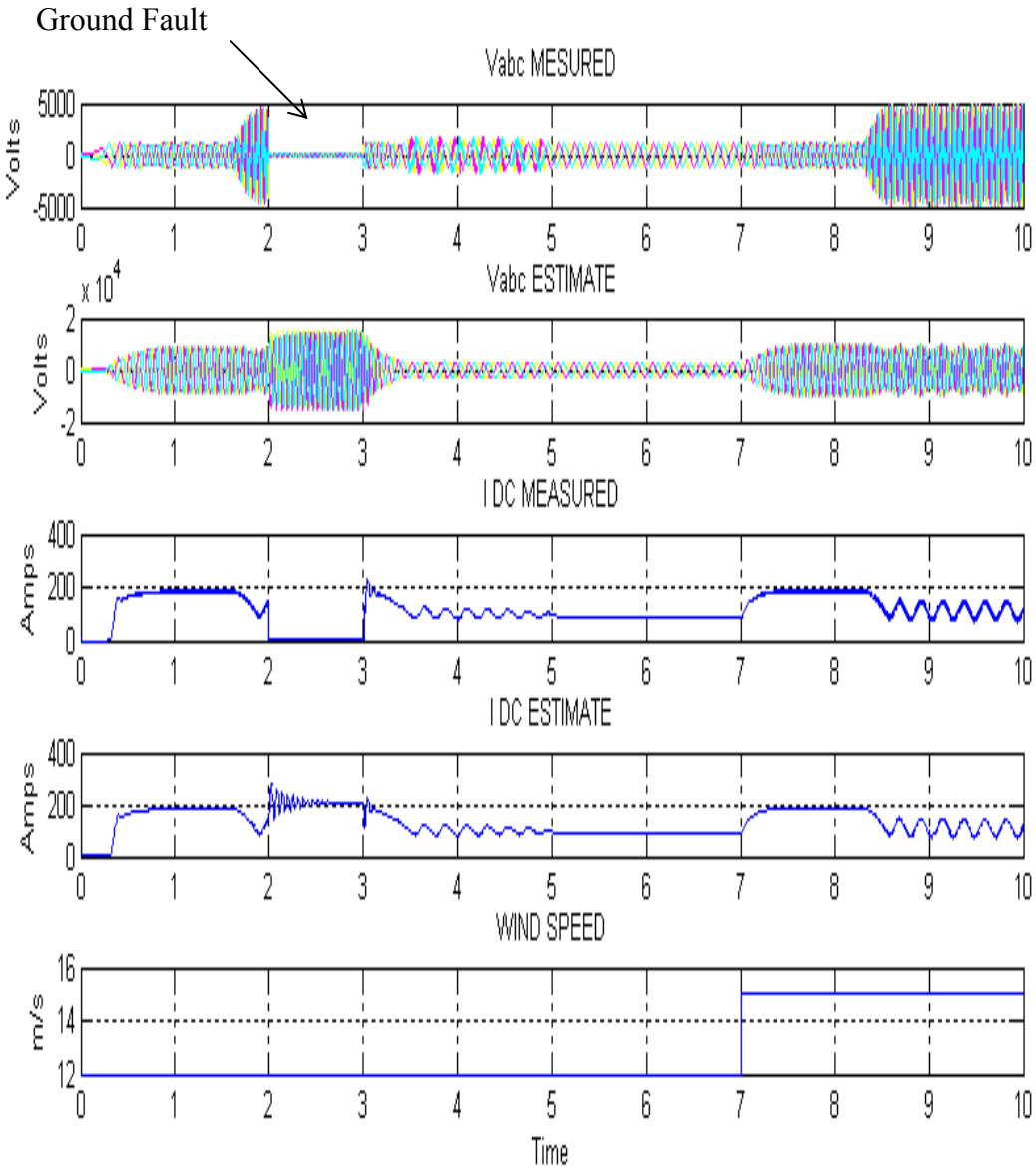

Figure 7.5 Simulation of a ground fault on this system.

7.3 Torque pulsation

A wind generator captures the power in the wind and converts the energy to mechanical torque. This torque is used to spin the rotor of the generator. The mechanical equation for the generator is given in equation (7.1). Tm is mechanical torque, Te is electrical torque, B is the friction coefficient and J is the inertia constant. ωm is the rotor speed in radians/second. We can see from this equation that any sudden changes in Te can affect Tm. This is a concern for a generator since torque pulsation can lead to premature failure of the mechanical components. Figure 7.6 is the simulation of the torque on the generator[31-40].

$$T_m = T_e + B\omega_m + J\frac{d\omega_m}{dt} \qquad (7.1)$$

The first plot is the electrical torque. The second plot is the wind speed and the last is the pitch angle. As the pitch angle has a step change the electrical torque of the generator has a sudden change. This is reflected throughout the system.

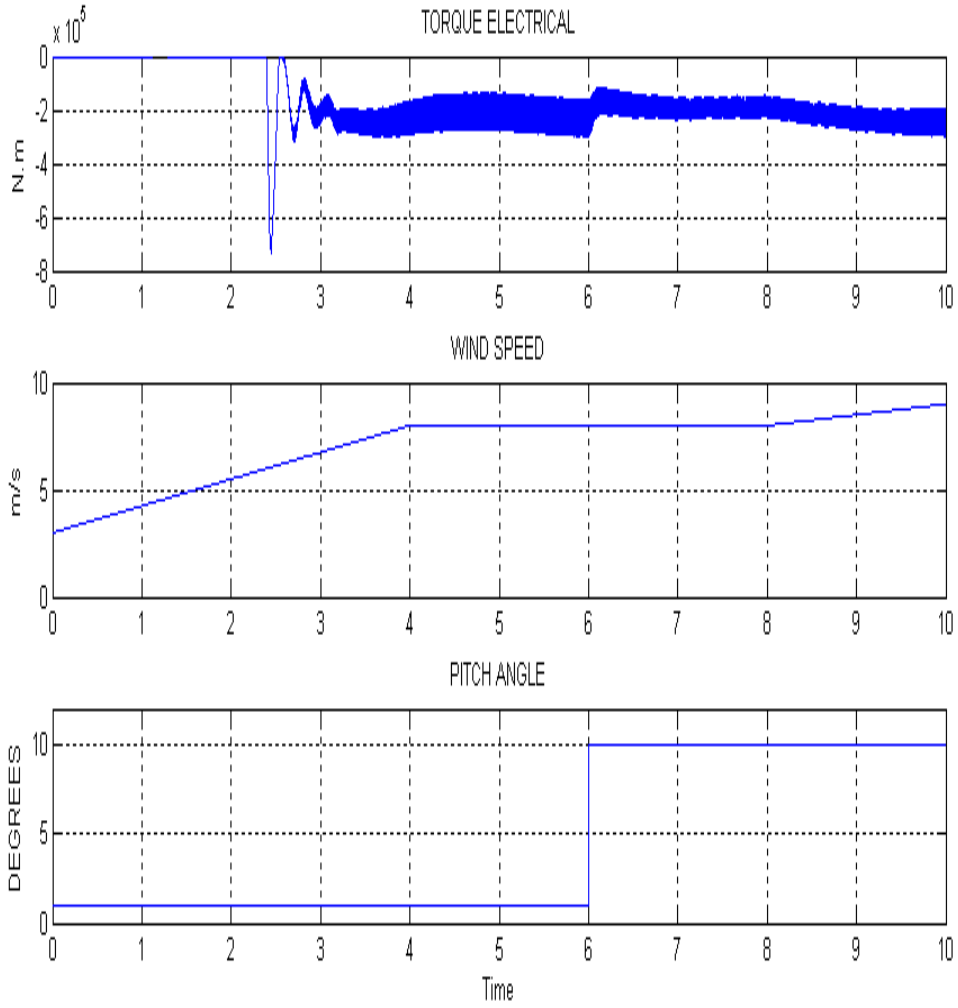

Figure 7.6 Simulation of torque pulsations.

Chapter 8

8.1 DC Power inversion to Grid

The power is collected from all the turbines and transferred to the grid side inverters via a DC bus. Multiple large size inverters transfer the power to the utility grid. The grid side inverters adjust the DC voltage of the system and perform grid side functions such as exporting reactive power. Energy storage components (ultra-capacitor and batteries) are directly connected to the DC system. They exchange power with the DC system to perform power ramp rate control, power smoothing, power shifting, and transient stability control at the wind farm output. The typical capacity factor of a wind farm is around 30-35%. The additional capacity of the inverter can be used to operate the energy storage elements when the system is not generating nominal power.

8.2 Selection of the inverter, converter and filter topologies

A three-phase 3-level Neutral Point Clamp (NPC) inverter is chosen as inverter of choice for this application. The 3-level NPC provides higher quality output voltage and current waveform and requires a reduced output LCL filter size and cost compared with two level inverters. Only half of the DC bus voltage has to be switched, which leads to reduced switching losses and higher efficiency. It also creates less Common Mode (CM) current at the output to grid. For this application, the switching frequency is around 2-4 kHz. An LCL filter is designed for the inverter, so the output current profile meets the IEEE 1547 standard [19]-[20]. A passive damping resistor is used to prevent the resonance in the filter [21].

8.3 Control of grid side inverter

Two techniques are employed to control the inverter. 1. Constant DC bus mode of operation 2. Direct active/reactive power control. In normal operation, when energy storage is not connected to the DC bus, the active power control is used to regulate the DC bus voltage. The current control forms the inner loop and the voltage control will form the outer loop. The current control loop equations are given as below [22]-[24]:

$$v_d = -\left(K_p + \frac{K_i}{S}\right)(i_{dref} + i_d) + \omega L i_q + e_d \tag{8.1}$$

$$v_q = -\left(K_p + \frac{K_i}{S}\right)(i_{qref} + i_q) - \omega L i_d \tag{8.2}$$

V_d, V_q, I_d and I_q are synchronous reference frame voltage and current. In this case, the DC bus voltage is controlled using the VSI side DC current. For the voltage control loop the equation (3) can be derived. V_{dc}, I_{dc} is DC bus voltage and current respectively.

$$i_{dref} \approx i_{dc} - i_L = \left(K_p + \frac{K_i}{S}\right)\left(V_{dc\,ref} - V_{dc}\right) \tag{8.3}$$

If energy storage is utilized on the DC bus, the active power output can be regulated independently, considering the state of charge of the storage and the power coming from the wind farm. In this case, several techniques such as power smoothing, power ramp rate control, grid frequency support, and/or grid reactive power support can be applied.

8.3 Frequency droop and voltage droop control

The proposed MVDC system can provide frequency and voltage support to the grid. Typically, renewable energy systems ride on grid frequency and voltage and do not provide significant ancillary services. However, as renewable installed capacity is rising to become a significant part of the total grid capacity, it must participate in grid support functions. There are several mechanisms including generator governor, automatic gain control and load shedding. The proposed system can provide an alternative mechanism, which can be applied faster than conventional methods. The proposed MVDC system with ultra-capacitors and battery backup with DC/DC converter can allow the VSI to support frequency droop for a short duration before automation generation control take appropriate action. Similarly it can support the system to keep the AC voltage within range by regulating the reactive power.

The main advantages of the proposed MVDC system are active and reactive power rate control, frequency droop control and voltage droop control.

The proposed complete system from the generator to the inverter that ties to the grid is given in figure 8.1. The controls for both the PMSG and the Inverter are presented.

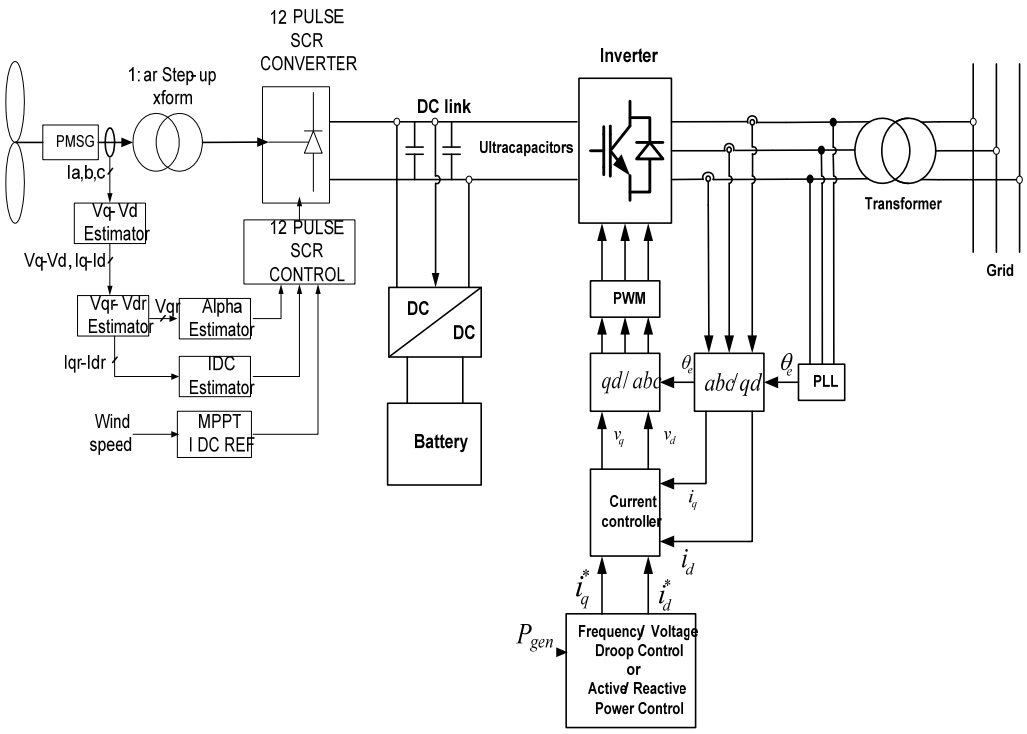

Figure 8.1 Wind energy conversion system with energy storage.

Chapter 9

9.0 Conclusion

In chapter 1, the importance that wind energy plays in the future energy generation is discussed. The current wind generator technology, the difference between a DFIG and PMSG generators are looked at. The problem and the solution that this work is centered around is stated and discussed. How wind generators connected to a HVDC/MVDC bus, tied to a grid via inverters are presented as a possible system.

Chapter 2 is dedicated to studying the HVDC/MVDC distribution. The different configuration of the HVDC distribution systems are presented. The advantages and disadvantages of the AC and DC distribution are evaluated. The converter used to convert AC power to DC power is looked at. Finally faults and redundancy in a DC distribution is analyzed.

Chapter 3 details this possible solution. The use of SCR as a power semiconductor device is presented. The system is modeled and simulated in MATLAB® and Simulink®. The parameter of a direct drive 1.5 MW generator is used in the simulation. The results of the simulation is discussed.

Chapter 4 focuses on the control system for the PMSG and 12 pulse SCR's. Three estimator are developed to aid in controlling this system. The first estimator estimates the PMSG generator voltages. The second estimator estimates the DC bus current and the third estimates the Alpha angle for firing the SCR's.

Chapter 5 is the Lab setup. The power section where the SCR's reside and how they are connected to the star and delta transformers are shown. A Texas instrument DSP is used to run this system in real time. The program flow as well as SCR gate and signal connection are illustrated. The system is run and data is gathered. The results are discussed and compared to the simulated results.

Chapter 6, the MPPT algorithm is developed. The wind turbine regions of operation and the Betz limits are discussed. Turbine energy capture and the necessary equations describing the mechanical system are presented. MPPT algorithm is simulated in MATLAB® and Simulink®.

Chapter 7 looks at how this system can be implemented in a wind farm. Two wind generators independently running and tied to a common DC bus is simulated. The results are presented. This proves the proposed system is viable for a wind farm. Another concern is how to protect such a system from faults. A possible fault isolation system is presented and simulated. Finally the torque that is generated by this system is studies as the power is varied.

Chapter 8, the final chapter looks at how the DC bus power is converted to the utility grid via inverters. The control of the inverter and interaction with the grid are stated. The inverters hold the DC bus voltage constant, enabling the wind generators to transfer power independently. This total generation, distribution and grid connection is presented in this chapter.

The following was accomplished in this work:

- Controls of a 12-pulse SCRs system to connect PMSG wind turbines to a HVDC bus was proposed.
- Three estimators are designed to estimate the generator terminal voltage, output DC current and firing angle in order to control the SCRs.
- The proposed system was fully simulated using Matlab/ Simulink.
- An experimental hardware setup was built to verify the operation of the system. This setup was connected to a synchronous generator and results are presented.
- Parallel wind generator setup was simulated. The results verifies that the proposed system will work for a wind farm.
- A fault isolation system was proposed and simulated , which shows how the system can tolerate faults and recover.
- Torque ripple on the generator was simulated to see the SCR's switching effecte on the generator.
- This setup was verified as a robust and a low cost method of implementing PMSG for HVDC distribution.

The following is proposed as future work:

- Explore different control methods for controlling the SCR's.
- Investigate reducing torque pulsations of the PMSG.

- Investigate using the proposed power conversion method for DFIG turbines.
- Explore options for communication/control between PMSG, circuit protection and grid-tied inverters.
- Investigate the best possible configuration for DC storage/connection to the HVDC/MVDC bus.
- Study the filtering needed to improve the DC bus voltage at the PMSG connections.

References

[1] M. Fatu, C. Lascu, G. Andreescu, R. Teodorescu, F. Blaabjerg, I. Boldea, "Voltage Sags Ride-Through of Motion Sensor less Controlled PMSG for Wind Turbines," in Proc. 42nd IEEE IAS Annual Meeting Industry Applications Conference, New Orleans, LA 2007, pp. 171 – 178,.

[2] Abedini, G. Mandic, and A. Nasiri, "Wind power smoothing using rotor inertia aimed at reducing grid susceptibility," Int. J. of Power Electronics, vol. 1, no. 2, pp. 227 - 247, 2008

[3] H. Peterson and P. Krause, Jr., "A Direct-and Quadrature-Axis Representation of a Parallel AC and DC Power System," IEEE Transactions on Power Apparatus and Systems, vol. PAS-85, no.3, pp. 210 – 225, March, 1966.

[4] L. Wang, K. Wang, W. Lee and Z. Chen, "Power Flow Control and stability Enhancement of Four Parallel Operated offshore Wind Farms Using a Line Commuted HVDC Link," IEEE Transaction on Power Delivery, vol. 25, no. 2, pp. 1190-1202, April 2010.

[5] Kun Han and Guo-zhu Chen, "A Novel Control Strategy of Wind Turbine MPPT Implementation for Direct-Drive PMSG Wind Generation Imitation Platform," IEEE 6th International Power Electronics and Motion Control Conference, May 2009, pp. 2255 – 2259, Wuhan, China.

[6] M. Eduardo, M. DJesus, D. Martin, S. Arnaltes and E. Castronuovo, "Optima Operation of Offshore Wind Farms With Line-Commutated HVDC Link Connection," IEEE transactions on energy conversion, vol. 25 no. 2, June 2010.

[7] Y. Weizheng, K. Woo, Z. Ruijie, G. Wei and W. Yue, "Analyze of Current Control Strategy based on Vector Control for Permanent-Magnet Synchronous Generator in Wind Power System," IEEE Power Electronics and Motion Control Conference, 2009, pp. 2209 – 2212.

[8] M. Li, K. Smedley, "One-Cycle Control of PMSG for Wind Power Generation," IEEE Power Electronics and Machines in Wind Applications, 2009.

[9] M. Chinchilla, S. Arnaltes and J. Burgos, "Control of Permanent-Magnet Generators Applies to Variable-Speed Wind Energy System Connected to the Grid," IEEE transactions on energy conversion, vol. 21, no,1,March 2006

[10] N.M Kirby,L. Xu, M. Luckett, and W. Siepman, "HVDC Transmission for Large Wind Farms", IEEE Power Engineering Journal, June 2002.

[11] J.B Ekanayake, L. Holdsworth, X.G. Wu and N.Jenkins, "Dynamic Modeling of Doubly fed Induction Generator Wind Turbines", IEEE Transactions on Power Systems", VOL1, pp.803-809, May2009

[12] Chan-Ki Kim, Vijaya K.Sood, Gil-Soon Jang, Seong-Joo Lim, Seoak-Jin Lee, "HVDC Transmission: Power Conversion Application in Power Systems"

[13] Vijaya K.Sood, "HVDC and FACTS Controllers: Applications of Static Converters in Power Systems"

[14] Ned Mohan, Tore M. Undeland, William P. Robbins "Power electronics: converters, applications, and design - Volume 1"

[15] P. Cartwright and L. Xu, "The Integration of large scale wind power generation into transmission network using power electronics" CIGRE General Session, Paris 2004

[16] S. Bozhko,R. Blasko-Gimenez,R. Li,J. Clare,G. Asher "Control of Offshore DFIG-based Wind Farm Grid with Line-Commutated HVDC Connection"

[17] Xie Lei,Xie Da,Zhang Yanchi "Offshore wind farm with dispersed wind turbines control and HVDC grid-connected control"

[18] D.Jovcic,J.Milanovic"Offshore wind farm Based on Variable Frequency Mini-Grids with Multiterminal DC Interconnections.

[19] Y. Patel, D. Pixler, A. Nasiri, "Analysis and design of TRAP and LCL filters for active switching converters," *IEEE industrial electronics international symposium* (ISIE), pp 638-643, 2010

[20] M. Liserre, F. Blaabjerg, and S. Hansen. "Design and Control of an LCLfilter based Three-phase Active Rectifier," *Conf Rec. of 36th IAS Ann. Meeting, Chicago*, 2001, pp. 297-307.

[21] M. Loserre, A. Dell'Aquila, F. Blaabjerg, "Genetic algorithm-based design of the active damping for an LCL filter three phase active rectifier," *IEEE Trans. Power electronics.*, vol. 19, no. 1, pp. 76–86, Jan. 2004.

[22] V. Blasko and V. Kaura, "A novel control to actively damp resonance in input LC filter of a three-phase voltage source converter," *IEEE Trans.Ind. Appl.*, vol. 33, no. 2, pp. 542–550, Mar./Apl. 1997.

[23] Y Lang; X Zhang; D Xu;, S. Hadianamrei; H Ma, "Nonlinear Feedforward Control of Three-phase Voltage Source Converter," *IEEE Industrial Electronics.,* vol. 2 pp. 1134-1137, Jul 2006

[24] R. M. Tallam, R. Naik, M. L. Gasperi, T.A. Nondahl, Hai Hui Lu, Yin Qiang, "Practical issues in the design for AC drives with reduced DC link capacitor," *Conf Rec. of 38th IAS Ann. Meeting,* vol. 3, pp. 1538-1545, 2003

[25] T. Ackermann, "Wind Power in Power Systems", John Wiley & Sons, 2005.

[26] L. H. Hansen, L. Helle, F. Blaabjerg, E. Ritchie, S. Munk-Nielsen, H. Bindner, P. Sørensen and B. Bak-Jensen, "Conceptual survey of Generators and Power Electronics for Wind Turbines", 2001.

[27] Johnson, Gary L. "Wind energy systems", Prentice-Hall, inc 1985.

[28] High Voltage Proven Technology -SIEMENS

[29] http://www.mathworks.com/products/simpower/blocklist.html

[30] Adaptive Torque control of variable speed wind turbine, Kathryn E. Johnson, NREL

[31] G. Mandic, A. Nasiri, E. Muljadi, and F. Oyague, "Active torque control for gearbox load reduction in a variable speed wind turbine," accepted of publication in *IEEE Trans. Ind. Appl.*, 2012

[32] Y. Hori, H. Iseki, and K. Sugiura, "Basic consideration of vibration suppression and disturbance rejection control of multi-inertia system using SFLAC (state feedback and load acceleration control)," *IEEE Trans. Ind. Appl.*, vol. 30, no. 4, pp. 889–896, Jul./Aug. 1994.

[33] M. Cychowski, K. Szabat, and T. Orlowska-Kowalska, "Constrained model predictive control of the drive system with mechanical elasticity," *IEEE Trans. Ind. Electron.*, vol. 56, no. 6, pp. 1963–1973, Jun. 2009.

[34] K. Szabat and T. Orlowska-Kowalska, "Vibration suppression in a two-mass drive system using PI-speed controller and additional feedbacks—Comparative study," *IEEE Trans. Ind. Electron.*, vol. 54, no. 2, pp. 1193–1206, Apr. 2007.

[35] A. Dixit and S. Suryanarayanan, "Towards Pitch-Scheduled Drive Train Damping in Variable Speed, Horizontal-Axis Large Wind Turbines," in *Proc. 44th CDC-ECC,* Seville, Spain, Dec. 12-15, 2005.

[36] S.H. Kia, H. Henao, and G.-A Capolino, "Torsional Vibration Effects on Induction Machine Current and Torque Signatures in Gearbox-Based Electromechanical System," *IEEE Trans. Ind. Electron.,* vol. 56, no. 11, pp. 4689-4699, Nov. 2009.

[37] H. Geng, D. Xu, B. Wu, and G. Yang, "Active Damping for PMSG based WECS With DC-Link Current Estimation," *IEEE Trans. Ind. Electron.,* vol.58, pp. 1110-1119, Apr. 2011.

[38] M. Molinas, J. A. Suul, and T. Undeland, "Torque transient alleviation in fixed speed wind generators by indirect torque control with STATCOM," in *Proc. 13th EPE-PEMC*, Poznan, Poland, Sep. 1–3, 2008, pp. 2318–2324.

[39] T. Zoller, T. Leibfried, and A.M. Miri, "Application of Power Electronics for Damping of Torsional Vibrations," in *Proc. 7th PEDS,* Bangkok, Thailand, Nov. 27-30, 2007.

[40] R. Muszynski and J. Deskur, "Damping of Torsional Vibrations in High-Dynamic Industrial Drives," *IEEE Trans. Ind. Electron.*, vol. 57, pp. 544-552, Feb. 2010.

[41] E. A. Bossanyi, "The Design of Closed Loop Controllers for Wind Turbines," *Wind Energy,* vol. 3, pp. 149-163, 2000.

[42] H. Polinder, F. F. A. van der Pijl, G. J. de Vilder, and P. J. Tavner, "Comparison of Direct-Drive and Geared Generator Concepts for Wind Turbines," *IEEE Trans. Energy. Convers.*, vol. 21, pp. 725-733, Sep. 2006.

[43] I. Boldea *Variable Speed Generators,* CRC Press, 2005

[44] J. L. Rodriguez-Amenedo, S. Arnalte, and J.C. Burgos, "Automatic generation control of a wind farm with variable speed wind turbines," *IEEE Trans. Energy Convers.*, vol.17, no.2, pp.279-284, Jun. 2002.

[45] Q.Q. Wang, "Maximum wind energy extraction strategies using power electronic converters", Ph.D. Dissertation, University of New Brunswick, 1996

[46] E.Koutroulis, and K.Kalaitzakis, "Design of a Maximum Power Tracking System for Wind-Energy-Conversion Applications," *IEEE Trans. Ind. Electron.,* vol. 53, no. 2, pp. 486-494, Apr. 2006.

[47] E. Muljadi and C.P. Butterfield, "Pitch-controlled variable-speed wind turbine generation," *IEEE Trans. Ind. Appl.,* vol.37, no.1, pp.240-246, Jan/Feb 2001.

[48] O. Anaya-Lara, N. Jenkins, J. Ekanayake, P. Cartwright, M Hughes, *Wind Energy Generation : Modeling and Control.* John Wiley & Sons, 2009.

[49] Y. Chen, P. Pillay, and A. Khan, "PM wind generator topologies," *IEEE Trans. Ind. Appl.*, vol. 41, no. 6, pp. 1619–1626, Nov./Dec. 2005.

[50] G. Mandic, and A. Nasiri, "Modeling and simulation of a wind turbine system with ultracapacitors for short-term power smoothing," IEEE ISIE 2010, Bari, Italy, July 2010.

CURRICULUM VITAE

RAVI NANAYAKKARA

2520 Rebecca DR., Racine, WI 53402 (262)-752-4854

ravin@ieee.org

EDUCATION:

Doctor of Philosophy – Electrical Engineering (Power Electronics)

University of Wisconsin Milwaukee, Milwaukee, Wisconsin December 2012

Master of Science in Electrical and Computer Engineering

Marquette University, Milwaukee, Wisconsin December 2001

Bachelor of Science in Electrical Engineering

University of Wisconsin Milwaukee, Milwaukee, Wisconsin May, 1997
commencement Honors

SUMMARY:

A highly motivated and analytical professional with 17+ years of work experience at a leading Industrial Automation and Controls Corporation. Hardware design, simulation and new product development experience coupled with strong interpersonal communication and project management skills.

PROFESSIONAL OVERVIEW:

ROCKWELL AUTOMATION-ALLEN BRADLEY

Milwaukee,Wisconsin

Project Engineer Hardware **February,2005 to Present**

Responsible for overseeing a project from inception to finish. Overall responsibility for setting the project technical direction. Responsible for working with cross-functional teams to establish customer requirements for new products.

- Design of next generation 690/480 volt three phase motor controller.
- MATLAB® and Simulink®. modeling.
- Power electronics/Digital/communication hardware design. Includes High speed SCR gate drive design, DSP, Input/output circuitry, Voltage and Current controller design as well as Power supply design.

Senior Hardware Design Engineer **April,2001 to February ,2005**

Team member of a new product development team responsible for designing the next generation HMI products.

- Project lead responsibility for design and development of a new display platform. This is the largest HMI display platform undertaken by the business with the largest estimated profit margins.
- In depth knowledge of display interfacing technology. Implemented DVI /LVDS interface in driving large-scale displays to reduce EMI. This in turn produced cost savings of half a million a year and ease of manufacturing by using board to board interconnects.
- Responsible for the new design of scalable inverter architecture for driving CCFL backlights for flat panel TFT displays of various sizes. Exceeded the cost; size and performance goals set in the design specification.
- Design of low power white LED drivers for battery operated hand held displays.
- Design of battery charging circuit for Lithium Ion. Embedded system development with 32 bit microprocessor, 8 bit micro programming experience, SDRAM, Flash, DDR, USB, CPLD, Ethernet 10/100 implementation experience.
- Familiarity with safety standards and EMC regulations world wide. Worked with UL representatives in obtaining agency approvals for designs. Designed products for CE, CUL, UL, Demco, Ctic and other industrial safety standards.
- Responsible for design specifications and cross-functional integration with mechanical, test engineering and manufacturing teams. Overall responsibility for all display heads design and pilot production.

Hardware Design Engineer July, 1997 to April, 2001

Responsible for overall power supply architecture for supporting the hardware platform of the next generation operator interface terminals.

- Design of distributed DC/DC power supplies for an embedded platform. Special emphasis on low voltage and high current core operation of microprocessors. High efficiency (85%-90%) DC power supply design using synchronous rectification. Low EMI power supplies using out of phase switching regulators.
- Design of AC/DC switch mode power supplies for industrial environment.
- Analysis of analog designs with Accusim simulation, Saber simulation , Mathcad and Matlab tools. Schematic capture using Mentor graphics.
- Worked with mechanical teams in thermal management and packaging of products. Component de-rating and analysis for meantime failure. Implemented accelerated life test for power supply testing.

Engineering Intern June,1995 to July,1997

Designed systems for testing Man Machine Interface (MMI) with Allen-Bradley Programmable Logic controllers.

Worked with DH+, DH485, DF1, RIO, Controllnet and DeviceNet protocols. Design and development of table driven test software using Visual Basic allowing faster functional evaluation of the development software.

PROFESSIONAL & ACADEMIC SKILLS

- Two patents have been filed as well as numerous innovation awards.
- Knowledge of modern control theory including state space control and non-linear adaptive control.
- Ability to analyze stability of a control loop, Optimize a control loop for desired response.
- Experience in designing power inductors and transformers
- IEEE Member